A Theoretical and Experimental Investigation of a Shell-and-Coil Heat Exchanger for a Solar Domestic Hot Water System

by

Ibrahim Gharbia

Submitted in partial fulfillment of the requirements
for the degree of Master of Applied Science

at

Dalhousie University
Halifax, Nova Scotia
September 2010

DALHOUSIE UNIVERSITY

DEPARTMENT OF MECHANICAL ENGINEERING

The undersigned hereby certify that they have read and recommend to the Faculty of Graduate Studies for acceptance a thesis entitled "A Theoretical and Experimental Investigation of a Shell-and-Coil Heat Exchanger for a Solar Domestic Hot Water System" by Ibrahim Gharbia in partial fulfillment of the requirements for the degree of Master of Applied Science.

Dated: September 03, 2010

Supervisor: _____

Co-supervisor: _____

Readers: _____

_____

DALHOUSIE UNIVERSITY

DATE: September 03, 2010

AUTHOR: Ibrahim Gharbia

TITLE: A Theoretical and Experimental Investigation of Shell-and-Coil Heat Exchangers for a Solar Domestic Hot Water System

DEPARTMENT: Department of Mechanical Engineering

DEGREE: MASc CONVOCATION: October YEAR: 2010

TABLE OF CONTENTS

LIST OF TABLES

LIST OF FIGURES

List of Abbreviations and Symbols Used

A	Area, m^2
AC	Alternating current, A
AWG	American wire gauge
C	Constant
C	Coil
CFD	Computational fluid dynamics
C_p	Specific heat at constant pressure, J/kg·K
CPU	Central processing unit
D	Diameter, m
DC	Direct current, A
De	Dean Number
D_i	Tube inner diameter, m
D_{hi}	hydraulic tube inner diameter, m
D_{ho}	hydraulic tube outer diameter, m
D_o	Tube outer diameter, m
H	Shell height, m
h_i	Inside convection heat transfer coefficient, $W/m^2 \cdot K$
h_o	Outside convection heat transfer coefficient, $W/m^2 \cdot K$
Hz	Hertz

I	Current, A
I	First loop
ID	Inner diameter, m
II	Second loop
k	Thermal conductivity, $W/m^2 \cdot K$
L	Total coil tube length, m
LPM	liter per minute
$\dot{m}$	Mass flow rate, kg/s
n	Number Coils
NCHE	Natural convection heat exchanger
Nu	Nusselt number
OD	Outer diameter, m
P	Pressure, kPa
P	Electric power, W
PF	Performance factor
Pr	Prandtl number
q	Heat transfer rate, W
q-hx	Heat transfer rate for the heat exchanger, W
R	Resistance, Ω
Ra	Rayleigh number
SCHX	shell-and-coil heat exchanger
S3CHX	shell-and-3coil heat exchanger
S4CHX	shell-and-4coil heat exchanger
S3CHX-W	shell-and-3coil heat exchanger, water is the working fluid on the tube side

S3CHX-G	shell-and-3coil heat exchanger, glycol is the working fluid on the tube side
S4CHX-W	shell-and-4coil heat exchanger, water is the working fluid on the tube side
S4CHX-G	shell-and-4coil heat exchanger, glycol is the working fluid on the tube side
SDHW	Solar domestic hot water
T	Temperature, °C
T_{co}	Temperature outlet on the cold side, °C
T_{ci}	Temperature inlet on the cold side, °C
T_{hi}	Temperature inlet on the hot side, °C
T_{ho}	Temperature outlet on the hot side, °C
t	Time, sec
UA	Overall heat transfer coefficient-area product, W/K
V	Voltage, V
V	Velocity, m/s

Greek Letters

β	Volumetric thermal expansion coefficient, K^{-1}
ρ	Density, kg/m^3
μ	Dynamic viscosity, $N \cdot s/m^2$
v	Kinematic viscosity, m^2/s

Subscripts

act	Actual
ave	Average
D	Diameter
elec	Electric
EXP	Experiment
g	Glycol (propylene glycol)
h_x	Heat exchanger
i	Inlet
i	Inside surface
lab	Laboratory
lm	Log mean
meas	Measured
o	Outlet, Outside surface
PR	Predicted
TH	Theoretical
w	Water

ABSTRACT

Solar energy is an important form of renewable energy that can be used as an alternative to fossil fuels. It can be used to produce electricity or to provide heat. One particular application is using solar energy for a domestic hot water system.

The purpose of this research is to improve the thermal performance of a solar domestic hot water (SDHW) system. Experimental research was conducted to study the thermal performance of a shell-and-3coil heat exchanger and a shell-and-4coil heat exchanger using either water or glycol as working fluids on the tube side.

An experimental set-up simulating a SDHW system was designed and constructed. The set-up contained a 270 L storage tank, a shell-and-three coil heat exchanger or a shell-and-four coil heat exchanger, and electrical heaters to simulate the solar collector. At the inlets and outlets of the storage tank and the heat exchanger the temperatures, pressures, and flow rates were measured to determine the thermal performance. The results from the experiment tests were analyzed in terms of the overall heat transfer coefficient product (UA) and the pressure drop (ΔP) between the inlet and outlet of the heat exchanger.

The UA value of the shell-and-4coil heat exchanger was higher than the UA value of the shell-and-3coil heat exchanger. For example, at a heat transfer rate of 2000 W for water, the UA values were 240 W/K and 270 W/K for the shell-and-3coil heat exchanger and the shell-and-4coil heat exchanger, respectively. With respect to glycol, at a heat transfer rate of 2000 W the UA values were 197 W/K and 215 W/K for shell-and-3coil, and shell-and-4coil heat exchanger, respectively. The degradation of the thermal performance of the shell-and-3coil was offset by benefits, such as reduction in mass, volume, labor cost and the final cost. A reasonable agreement between theoretical and experimental results in terms of the UA value was observed.

The thermal performance of each coil in both heat exchangers was below that predicted by the relevant heat transfer correlations. A performance factor was calculated for each coil. For both glycol and water, and both heat exchangers, the performance factors for the inner most and outer most coils were 0.70 and 0.53, respectively. However, there is a slight difference in the performance factors of coils between the inner most and the outer most coils for the 3-coil and 4-coil heat exchangers. For these coils the performance factors varied from 0.55 to 0.67.

ACKNOWLEDGEMENTS

I am heartily thankful to my supervisor Dr. Peter Allen, whose encouragement, guidance and support from the initial to the final level enabled me to develop an understanding of the subject and to my co-supervisor Dr. Dominic Groulx for his guidance. Secondly, thanks are due as well to the other members of the supervisory committee, Dr. N. Ben-Abdallah and Dr. Prabir Basu.

Finally, I would like to express special thanks to my parents Hana Aljreo and Abdullah Gharbia and all my sisters and brothers for their unending love, interest and support during my academic years.

CHAPTER 1

INTRODUCTION

1.1 Background

Solar domestic hot water (SDHW) systems transform solar radiation from the sun into thermal energy stored. A SDHW system consists of the solar collector, pump, heat exchanger and storage tank.

Heat exchangers are widely used in many applications such as heat recovery systems, power plants, nuclear reactors, food industries, chemical processing, refrigeration and air conditioning systems. When the performance of a heat exchanger is enhanced, the heat transfer improvement enables the size of the heat exchanger to be decreased, Salimpour [1].

A natural convection shell-and-coil heat exchanger consists of a cylindrical shell with helical coils placed inside it. On the tube side the flow is forced by a pump through the coils while buoyancy forces are the cause of flow on the shell side, Taherian [2]. Helical coils are widely used as heat exchangers due to the high heat transfer coefficients. Several studies have indicated that helically coiled tubes are superior to straight tubes when employed in heat transfer applications, Shokouhmand, Salimpour and Behabadi [3]. In the coiled tubes, the modification of the flow is due to the centrifugal forces caused by the curvature of the tube, which produce a secondary flow field with a circulatory motion pushing the fluid particles toward the core region of the tube, Kumar, Mridha, Gupta and Nigam [4].

In a typical SDHW system an antifreeze solution of propylene glycol and water is circulated through the solar collector and heat exchangers using a pump. Due to the lower density of the water on the shell-side of the heat exchanger compared to the water at the heat exchanger inlet, the circulation of water is driven by natural convection.

With A natural convection heat exchanger (NCHE) in the SDHW system, the flow through the storage tank is driven by buoyancy forces due to the temperature difference between the heat exchanger and the storage tank. Thus, only one pump is required instead of two pumps for the two loops associated with the typical SDHW system.

Figure 1.1 shows a schematic of the double loop SDHW system (collector loop I and tank loop II). The two loops are between the storage tank and the heat exchanger, and between the heat exchanger and the solar collector. A pump powered by a photovoltaic module circulates the liquid in the solar collector loop.

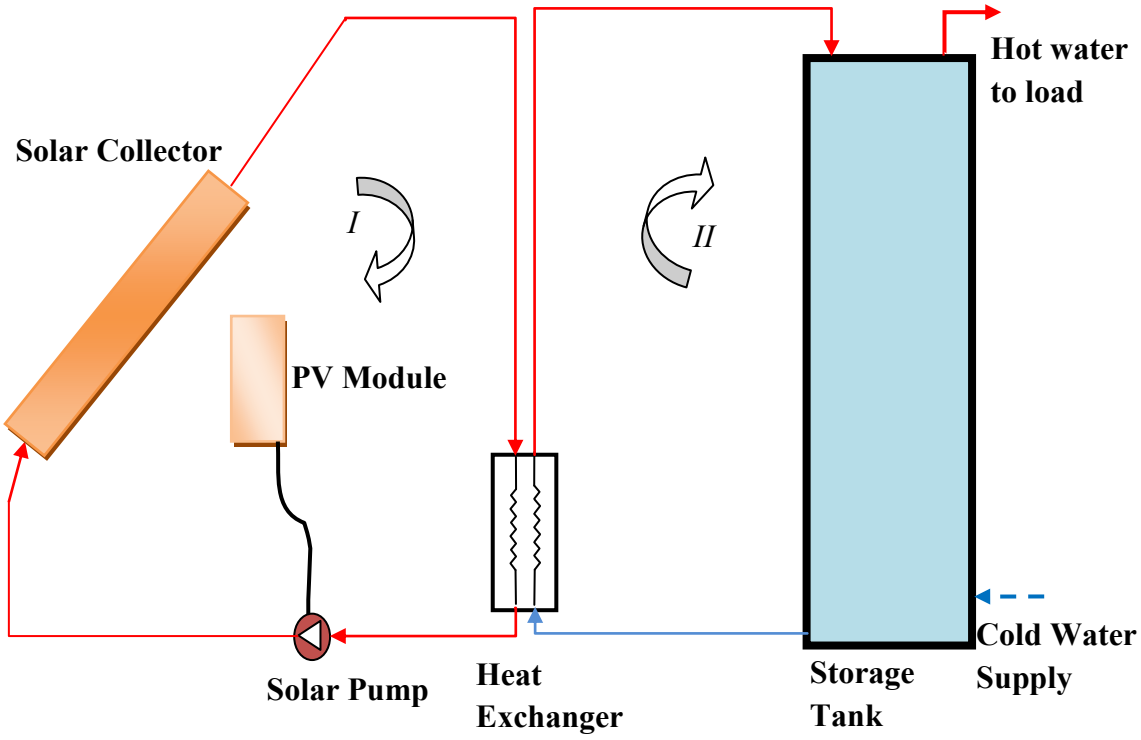

Figure 1.1. SDHW system with two loops

A NCHE is a heat exchanger in which the dominant mode of heat transfer in one or both flows is natural convection, as opposed to forced convection dominating on both sides of the heat exchanger. Though the natural convection heat exchanger is relatively new,

several studies have been performed on this topic and the traditional shell-and-coil heat exchangers were adapted to be used as natural convection heat exchangers.

Some NCHE systems have been shown to perform better than pumped systems, Bergelt et al. [5] Moreover, these systems have lower initial cost and less maintenance than the alternatives. Srinivasan et al. [6] performed experiments on a shell and coil NCHE for the case where the buoyancy driven flow occurs in the shell. They also studied NCHE's with fluted tubes instead of smooth circular ones. Whit et al. [7] recently introduced NCHE's with multiple helical coils in a cylindrical shell, in which the natural convection occurs in the shell-side flow configuration. Other works include those of Richmond and Hollands [8] and Parent [9], which involve shell and tube natural convection heat exchangers where buoyancy driven flow occurred inside the tubes. Also Ajele [10], Avina [11], and Bergelt et al. [5] have investigated shell-and-coil heat exchangers.

The purpose of the current study is to determine the performance of different shell-and-coil heat exchangers as well as the relative performance of the individual coils by using different fluid on the tube side experimentally and comparing it with an analytical model and comparing the thermal performance with the economic performance.

1.2. Objective

The objective of this research is to obtain and compare the thermal performance of two different external shell-and-coil heat exchangers through experimental analysis and a computer model. To accomplish this, the following specific objectives were outlined:

1. To compare two designs of external shell-and-coil heat exchangers and to analyze their thermal performance in terms of the overall heat transfer coefficient-area (*UA*) product.
2. To understand and analyze the hydraulic performance of the external heat exchanger in terms of pressure drop.
3. To predict the thermal performance (*UA*-value) of different external shell-and-coil heat exchangers, using computer simulation models combining experimental data,

and gain information on the values based on natural convection and forced convection heat transfer coefficients.

1.3. Scope of the study

Previous studies of shell-and-coil heat exchanger for SDHW systems have used controlled experimental conditions such as constant storage tank temperature, constant flow rate, and constant water heat exchanger inlet temperature.

In this study, which is focused on the thermal performance of shell-and-coil heat exchangers within the context of the two loops using heaters instead of solar collectors with the same operational conditions as a real SDHW system, tests were performed from morning at 200 W to 3000 W at noon on a sunny day using both glycol and water as the working fluid in the tube side for both shell-and-3coil and shell-and-4coil heat exchangers.

CHAPTER 2

LITERATURE REVIEW

2.1 Solar domestic hot water systems

SDHW systems can be defined as the complete assembly of subsystems and components necessary to convert solar energy to heat potable water to supply domestic water needs. SDHW systems are one of the major applications of shell-and-coil natural convection heat exchanger.

Salimpour [12] investigated three heat exchangers with different coil pitches and found that the shell-side heat transfer coefficient of coils with larger pitches is higher than those with smaller pitches. Also, two correlations were developed to predict the inner heat transfer coefficients and the outer heat transfer coefficients of the coiled tube heat exchanger.

Furbo [13] carried out experimental and analytical studies of smart solar tanks for small SDHW systems. A smart tank is a hot water tank in which the domestic water can be heated by solar collectors and by means of an auxiliary energy supply system. The auxiliary energy supply system in this study electric heating elements—heats up the hot-water tank from the top and the water volume heated by the auxiliary energy supply system is fitted to the hot-water consumption and consumption pattern. In periods with a large hot-water demand, the volume is large; in periods with a small hot-water demand, the volume is small. Two small SDHW systems, based on differently designed smart solar tanks and a traditional SDHW system were investigated by means of laboratory experiments and theoretical calculations. The investigations showed that the yearly thermal performance of SDHW systems with smart solar tanks is 5–35% higher than the thermal performance of traditional SDHW systems. Furbo [13] also concluded that the risk of oversized solar heating systems and oversized tank volume was reduced by using smart solar tanks.

Bojic [14] performed a simulation of a solar domestic water heating system using a time marching model. They used the mathematical model to evaluate the annual variation of the solar fraction with respect to the volume of the tank, demand hot water temperature required, difference of this temperature, and consumption profile of the domestic hot water demand. The results of this investigation could be used to design a solar collector system, and to operate already designed systems, effectively. The results for a number of designs with different storage tank volumes indicate that the systems with greater volume yield higher solar fraction values. The solar fraction of the system increases with lower hot water demand temperature and higher differences between the mean storage water and the demand temperatures.

Hollands [15] studied the optimum flow rates in solar heating systems with a counter flow heat exchanger. He showed that optimum flow rates exist on both sides of the heat exchanger when the overall exchanger conductance *UA*-values is fixed. They also stated that determining the optimum storage loop flow rate of systems with heat exchangers requires simulation of systems of various collector areas without exchangers.

2.2 Natural convection heat exchangers

Several studies have been carried out on natural convection heat exchangers due to its economic and practical applications. In this section some of the research on this topic will be discussed.

Gertzos et al. [16] experimentally and numerically studied the heat transfer phenomena inside a flat-plate integrated collector storage solar water heater with indirect heat withdrawal. The researchers reported that recirculation played an important role in the temperatures profiles, and that without recirculation, results obtained for the heat exchanger middle temperature were lower. Also a strong stratification of the tank water temperature up to 15˚C was observed. Gertzos et al. [16] also reported that numerical results obtained by using a computational fluid dynamics (CFD) model were in agreement with the experimental measurements, for both situations with and without recirculation.

Rao et al. [17] investigated the stability of a natural circulation loop in a heat exchanger. The researchers used the finite element program to solve the one-dimensional transient conservation equations of the loop fluid and the two fluid streams of hot-end and cold-end heat exchangers simultaneously. They stated that the stability may depend on a number of parameters and that the two non-dimensional parameters studied were the heat capacity rate of the fluid and the loop Grashof number. Three different stability cases: stable, neutrally stable, and unstable combinations of the two parameters, were used and the stability was scanned over a wide range of the two parameters values. The stability envelope was also constructed.

Prabhanjan et al. [18] experimentally investigated the natural convection heat transfer from helically coiled tubes in water. They reported that different lengths were used to correlate the outside Nusselt number to the Rayleigh number. Models were developed to predict the outer temperature fluid flow through the helical coiled heat exchanger. The best correlation employed the total height of the coil as the characteristic length. They developed a model to predict the outlet temperature of a fluid flowing through a helically coiled heat exchanger, given the inlet temperature, bath temperature, coil dimensions, and fluid flow rate. The predicted outlet temperature was compared to measured values from an experimental setup. The results of the predicted temperatures were close to the experimental values and suggest that the method presented has promise as a method of predicting outlet temperatures from similarly dimensioned heat exchangers.

Taherian [2] performed a study to find the effect of tube diameter, coil surface area, coil diameter, coil pitch, shell diameter and height on the shell-side heat transfer coefficient for different configurations of shell-and-coil NCHE's. Results showed that the shell-side coefficient were inversely proportional to both the coil surface area and the shell diameter. Taherian showed that the variations in coil tube diameter, glycol flow rate, and shell height do not affect the heat transfer coefficient. The *UA* value for the heat exchanger was found to be proportional to the coil surface area to the power 0.67 and that based on the experiment that plotted (variation of the overall heat transfer coefficient with

the total coil surface area). The effect of an increased coil surface is to increase the value of *UA*-value.

Taherian also found the shell-side heat transfer coefficient decreased with increasing coil surface area and that the tube diameter had little influence on the shell-side heat transfer coefficient. Increasing the height of the heat exchanger slightly increased the shell-side heat transfer coefficient. Taherian also concluded that the smaller diameter coils in single-coil configurations were more likely to encounter recirculation flows at the bottom of the heat exchanger. The shell-side heat transfer coefficient was not affected by the coil tube diameter. The value of the heat transfer coefficient was slightly higher for the smaller diameter coils, and increased by decreasing the shell diameter. The heat transfer coefficient *ho* for the natural flow did not have any significant effect on the glycol flow rate on the tube side.

MacLeod [19] performed a test on a full scale model of a shell-and-coil NCHE that consisted of four helical copper coils with inner diameters of 25.4 mm, 41.4 mm, 60.4 mm and 79.5 mm. The coils had vertical orientations made of 6.35 mm outer diameter copper tube, and were placed inside a copper shell of 102 mm diameter. A 40/60 propylene glycol solution was pumped on the tube side, while tap water flowed naturally on the shell side. Results from the experiment showed that the ratio of natural convection mass flow rate to forced convection mass flow rate followed a generally decreasing trend over the course of the experiment.

Xin [20] studied the natural convection heat transfer from helical tubes to air. The three helical coils tested were made of 25.4 mm, 12.7 mm and 12.7 mm tube diameters, with coil diameters of 259 mm, 127 mm, 127 mm and pitches of 62.5 mm, 28.5 mm and 76.0 mm respectively. Two coil turns were used, either five or 10 turns. Results show that natural convection heat transfer from vertical helical coil differs from the vertical array of horizontal cylinders. In the experiment, the heat transfer from the first turn was formed to be the same as for a single horizontal cylinder. Local Nusselt numbers were calculated for horizontal and vertical coils.

Ajele [10] studied the coil and shell NCHE experimentally. Ajele determined that the natural convection heat transfer coefficient was a function of the Rayleigh number and the flow space, which is a dimensionless parameter that accounts for the number of coils inside the heat exchanger shell. The copper tube coil had an outside diameter of 6.35 mm and the pitch was fixed at an average of two tube diameters. The coil diameter varied from 26.8 mm to 88.7 mm. A cylindrical shell of 100 mm inner diameter and 400 mm in height for eleven combinations of one to four coils were tested.

Avian [11] modeled a NCHE in SDHW system and used the empirical correlations for heat transfer from an array of tubes to predict the Nusselt number for the shell-and-coil NCHE. Technical and economical factors were evaluated, and an optimum heat exchanger configuration formed by two coils made of 6.35 mm tube, with inner diameters of 25.4 mm and 44.5 mm and a height of 450 mm, were suggested. Avian showed that heat exchanger height and number of coils appeared to have a strong influence on the overall thermal performance of the heat exchanger.

Fraser [21] presented an empirical model based on experimental data for a commercially available shell-and-coil heat exchanger. Plots of both pressure drop and effectiveness, as a function of water flow rate, were obtained for the heat exchanger and then used as input data for the model. Fraser used standard hydraulic equations to compute the pressure drop in the connected pipes. Fraser also determined the pressure drop in the heat exchanger experimentally by summing the two components. The first component resulted from the drag force extended by the heat exchanger surfaces on the flowing fluid.

Ali [22] performed an experimental investigation of natural convection from vertical helical coiled tubes. The helical coiled tubes made of brass were tested in a tank filled with water. The outer diameters of the two tubes were 8 mm and 12 mm; five coil diameters and five pitches were tested. The coils were made of either 5 or 10 turns and pitches of 1.5 or 4 tube diameters. Ali concluded that the number of coil turns does not affect the heat transfer coefficient.

2.3 Thermal performance of heat exchanger

Conte et al. [23] numerically and experimentally investigated the heat transfer performance of a single round pipe coiled in a rectangular pattern. Steady laminar fluid flow in the bent and straight portion of the coiled pipes were used to find the flow behavior and how it would affect the temperature distribution and heat transfer in the system. The four different straight tubes were inclined at angles of 9º, 15º, 30º and 45º. The calculation on four rectangular coiled pipes was performed using Reynolds numbers of 300; 700 and 1400. The numerical and experimental results showed that coiling a pipe so that an exterior fluid flows over or in tube bundle can help to induce the turbulence without increasing the velocity. It was also reported that the temperature gradient on one side of the pipe wall would increase and the other side would decrease.

Jayakumar [24] performed an experimental and CFD estimation of heat transfer in helical coiled heat exchangers. Experiments were conducted for five different flow rates through the coil and at the helical pipe inlet for three different temperatures. Measurements of the flow rates (hot and cold fluids), inlet and exit temperatures, the heater power input, and the pump were carried out at steady state. They compared the experimental result with predictions using the CFD code Fluent, which showed good agreement within experimental error limits. Empirical correlations were used to estimate the heat transfer and pressure drop in the helical coils to calculate the inner heat transfer coefficient of the helical coil.

Shokonhmand [3] carried out an experimental study of shell-and-coil heat exchangers using Wilson plots, where Wilson plot is a technique to estimate the heat transfer coefficients in several types of heat transfer processes and to obtain general heat transfer correlations. This method is an outstanding tool in practical applications and in laboratory research activities that involve analysis of heat exchangers. They tested three heat exchangers for both parallel-flow and counter-flow configuration. These heat exchangers have different coil pitches and curvature ratios, and Wilson's plot was used to calculate

the overall heat transfer coefficients of the heat exchangers. They reported that the empirical correlations for a constant temperature boundary condition agreed with the present data in the low Dean number region in counter-flow, while these correlations overestimated the results in parallel-flow. The researchers stated that the shell-side heat transfer coefficients of the coils with larger pitches are greater than those with the smaller pitches, and the Nusselt numbers of the smaller and of the counter-flow configuration of the shell-side were less than those of the parallel-flow configuration. Therefore, the overall heat transfer coefficients of the counter-flow configuration were 0-40% more than that of the parallel-flow configuration.

Gupta et al. [25] performed experimental research to determine correlations for designing the coiled finned-tube heat exchangers used in cryogenic applications. The research team developed a cross-counter flow coiled finned-tube heat exchanger that was used in a refrigeration cycle, and carried out the experiment with an effective Reynolds number of 500-1900. The experimental values of the overall heat transfer coefficient for different mass flow rates at different temperature levels were compared with the calculated corresponding values of the overall heat transfer coefficients, and results showed that different correlations chosen in the study can be used for designing the coiled finned-tube heat exchangers with a reasonable degree of accuracy. However, Prabhat recommended that an appropriate method of calculating the free-flow area should be chosen for correct application of these correlations.

Coronel [26] carried out a study to determine the convective heat transfer coefficient in both helical and straight tubular heat exchangers under turbulent flow conditions. They used a method to determine the overall heat transfer coefficient of an industrial helical heat exchanger. The method permits the calculation of the inside and outside convective heat transfer coefficients based on the values of the inlet and outlet temperatures of product and heating medium, flow rate, and the properties of the product. The results of this analysis show that previously published correlations yield similar results to the one obtained by this method. Under turbulent flow conditions, and non-isothermal, non-

constant heat flux conditions, the arithmetic mean temperature of the product was used to calculate its properties, and subsequently in computing Reynolds and Prandtl numbers. The use of the mean temperature allows the calculation of the convective heat transfer coefficients in a similar way to the case of isothermal product.

Gupta et al. [25] investigated the hydrodynamics and heat-transfer characteristics of a coiled flow inverter as a heat exchanger at the pilot plant scale. The researchers performed the experiment in a counter-current mode operation with the hot fluid in the tube side and cold fluid in the shell side, with a Reynolds number range of 1000 to 16,000, using water in the tube side of the heat exchanger while the fluids in the shell side were cooled water or ambient air. Based on the configuration of the coiled flow inverter, pressure drop and the overall heat transfer coefficient were calculated during various process conditions of the tube and shell. Results showed that in the tube side, increases in the Reynolds number for a constant flow rate in the shell side meant the overall heat transfer coefficient increased. An increased overall heat transfer coefficient also occurred for different flow rates in the shell side but with a constant flow rate in the tube. Based on the results, an empirical correlation was developed for the friction factor and heat transfer for the shell side and tube side of the heat exchanger. Gupta et al [25] concluded that for a low Reynolds number the heat transfer was 25% higher, while at higher Reynolds numbers the heat transfer was 12% higher, as compared to the coiled tube data reported in the literature review of Kumar et al. [4]

Hosseini et al. [27] performed experiments to determine the heat transfer coefficient and pressure drop on the shell side of a shell-and-tube heat exchanger for three different copper tubes (smooth, corrugated and micro-fins). In order to investigate the effect of surface configuration on the shell side heat transfer as well as the pressure drop of the three types of tube bundles, the researchers built and modeled a shell-and-tube heat exchanger from oil cooler. Results obtained from their experiment showed that due to the larger surface area of the micro-finned tube, a higher Nusselt number and a higher pressure drop were recorded, while corrugated tubes at the experimental range had lower

Nusselt numbers, but similar pressure drops, comparatively. It was also reported that the experimental results were compared with theoretically available data and correlations to determine both pressure drop and Nusselt numbers for the three tube types.

Fernando et al. [28] developed a mini-channel aluminum tube heat exchanger to evaluate a single phase heat exchanger coefficient by the Wilson Plot method. The researchers successfully applied the Wilson Plot method to determine the heat transfer coefficients in the laminar and transition flow regimes of a liquid-to-liquid heat exchanger. They reported that, for the tube–side of the heat exchanger, experimental average Nusselt numbers for Reynolds numbers in the range $2300 < Re < 6000$ were in good agreement with the average predicted Nusselt numbers of the Gnielinski correlation. The researchers could not give a clear reason why in the laminar flow range the tube-side Nusselt numbers were not well correlated to any of the correlations from the literature or why the experimentally determined Nusselt numbers were considerably lower than expected. It was also reported that the heat transfer coefficients on the shell side were not well predicted from available correlations and the experimental heat transfer coefficients were higher than expected.

Naphon [29] studied the thermal performance and pressure drop of the helical-coil heat exchanger with and without helical crimped fins. Cold and hot water were used as working fluids in the shell and tube sides, respectively, at different flow rates and different inlet temperatures. Naphon [29] reported that for increases in mass flow rate of hot water, the outlet cold water temperature increases. The average heat transfer rate increased as hot and cold water mass flow rates increased. It was also reported that heat exchanger effectiveness was affected by inlet hot and cold water mass flow rates and inlet hot water temperature.

Prabhanjan [30] studied the relative advantage of using a helical coiled heat exchanger over a straight tube heat exchanger for heating liquids. They reported that the particular difference in the study was the boundary conditions for the helical coil, and results showed that the heat transfer coefficient was affected by the geometry of the heat

exchanger and the temperature of the water bath heat exchanger. It was also reported that the helical coil heat exchanger increased the heat transfer coefficient when compared to a similarly dimensioned straight tube heat exchanger. The heat transfer coefficient was not affected by flow rate, because the flow was turbulent and flow rate increase does not change the wall effect significantly.

Gupta [25] designed and optimized coil finned–tube heat exchangers for cryogenic applications. They stated the efficiency of the cryogenic systems strongly depends on the thermal and pressure drop performance of the heat exchangers. Their results showed that the predictions of the four end temperatures from present design methods were compared with the actual experimental results of one of the prototypes, and the possibility of adjusting the thermal and pressure drop performance was completed by varying the clearance. Gupta [25] found that only for a range of mean shell diameter did the shell side pressure drop decrease, while the tube side pressure drop remained nearly constant at the expense of increase in surface area.

Camacho-Duke [31] designed and built five configurations of shell-and-coil immersion heat exchangers to examine the performance of SDHW systems. Camacho-Duke used the heat exchanger *UA*-value to characterize and compare the thermal performance of the heat exchangers. Camacho-Duke concluded that the thermal performance of the heat exchangers was as expected and observed to be a function of storage tank temperatures. As well, the flow rate on the tube side was a function of both the area and heat transfer coefficients outside and inside the tube surfaces.

CHAPTER 3

EXPERIMENTAL SETUP

3.1 Experimental apparatus

The solar domestic hot water system used in this study, consisting of heaters, flow meters, glycol pump, glycol reservoir, piping, thermocouples, data acquisition device, pressure gages, storage tank and the heat exchanger, is described below, with each section focusing on one particular component.

Figure 3.1 is a schematic diagram of the experimental apparatus. A photograph of the experiment is provided in Appendix A, Figure A.3. The working fluid (glycol or water) from the heater to the system is shown with red lines, and the water piping is shown with blue lines. The thermocouple wires and the electrical connection between the power station and the heaters are not shown in Figure 3.1 in order to reduce complexity. All the thermocouple wires were connected to the data acquisition device, and from this point to the CPU for monitoring data.

3.1.1 Auto transformer

An auto transformer CVS manufactured by Sola was used for this experiment setup to provide a constant 240 VAC during the day. The voltage in the electrical grid varied during the day from 220 to 240 VAC depending on how much electricity was used in the building. At night the voltage was close to 240 VAC, but during the day it was considerably less. More details about this auto transformer are presented in Appendix A

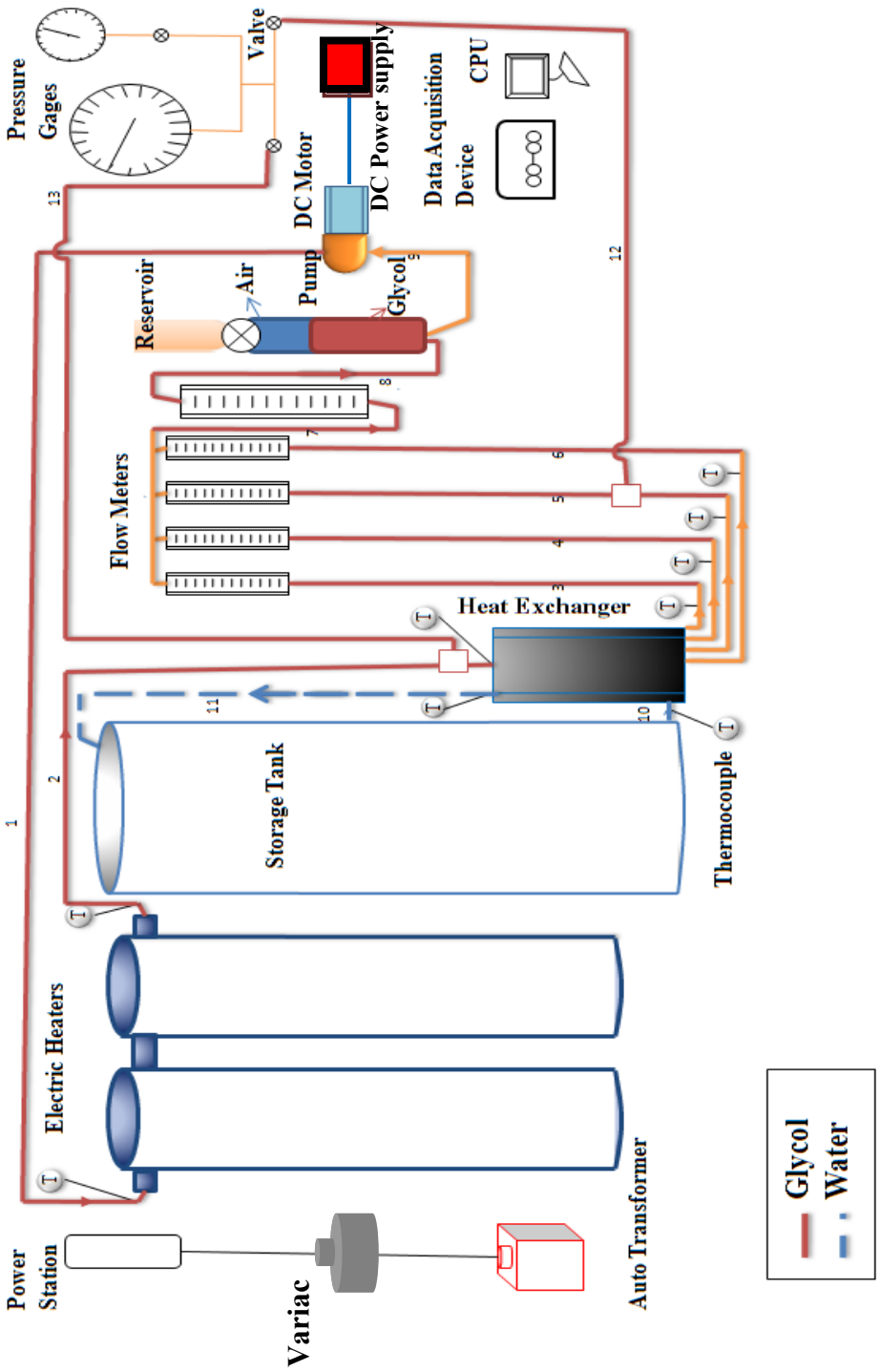

Figure 3.1. Experimental apparatus

3.1.2 Variable transformer (Variac)

A variable transformer, type 136B, was used to vary the output voltage for a steady AC input voltage to the electric heaters. Manually operated units have standard dials graduated 0-100. General and electrical characteristics for the 136B are given in Appendix A.

3.1.3 Heaters

The two heaters simulated two 3 m^2 flat plate solar collectors and performed the function of heating the glycol to the required temperature. These two electric heaters had a power rating of 2500 W at 240 VAC. The heaters were wired in parallel and plumbed in series, and are manufactured by Chromalox Canada. The Variac was used to control the voltage to the heaters.

3.1.4 Flow meters

Four Cole-Parmer 150 mm variable-area flow meters were used (three flow meters for the shell-and-3coils and four for the shell-and–4-coils) to measure the flow rate (glycol solution or water) in the individual coils of the heat exchanger. The calibration of the flow meter was performed by running the glycol solution through each of the flow meters at different rates, while measuring the flow rate was completed by recording the time needed to collect a certain amount of glycol by volume. The flow meters have a ± 2% full scale measuring accuracy. The glycol was a solution of 38% by volume of propylene glycol in water.

A Krohane model G 19.12 flow meter calibrated in GPM, was used to measure the total flow rates of the working fluid in the tube side. 0.01-1.00 GPM was the range of flow measurement for this model. The calibration of the flow meter was performed by running the glycol solution through each of the flow meters at different rates while measuring the flow rate was completed by recording the time needed to collect a certain amount of glycol or water by volume.

The calibration plots are shown in Figure B.1 (D). The linear behavior of the flow meters and the density effects on the flow meters reading were observed. Calculation of the flow rate based on this equation was performed by the computer, depending on the mean temperature of glycol flowing through the flow meter. The temperature effects were accounted for, based on the interpolated results. The equation of the calibration was included in the computer code.

3.1.5 Glycol pump

A brass, positive displacement, sliding-vane type pump, model CO1305AF, with a capacity of 4.4 LPM manufactured by Procon, was used to circulate the glycol solution or water on the tube-side of the SCHX. This pump was driven by a Thermo Dynamics DC electrical motor, model 3A-1402072B with a nominal voltage of 12 VDC and a maximum current of 3 ADC. An Anatek model 50-05S DC power supply was used to control the voltage to the motor.

3.1.6 Glycol reservoir

The glycol solution or water was pumped from a reservoir, circulated through the heater, the heat exchanger, the flow meters and other parts of the loop and back to the reservoir. The reservoir was comprised of a 0.65 liter copper cylinder and filled with a 38% propylene glycol solution, or water.

3.1.7 Piping

In this experiment, four different sizes and two different materials for pipes were used. For the glycol loop, 9.52 mm nylon tubing was used. From the heater outlet to the heat exchanger inlet (tube side) and from the inlet line (reservoir) to the pump 9.52 mm copper tube was used. From the outlet heat exchanger (tube side) through to the reservoir 9.52 mm nylon tube was used.

Two nylon tubes with a diameter of 6.35 mm were used from the outlet heat exchanger on the tube side (low pressure) at coil #3 to the pressure gages and at the inlet of the heat exchange on the tube side to pressure gages, to measure the pressure drop heat exchanger (high pressure). Table 3.1 shows the dimensions and the materials of each pipe in this experiment setup

Table 3.1 Specifications of the pipes

Pipe Number	Location	Material	Outer diameter (mm)	Length (mm)
1	Pump to the electric heaters	Nylon	9.52	1060
2	Electric heaters to HX(tube side)	Copper	9.52	1300
3,4,5&6	Coil #4,3,2 and1 to the flow meters	Nylon	9.52	960
7	Flow meters to the major flow meter	Nylon	9.52	500
8	Major flow meter to	Nylon	9.52	500
9	to the pump	Copper	9.52	550
10	tank bottom to bottom HX(shell side)	Copper	22	80
11	HX(shell side)-top to tank-top	Copper	22	1200
12	Pipe #5 to pressure gages	Nylon	6.35	1000
13	HX-top (tube side) to pressure gages	Nylon	6.35	900

3.1.8 Thermocouples

Copper-constanta (T-type) thermocouples, sizes 26 AWG, were used to measure the temperatures. The insertion type thermocouples, of 3.2 mm diameter, were installed at heater inlet and outlet and at the heat exchanger inlets and outlets (for both shell and each coil) except for the shell outlet, where the wire thermocouple was attached by using aluminum tape. The ambient temperature in the laboratory was measured by using a 4.8 mm thermocouple.

3.1.9 Data acquisition device

A Sciemetric electronic measurement system (Manotick, Ontario), model 8082A, was used as the data acquisition device to measure the voltage differences across the thermocouple leads. The data acquisition device has the following specifications: DC current in the range +/- 4.096 mA with 0.1 μA resolutions, DC voltage in the range +/- 4.096 V with 2 μV resolutions, resistance of up to 1.3 MΩ with 0.5Ω resolution and frequencies with average of 0.03 to 3.8 Hz.

A total of 77 independent input channels were provided, of which 64 were general purpose analog channels; however, only 7 analog channels were used in this experiment. The CPU converts the measured voltage to temperatures as the data acquisition device was connected to a SCIEMETRIC CPU module (model 901). The CPU module also performed the function of continuously reading the temperature over certain periods of time. The communication between the data acquisition CPU and the computer was made via the serial port of the computer. The maximum transmission speed was 9600 bits of data per second (Baud). An Apple Macintosh SE/30 computer was used for monitoring the data. To monitor the measurements, temperature graphs were produced and other calculations such as the heat transfer were computed and a computer code was developed using Microsoft QuickBasic 1.0.

3.1.10 Pressure gauges

In this experiment two different graduation pressure gauges were used to measure the pressure drop of water and glycol from the coil inlet to the outlet of the heat exchanger.

Initially when measuring the pressure drop, the low pressure valve (heat exchanger outlet) was closed and the high pressure valve (heat exchanger inlet) was open. The 0-15 psi pressure gauge was first used, while the valve leading to the smaller pressure gauge (greater graduation range 0-5 psi) was closed. If the reading was less than or equal to 5 psi, the valve was opened and the smaller pressure gauge was used to measure the

pressure drop. If the reading was greater than or equal to 5 psi, the reading was taken from the larger pressure gauge (with less graduation range).

To measure the pressure drop from the coil outlet of the heat exchanger, the high pressure valve was closed and the low pressure valve open and the same process was repeated, between the small and the large pressure gauges .

In the second experiment, glycol was used instead of water and the same process was followed to measure the glycol inlet and outlet pressure drop from the heat exchanger.

Experiments using water and glycol were performed for shell-and-3coil then shell-and-4coil heat exchangers in each case.

3.1.11 Water storage tank

The tank was an insulated tank of 270 liters capacity and model number PR0612T manufactured by Rheem Canada Ltd. Water flows from the bottom of the tank to the heat exchanger then to the top of the tank.

3.1.12 Heat Exchanger

Two different shell and coil heat exchangers were designed and tested for using both glycol and water working fluids in the tube side. The system utilizes a shell-and-coil heat exchanger (SCHX), natural convection heat exchanger (NCHE) manufactured by Thermo Dynamic Ltd (TDL). Both shell-and-3coil (S3CHX) and shell-and-4coil (S4CHX) consist of three and four concentric helical copper coils enclosed in copper shells and are counter flow heat exchangers. For both heat exchangers, a total of 14 (7-each) tests were conducted for the sake of repeatability. Tests runs were performed for this study, based on the design of a vertical coil natural convection heat exchanger. The 38/62 propylene glycol/water came from the heaters and went through the pipe to the heat exchanger inlet. On the tube side forced circulation by the pump transferred the heat to the shell side by

natural convection of the water to the storage tank. These tests were conducted using (i) water and (ii) propylene glycol (38/62) as the working fluid in the tube side.

The heat exchanger was located at ground level, next to the storage tank. A 22 mm diameter and 112 cm long copper tube insulated with flexible elastomeric insulation (Armstrong AP/Armflex) was used to connect the heat exchanger (hot natural convection loop) and the storage tank. A 22 mm diameter, 80 mm length copper tube was used as the connection between the tank (cold natural loop) to the heat exchanger inlet in the shell side.

3.1.12.1 Shell-and-3Coil heat exchanger (S3CHX)

A standard copper water tube, type M, of 3 inches nominal diameter (77 mm) with height of 406 mm, was used for the shell with 2.4 mm thick rectangular copper plates in size of 125 mm length and 112 mm width for each end. The heat exchanger was insulated using 25.4 mm of flexible elastomeric insulation. Figure 3.2 shows the schematic diagram of the S3CHX.

The three tubes used to form the coils, before bending, have inner and outer diameters of 4.83 mm and 6.35 mm respectively. Figure 3.3 depicts the shell-and-3coil with different major and minor axes after bending along the axis of the copper tube in the S3CHX. Coil #1, Coil #2 and Coil #3 represent the inner, second and the outer coils respectively. Table 3.2 shows the dimensions of the three coils, some of which are the mean diameter and elliptical dimensions (major and minor). In the centre of the heat exchanger was a 12.7 mm outer diameter copper tube, running from the top to the bottom.

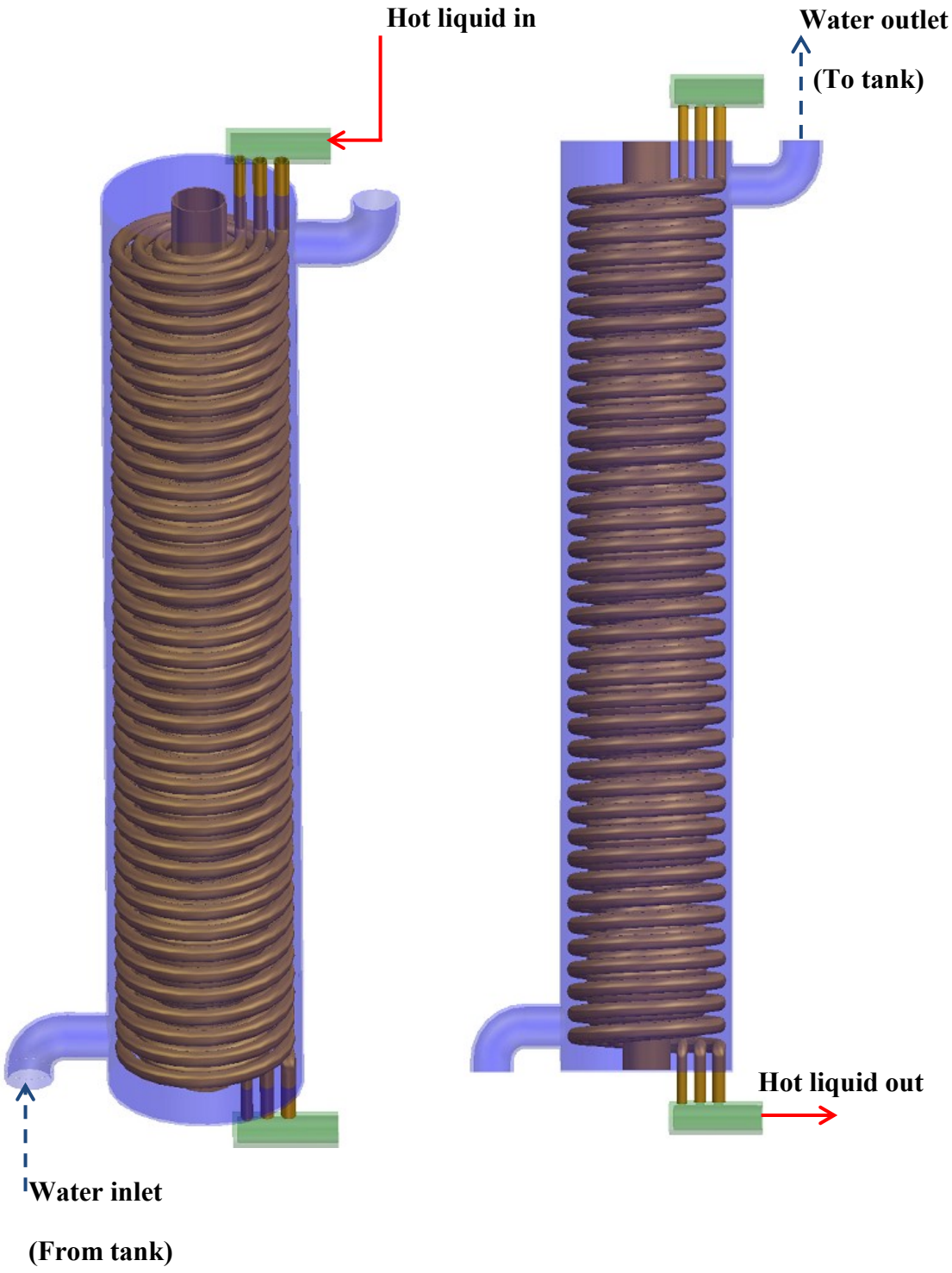

Figure 3.2 Schematic diagram of the S3CHX.

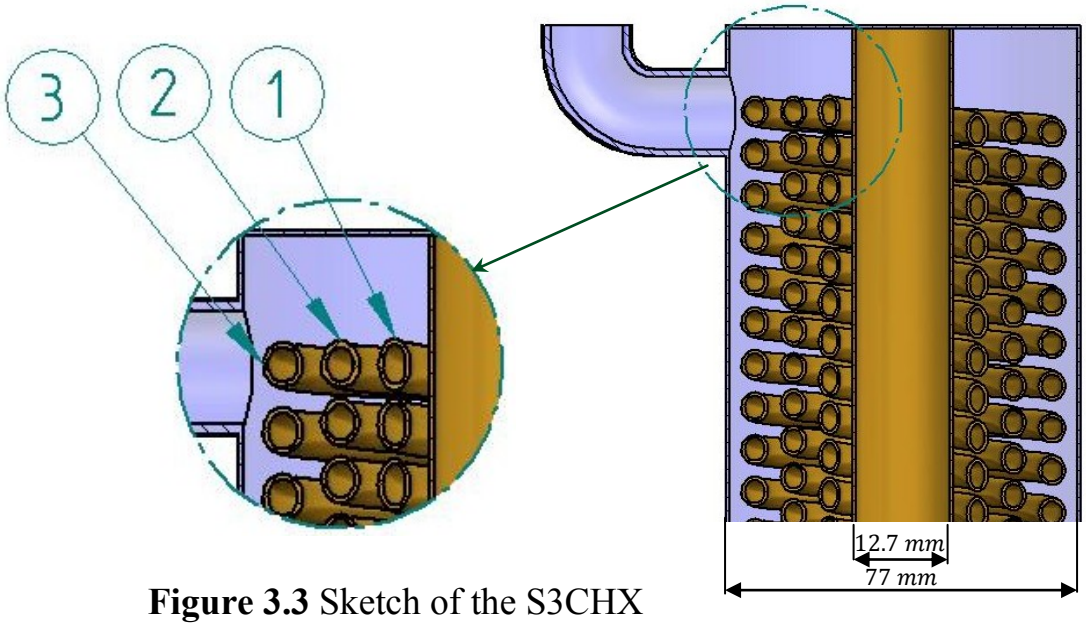

Figure 3.3 Sketch of the S3CHX

Table 3.2 Specifications of S3CHX

Specifications	Coil #1	Coil #2	Coil #3
Major axis, outer, mm	**7.51**	**6.74**	**6.72**
Minor axis, outer, mm	**4.87**	**5.68**	**6.00**
Major axis, inner, mm	**5.99**	**5.22**	**5.20**
Minor axis, inner, mm	**3.35**	**4.16**	**4.48**
Number of turns	**43**	**45**	**39**
Space between tubes, mm	**1.93**	**2.28**	**3.69**
Coil pitch	**1.26**	**1.34**	**1.55**
hyd. diameter, mm	**4.13**	**4.60**	**4.80**
coil mean diameter., mm	**31.6**	**48.6**	**67.6**
coil outer diameter., mm	**36.5**	**54.3**	**73.6**
coil inner diameter., mm	**26.7**	**42.9**	**61.6**

3.1.12.2 Shell-and-4Coil heat exchanger (S4CHX)

The material used in the S4CHX was the same as used in the S3CHX, but the S4CHX used a 4 inch nominal diameter copper water tube for the shell. The shell had a 102 mm inner diameter and was 406 mm in height. Square copper plates with 2.4 mm thick in size of 125 mm length and 125 mm width for each end were used for S4CHX. In the centre of the heat exchanger was a 12.7 mm outer diameter copper tube, running from the top to the bottom. 12.7 mm thick Armstrong AP/Armflex was used to isolate the heat exchanger. Figure 3.4 shows the schematic diagram of the S4CHX.

Inside the shell are 4 concentric vertical helical coils. The tubes used to form the coils, before bending, have inner and outer diameters of 4.83 mm and 6.35 mm respectively. Figure 3.5 shows the sketch of the shell-and-4coil with different major and minor axis after bending along the core of the copper tube in the S4CHX. Coil #1, Coil #2, Coil #3 and Coil #4 represent the inner, second, third and the outer coils from the centre of the core tube respectively. Table 3.3 shows the dimensions of the four formed coils, some of which are the mean diameter and elliptical dimension (major and minor).

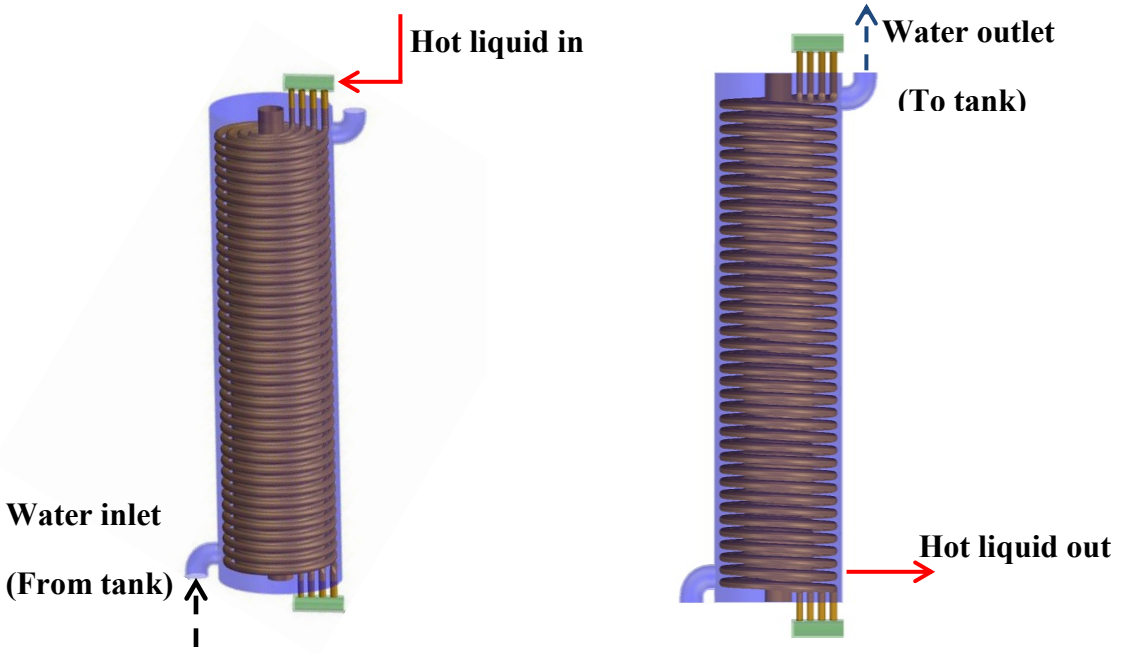

Figure 3.4 Schematic diagram of the S4CHX

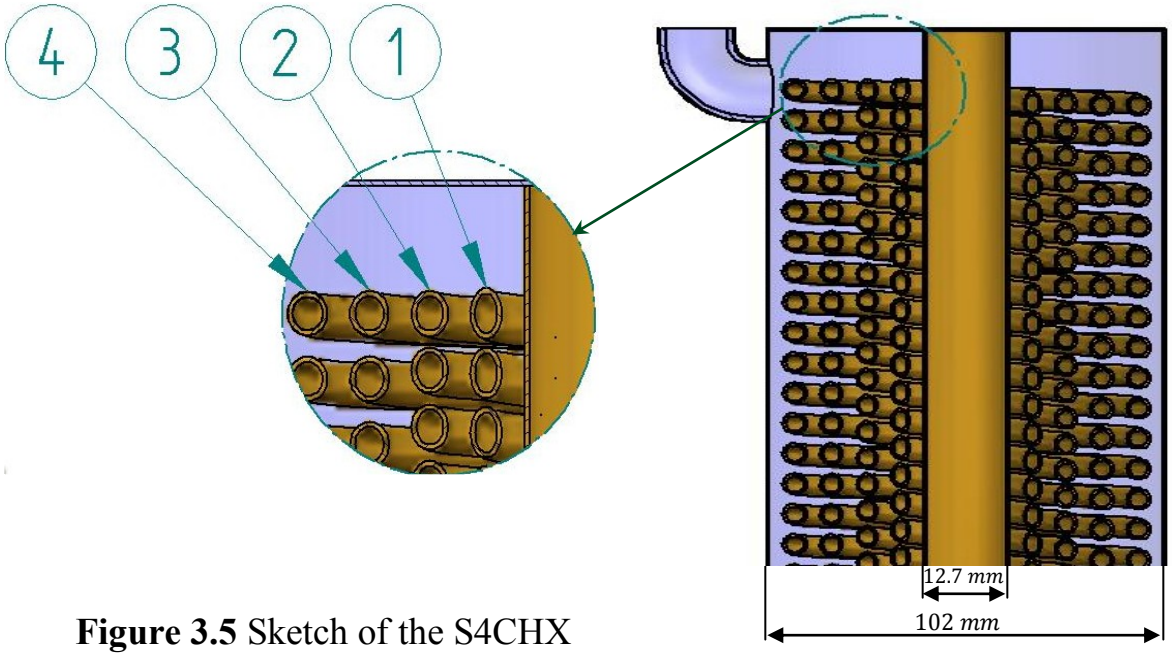

Figure 3.5 Sketch of the S4CHX

Table 3.3 Specifications of S4CHX

Specifications	Coil #1	Coil #2	Coil #3	Coil #4
Major axis outer, mm	**7.51**	**6.74**	**6.72**	**6.55**
Minor axis outer, mm	**4.87**	**5.68**	**6.00**	**6.15**
Major axis inner, mm	**5.99**	**5.22**	**5.20**	**5.03**
Minor axis inner, mm	**3.35**	**4.16**	**4.48**	**4.63**
Number of turns	**43**	**45**	**39**	**36**
Space between tubes, mm	**1.93**	**2.28**	**3.69**	**4.73**
Coil pitch	**1.26**	**1.34**	**1.55**	**1.72**
Hydraulic diameter, mm	**4.13**	**4.60**	**4.80**	**4.82**
Coil mean diameter, mm	**31.6**	**48.6**	**67.6**	**90.6**
Coil outer diameter, mm	**36.5**	**54.3**	**73.6**	**96.8**
Coil inner diameter, mm	**26.7**	**42.9**	**61.6**	**84.5**

3.1.12.3 Clearance between coils for S3CHX and S4CHX

For both the S3CHX and S4CHX, the radial and axial clearances establish a spiral flow path and an axial flow path, which are sized to cause the first fluid to travel in a spiral motion, thus enhancing heat transfer between the first fluid and the second fluid. The clearance between the coils varies from one to another, and the geometric characteristics of the coil are only averagely uniform. Figure 3.6 and Figure 3.7 show the clearances in millimeters for the S3CHX and S4CHX respectively.

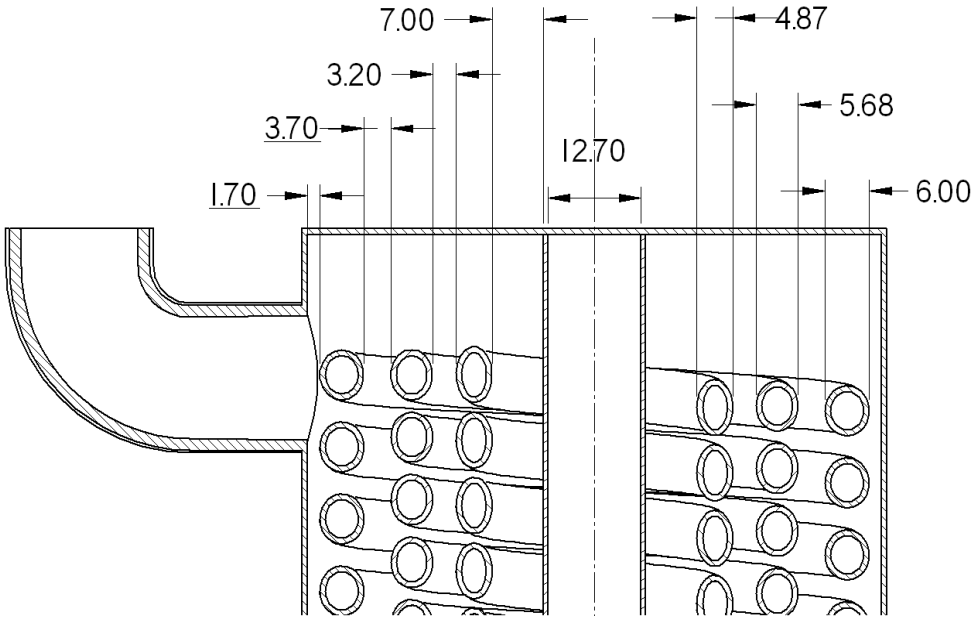

Figure 3.6 Clearances between coils inside S3CHX

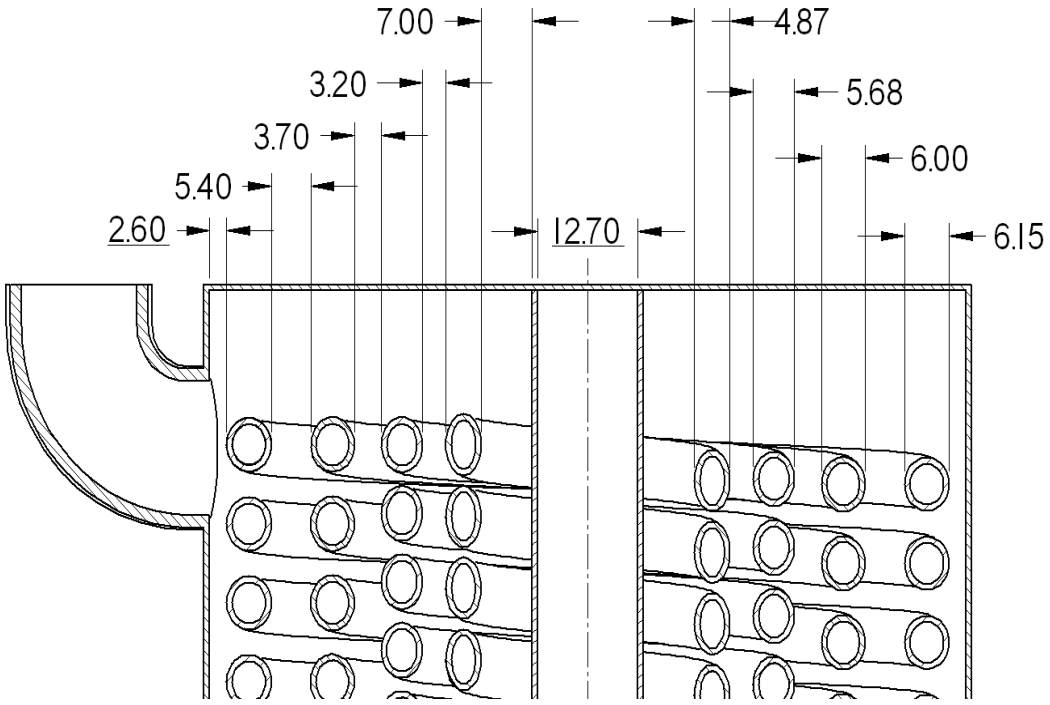

Figure 3.7 Clearances between coils inside S4CHX

CHAPTER 4

EXPERIMENTAL PROCEDURE AND ANALYSIS

4.1 Experimental Procedure

The experimental procedure was initiated after assembling the equipment: the shell-and-coil heat exchanger, two heaters connected in parallel, DC motor, pump, storage tank, reservoir, piping, flow meters, pressure gages, thermocouples attached in different locations of the system, data acquisition to collect data that can be manipulated by a computer, and a Mac computer to collect the data from the data acquisition. All experiments were conducted at the Solar Thermal Laboratory located at Dalhousie University, Halifax, NS, Canada.

4.1.1 Test Description

The tests began after determining the functionality of each heat exchanger configuration by carrying out heat transfer and pressure drop calculations. The heat exchanger was insulated and installed close to the storage tank to avoid heat losses. The storage tank was filled with water from the water supply. Adjustments were made to ensure the system worked properly. Threaded connectors and sealant were used on the heat exchanger and heaters to avoid leaks. Thermocouples were attached at the inlet and outlet of the heat exchanger (shell and tube side) and the heater to measure the temperatures. Pressure relief valves were attached at the heaters inlet and at the top of the tank to protect from high pressure and to remove the air from the system. All piping was installed and insulated except the outlet pipes from the heat exchanger (tube side). The pump was turned on and water filled the reservoir to check for leaks.

4.1.2 Test procedure

The first step to collect the data from the system was to operate the heaters and the pump. The flow rates were based on experimental data obtained from a sunny day from a real system. The experiment was carried out based on the data obtained from Figure 4.1, on Feb. 8, 2001 because it was a sunny day and heat transfer up to 3000 W was recorded compared to Figure 4.2 and Figure 4.3 for the experimental results obtained on June 2, 1998 and June 7, 1998 respectively, that recorded a maximum heat transfer of 2600 W and 2450 W respectively. In order to study the thermal performance of the heat exchanger at higher heat transfer, 3000 W was used for the experiment.

The test was initiated by adjusting the Variac to supply 200 W of power to the electrical heaters. Every 30-45 minutes the wattage was increased to the following levels: 500, 1000, 1500, 2000, 2500 and 3000 W. 3000 W was chosen as the maximum value for heat transfer rate (*q-hx*) because it was the highest value for the solar collector as seen in Figure 4.1. The DC power to the solar pump was adjusted based on the flow rates of 0.90, 1.17, 1.56, 1.86, 2.06, 2.17 and 2.20 LPM respectively. The flow was varied because the greater the solar flux, the greater the power to the pump and that lead to the greater thermal energy in the solar collector and increasing the heat transfer rate. Data at the 200 W levels was ignored due to the fluctuations experienced in the results obtained during the adjustment of the solar pump. The power levels and corresponding flow rates are shows in Table 4.1

Table 4.1 Flow rates at particular heat transfer values

***q-hx* (W)**	**Flow rate (LPM)**
200	0.90
500	1.17
1000	1.56
1500	1.86
2000	2.06
2500	2.17
3000	2.20

Figure 4.1 presents the result of the experimental data for the glycol flow rate on Feb 8, 2001, which illustrates the flow rate for the glycol versus the heat transfer rate of the heat exchanger on that date. The higher the heat transfer, the higher the flow rate, the higher flow rate the higher the efficiency, and greater the temperature change. On a typical sunny day the solar flux on the solar collector increases from sunrise until noon then decreases till sunset, while the pump is powered by a PV module. Based on this experimental data, the mass flow rate was increased, and also the heat transfer for the heaters was increased for the experiment as set out in Table 4.1.

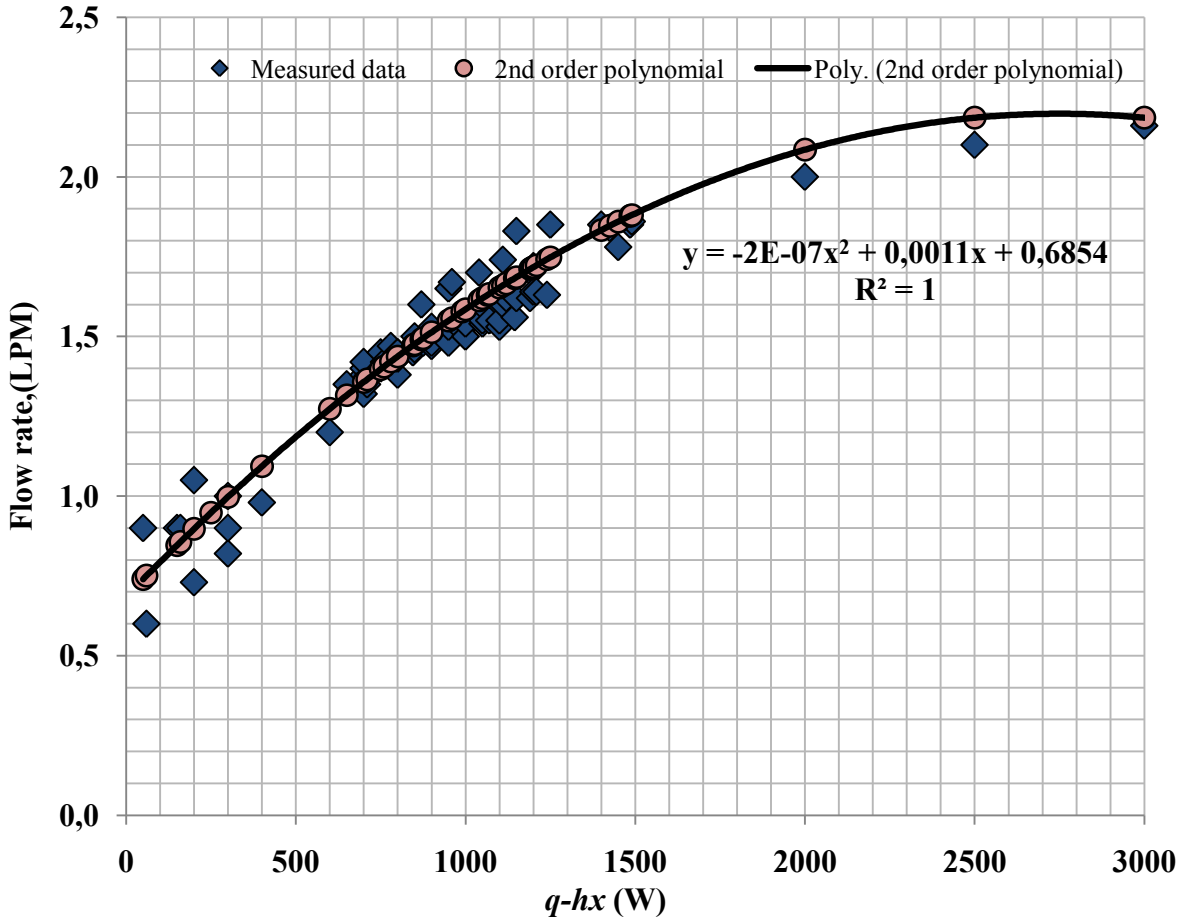

Figure 4.1 Experimental data for flow rate on Feb. 8, 2001

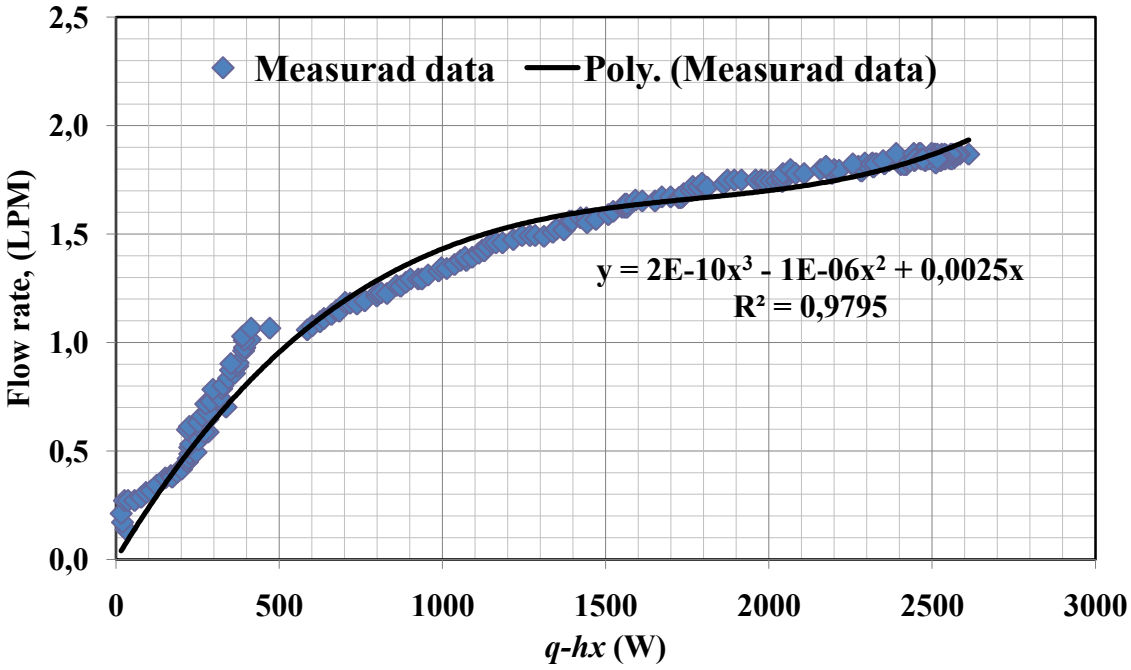

Figure 4.2 Experimental data for flow rate on June 2, 1998

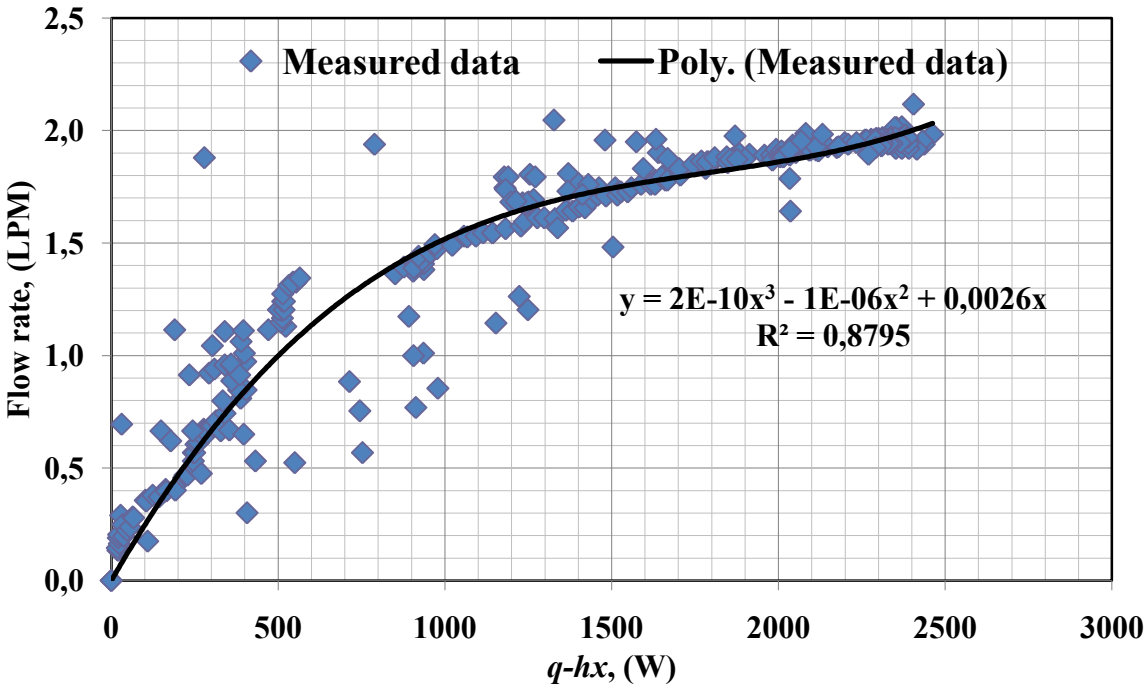

Figure 4.3 Experimental data for flow rate on June7, 1998

A Macintosh computer was used to monitor the data from the system. Code was developed using Microsoft QuickBasic 1.0. This code monitored:

1. Data temperatures on the screen. According to the information received from the data acquisition CPU device, temperatures were constantly updated. It took 13 second to complete one cycle of reading.
2. Heat transfer parameters based on the equations in the program.

4.2 Analysis

To study the heat transfer and fluid flow in the shell-and-coil heat exchangers there are some considerations inside the shells and coils. Only important parameters were presented that are relevant to the thermal performance of shell-and-coil heat exchanger configurations. The thermal performance of the heat exchanger can be expressed by its effectiveness, and the overall heat transfer coefficient.

The overall performance of a SDHW system depends upon many interdependent variables. An evaluation of heat exchangers for use in solar systems must include a measure of how well such configuration performs within the context of the system as well as the analysis of a specific configuration as an isolated unit.

4.2.1. Heaters Performance

Based on the actual solar collector data for a peak of 3000 W for a sunny day, electrical heaters of approximate rating 5000 W were used for the experimental set-up (5000 W at 240 VAC).

The heaters were plumbed in series; however, they were wired in parallel as shown in Figure 4.4 with a total electric resistance of 12 Ω.

$$\text{Electric Power } P = I(current) \times V(Voltage) \qquad [4\text{-}1]$$

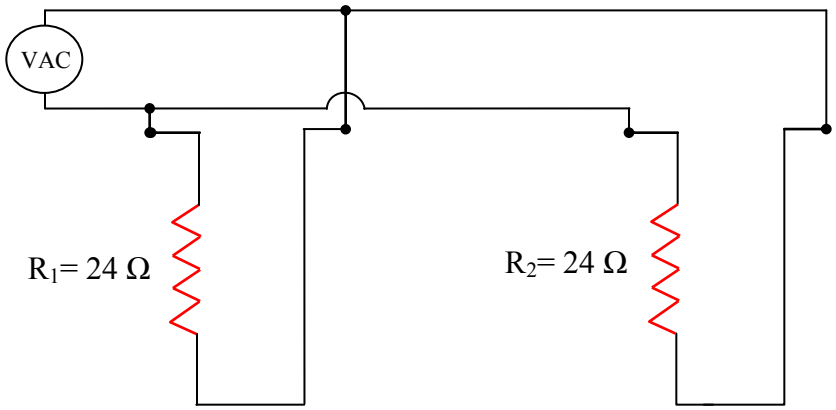

Figure 4.4 Electric diagram of two electric heaters

$$R_{Total} = \left(\frac{1}{R_1} + \frac{1}{R_2}\right)^{-1} \quad [4\text{-}2]$$

Where,

R_{Total} = Total resistance of the heaters

$$R_{Total} = \left(\frac{1}{24} + \frac{1}{24}\right)^{-1} = 12\ \Omega$$

$$P = \frac{V^2}{R} \quad [4\text{-}3]$$

The 2.5 kW at 240 V was not enough to simulate a 3 kW solar collector array. By choosing 2 electrical heaters the maximum electrical power is:

$$P = \frac{(240)^2}{12} = 4800\ W$$

190 volt was the voltage required to meet the requirement of wattages (3000 W).

$$P = \frac{(190)^2}{12} = 3008\ W$$

For experimental purposes it is important to determine the heat losses to obtain reasonable result. These losses vary from one system to another and it depends on factors

such as quality of insulation, piping layout and location. With all those variables fixed, the type and locations of the heat exchangers employed becomes critical.

4.2.2 Heat Exchanger Performance

For an external shell-and-coil heat exchanger, the absence of free velocity requires use of a mean internal flow, the absence of a fixed free stream temperature necessitates using a mean temperature. For designing or predicting the performance of a heat exchanger, it is essential to relate the total heat transfer rate to quantities, for example, the total surface area for heat transfer, inlet and outlet fluid temperatures and the overall heat transfer coefficient.

The thermal performance of the heat exchangers was quantified by the overall heat transfer coefficient-area product, *UA*-value. Generally, the heat transfer rate in the heat exchanger on the tube side can be expressed by measuring quantities using equation [4-4].

$$q_{hx} = \dot{m}_{(w,g)} c_{p(w,g)} (T_{hi} - T_{ho}) \quad [4\text{-}4]$$

Where,

q_{hx} is the heat transfer rate for the heat exchanger (W),

$\dot{m}_{(w,g)}$ is the water or glycol mass flow rate on the hot side (kg/s),

$c_{p(w,g)}$ is the water or glycol specific heat (J/kg·K),

T_{hi} is the temperature heat exchanger inlet on the hot side (℃)

T_{ho} is the temperature heat exchanger outlet on the hot side (℃)

The heat transfer rate is calculated using equation [4-5] using either glycol or water information when glycol used as the working fluid on the tube sides.

$$q = \left(\dot{m} c_p\right)_g \Delta T_g = \left(\dot{m} c_p\right)_w \Delta T_w \quad [4\text{-}5]$$

The proportionality between the overall thermal conductance of the heat exchanger, U, the total surface area for heat transfer, A, and total heat transfer rate, q_{hx}, is expressed by equation [4-6].

$$UA = \frac{q_{hx}}{\Delta T_{lm}} \quad [4\text{-}6]$$

Where,

UA is the overall heat transfer coefficient-area product for the heat exchanger (W/K),

ΔT_{lm} is the log mean temperature difference between the working fluid on the tube side and the fluid on the shell side.

Equation [4-6] is an extension of Newton's law of cooling. It relates the total heat transfer rate to the temperature difference between the two working fluids, shell and tube sides. Once the heat transfer is known, an appropriate form for $\Delta T_{lm,}$ i.e., one that reflects the variation of local temperature difference with position in the heat exchanger, is required for common arrangements, e.g., for counterflow heat exchangers, the appropriate ΔT_{lm} is well-known in many textbooks and publications as the log-mean temperature difference,

$$\Delta T_{lm} = \frac{\Delta T_1 - \Delta T_2}{ln\left(\Delta T_1 / \Delta T_2\right)} \quad [4\text{-}7]$$

Where,

$\Delta T_1 = T_{hi} - T_{co}$

$\Delta T_2 = T_{h,o} - T_{ci}$

And where,

T_{co} is the temperature water outlet from the heat exchanger (cold side)(℃).

T_{ci} is the Temperature water inlet to the heat exchanger (cold side)(℃).

The inlet and outlet for both side (shell and coil) are shown in shell-and-4coil heat exchanger in Figure 4.5

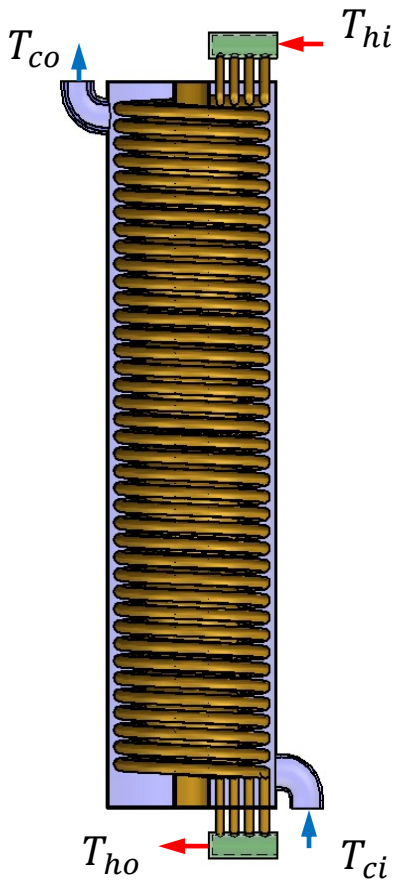

Figure 4.5 Inlets and outlets shell-and-coil heat exchanger

For the counterflow heat exchanger, the hot and cold fluid temperature distributions are shown in Figure 4.6. This configuration for this heat exchanger provides for transfer between the hotter portions of the two fluids at one end, likewise between the colder portions at the other, that is why the temperature difference, $\Delta T=T_h-T_c$ changes with respect to x. The outlet temperature of the cold fluid may exceed the outlet temperature of the hot fluid. Incropera [32]

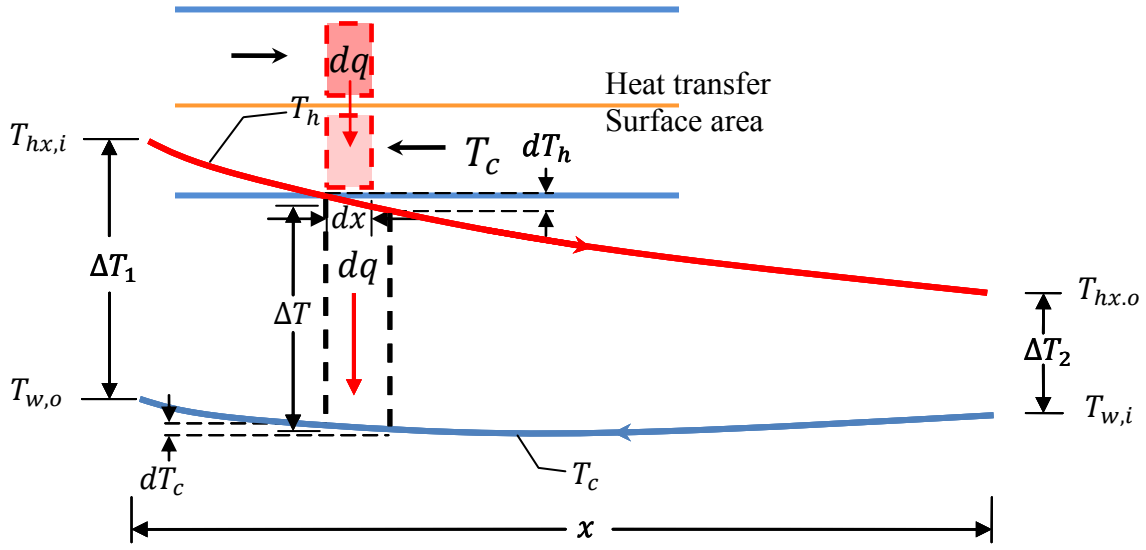

Figure 4.6. Temperature distributions for a shell-and-coil heat exchanger

The mechanism of the heat exchanger simply transfers the heat from one fluid to another. Viscosity is the quantity that describes a fluid's resistance to flow. Fluids resist the relative motion of immersed objects through them as well as to the motion of layers with differing velocities within them. The fluid that has a higher temperature has a lower viscosity so, as the temperature goes up the viscosity goes down. The relationship between the temperature and the viscosity of this agreement is provided in Appendix B from the experimental data (propylene glycol).

For each coil, knowing the tube side heat transfer coefficient, h_i, (see section 4.2.4.1) and the overall heat transfer coefficient, UA, (see equation [4-6]) the shell side heat transfer coefficient, h_o, can be determined using equation [4-8].

$$\frac{1}{UA} = \frac{1}{h_i A_i} + \frac{ln(d_o/d_i)}{2\pi kL} + \frac{1}{h_o A_o} \qquad [4\text{-}8]$$

Where,

$$(A_i)_n = \pi(D_i L)_n \quad [4\text{-}9]$$

$$(A_o)_n = \pi(D_o L)_n \quad [4\text{-}10]$$

And where,

D_i is the inner diameter of the tube

D_o is the outer diameter of the tube

$L_1,\ L_2, L_3 and\ L_4$ are the lengths of coil 1, 2, 3 and 4 respectively

n = 1, 2, 3

or n = 1, 2, 3, 4

The thermal resistance, $\frac{ln(d_o/d_i)}{2\pi kL}$, of the tube walls for tubes made from high thermal conductivity materials can be neglected. However, in this research the thermal resistance of the tube has been neglected.

The total overall heat transfer coefficient for the heat exchanger is the summation of the overall heat transfer coefficient for each coil, for example the overall heat transfer coefficient for the S4CHX is presented in equation [4-11].

$$UA = (UA)_{coil\ \#1} + (UA)_{coil\ \#2} + (UA)_{coil\ \#3} + (UA)_{coil\ \#4} \quad [4\text{-}11]$$

4.2.3 Error detection and correction

During the course of the experiments it was observed that the performance of the heat exchangers was affected by some independent variables, such as temperature, inlet and outlet and mass flow rate for the shell side and tube side of the heat exchanger. It was observed that the flow meter was not reading accurately based on the results obtained from the preliminary tests. This section describes the correlation used in solving the problem.

The heat loss from the heat exchanger loop, Δq, is presented in equation [4-12] for the S3CHX and equation [4-13] for the S4CHX. These equations were used to determine the actual heat transfer (q_{act}), which are presented in equation [4-14] for both heat exchangers

$$\Delta q = 6.3(T_{ave} - T_{lab}) \quad [4\text{-}12]$$

Where,

T_{lab} is the laboratory temperature while running the experiments. It was 21.0℃ for the S3CHX and was 24.4 ℃ for the S4CHX as recorded from the thermocouple.

T_{ave} is the average temperature of the inlet and outlet hot fluid on the tube side.

$$\Delta q = 6.3 \times T_{ave} - 154 \quad [4\text{-}13]$$

The actual heat transfer in the heat exchanger is

$$q_{act} = q_{elec} - \Delta q \quad [4\text{-}14]$$

Since the flow meter was not reading properly, the actual mass flow rate used is represented by equation [4-15]

$$\dot{m}_{act} = \dot{m}_{meas} \times R \quad [4\text{-}15]$$

And,

$$R = \frac{q_{elec} - \Delta q}{q_{hx,meas}} \quad [4\text{-}16]$$

Where,

q_{elec} is the heat transfer rate from the electric heaters (W)

Δq is the heat loss from the heat exchanger loop defined as

n= 1, 2, 3 and 4 for the four coils

$\dot{m}_{act}$ is the actual mass flow rate (LPM)

$\dot{m}_{meas}$ is the mass flow rate measured (LPM)

$q_{hx3c,meas}$ is the heat transfer for the 3 coils, and $q_{hx4c,meas}$, for the S4CHX

Where,

$q_{hx,meas}$ for each coil represent in equation [4-17]

$$q_{hx,meas} = \dot{m}_{meas} c_p \Delta T \quad [4\text{-}17]$$

Where,

c_p is the specific heat for the glycol or water (J/kg. K)

$$\Delta T = T_{hi} - T_{ho} \quad [4\text{-}18]$$

Where,

T_{hi} is the temperature fluid inlet on the tube side.

T_{ho} is the temperature fluid outlet on the tube side.

In order to obtain the actual mass flow rate of the glycol, the flow meter was calibrated because of the discrepancies experienced in the flow.

Two tests were performed with the S4CHX-G and results obtained are shown in Tables B.1 and B.2 in Appendix B for test #1 and test #2 respectively. The results were plotted as shown in Figure B.1 (D) in appendix B, which is the calibration equation [4-19] generated based on the result of the two tests performed.

$$R = -2.41 \times GPM^2 + 2.61 \times GPM + 0.159 \quad [4\text{-}19]$$

This equation was input to the computer program, which was used to correct the discrepancies experienced in the flow meter, as readings obtained from the flow meter were corrected by the computer program using the equation to obtain the actual value of the glycol mass flow rate, $\dot{m}_{act}$, value in the S4CHX-G for all the 4 tests conducted.

This computer program using the calibration equation was also used to find the actual mass flow rate of glycol for the 4 tests conducted in the S3CHX-G, since the discrepancies only affected the flow meter not the heat exchanger.

4.2.4 Shell-and-coil heat transfer coefficients

As an experimental method is employed in this study, theoretical models (see Appendix C.2) were developed to validate the experimental results. Based on experimental data, a computer program calculated the inside heat transfer coefficient (h_i) the outside heat transfer coefficient (h_o) based on forced water flow and proportioning water flow over the coils, (h_o) for each coil, assuming natural convection only and calculated *UA*-value for each coil and (*q*-*hx*) for each coil. The heat transfer coefficients used for this study consists of 3 and 4 concentric vertical coiled tubes within cylindrical shells. On the tube side is a forced flow while natural convection occurs on the shell side.

4.2.4.1 Calculation of heat transfer coefficients inside the coils (h_i)

The heat transfer coefficient inside the tube (h_i) is an important factor in any convection problem. The heat transfer inside a helical coil is always greater than in a straight tube heat exchanger and that fact is due to the secondary flow caused by centrifugal forces as shown in Figure 4.7

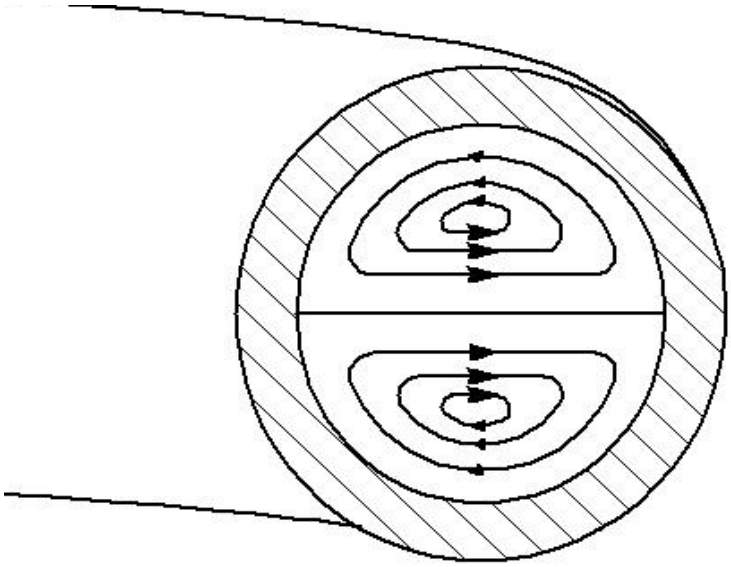

Figure 4.7 Secondary flow inside helical coils

The heat transfer coefficients, *h*, originated with Newton's law of cooling, and it depends on a material's physical properties and also depends on fluid condition and geometry when passing over a surface. The Nusselt number is the dimensionless form of the heat transfer coefficient.

Ajele[10] and Taherian [2] investigated the heat transfer within helical coils experimentally and numerically. They conducted experiments with shell-and coil heat exchangers similar to the one used for this study, and found that the experimental correlation presented by Manlapaz and Churchill [33] was appropriate for the conditions of glycol and water flow. Equation [4-20] was used to calculate the Nusselt number in this research.

$$Nu_i = \left[\left(4.364 + \frac{4.364}{X3}\right)^3 + 1.816\left(\frac{De}{X4}\right)^{1.5}\right]^{0.333} \quad [4\text{-}20]$$

Where $X3$ is defined as,

$$X3 = \left(1 + \frac{1342}{(De^2 \times Pr)}\right)^2 \quad [4\text{-}21]$$

And $X4$ is defined as,

$$X4 = \left(1 + \frac{1.15}{Pr}\right) \quad [4\text{-}22]$$

Where, Pr is the Prandtl number. The Dean number, De, is a dimensionless group in fluid mechanics, which occurs in the study of flow in curved pipes and channels, and is defined as

$$De = Re_D \left(\frac{D_{hi}}{D_c}\right)^{0.5} \quad [4\text{-}23]$$

Where D_{hi} is the hydraulic tube inner diameter and is defined in equation [4-24]

$$D_{hi} = \frac{a_{in}\, b_{in}}{\sqrt{\frac{a_{in}^2 + b_{in}^2}{2}}} \quad [4\text{-}24]$$

Figure 4.8 shows the major axis inner diameter, a_{in}, minor axis inner diameter, b_{in}, major axis outer diameter, a, and minor axis outer diameter, b.

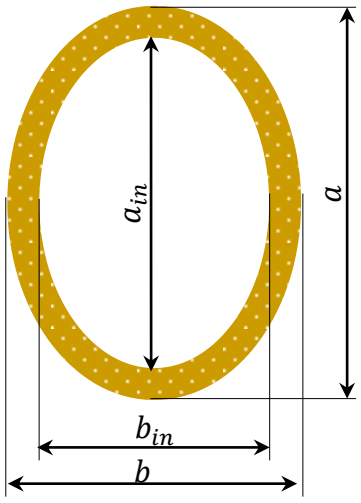

Figure 4.8 Major and minor tube diameters

The Reynolds number, Re is given by

$$Re_D = \frac{\rho\, D_{hi}\, u_m}{\mu} \quad [4\text{-}25]$$

Where ρ and μ are the density and the dynamic viscosity of the fluid inside the tubes and u_m is the mean velocity of the flow.

$$u_m = \frac{\dot{m}}{\rho\, A_C} \quad [4\text{-}26]$$

Where,

$$A_c = \frac{\pi\, a_{in} b_{in}}{4} \quad [4\text{-}27]$$

Where A_C is the cross-sectional area of the tube and $\dot{m}$ the mass flow rate of the fluid flow in the tube.

The Nusselt number is obtained by applying the correlation of Manlapaz and Churchill as stated in equation [4-20]. The heat transfer coefficient inside the tube, h_i, follows from the Nusselt number.

$$h_i = \frac{Nu_i\, k}{D_{hi}} \quad [4\text{-}28]$$

k is the thermal conductivity of fluid (glycol solution or water)

4.2.4.2 Calculation of heat transfer coefficients outside the coils (h_o)

Natural convection is caused by buoyancy forces due to density differences caused by temperature variations in the fluid. A fluid is heated, the density changed will cause the fluid to rise and be replaced by cooler fluid that also will be heated and rise. Figure 4.9 shows the natural fluid flow on the shell side. The heat transfer coefficient on the tube side (h_i) will be used to calculate the heat transfer coefficient on the shell side (h_o), using equation [4-8].

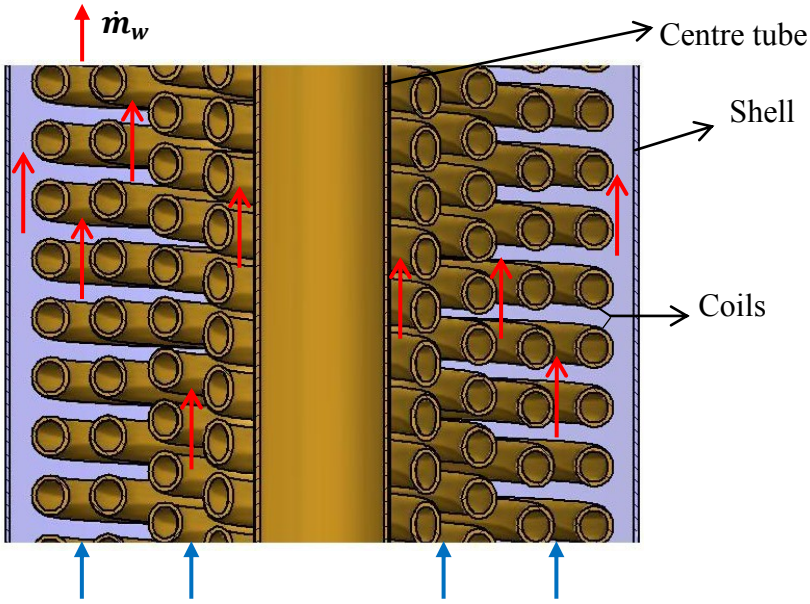

Figure 4.9 flow rate on the shell side of the heat exchanger

The energy balance equation governing the two fluids streams in the shell-and-coil heat exchanger is

$$q_{hx} = (\dot{m}\, c_p)_h (T_{hi} - T_{ho}) = (\dot{m}\, c_p)_c (T_{co} - T_{ci}) \qquad [4\text{-}29]$$

By knowing the heat transfer rate, the *UA*-value, is then found using equation [4-6]. Knowing the tube side heat transfer coefficient, h_i, and the overall heat transfer coefficient, *UA*-value, the shell side heat transfer coefficient, h_o, can be determined using equation [4-8].

$$h_o = \left\{ A_o \left(\frac{1}{UA} - \frac{1}{h_i A_i} \right) \right\}^{-1} \qquad [4\text{-}30]$$

For the mathematical model there are two methods to calculate the heat transfer coefficient outside the tube, h_o.

The first method is based on forced water flow and proportioning the water flow over the coils. The velocity on the shell side over each coil can be calculated.

In calculating the heat transfer coefficient h_o, based on forced water flow, the empirical correlation due to Hilpert was applied Incropera [32].

$$Nu_{Df} = CR_e{}^m Pr^{1/3} \quad [4\text{-}31]$$

For, $Re_D < 40$ $\quad C = 0.911, m = 0.385$

And for, $Re_D > 40$ $\quad C = 0.683, m = 0.466$

Where,

Nu_{Df} is the Nusselt number for the forced flow over a cylinder, in cross flow.

Re_D is Reynolds number.

$$Re_D = \frac{\rho\, D_{ho}\, V}{\mu} \quad [4\text{-}32]$$

Pr is the Prandtl number

$$h_{ocf} = \frac{Nu_{Df} k}{D_{h,o}} \quad [4\text{-}33]$$

Where,

h_{ocf} is the heat transfer coefficient for forced flow on the outside for each coil

D_{ho} is the hydraulic tube outer diameter. See Figure 4.8

$$D_{ho} = \frac{ab}{\sqrt{\frac{a^2 + b^2}{2}}} \quad [4\text{-}34]$$

The calculation of h_o for each coil can also be based on the assumption of natural convection only. The calculation of the heat transfer coefficient h_o was based on the Rayleigh number when considering natural convection. Equation [4.35] presents the Nusselt number for the natural convection over the coils Incropera [32].

$$Nu_{DX} = 0.48 {Ra_D}^{1/4} \quad [4\text{-}35]$$

Rayleigh number,

$$Ra_D = \frac{g\beta}{\vartheta\alpha}(T_{msoc} - T_{mw})D_{ho}^3 \quad [4\text{-}36]$$

Where, g is the acceleration due to gravity (9.8 m/s^2)

β is the thermal expansion coefficient for water

ϑ is the kinematic viscosity for water

α is the thermal diffusivity for water

T_{msoc} is the mean temperature on the outside surface of the coil. (°C)

T_{mw} is the mean water temperature in the heat exchanger. (°C)

$$h_{oc} = \frac{Nu_{DX}k}{D_{h,o}} \quad [4\text{-}37]$$

h_{oc} is the heat transfer coefficient for natural convection on the outside of each coil.

The forced flow method appears to be more accurate, because the flow of water is virtually forced by a natural convection system and that natural convection system is the chimney. The chimney works as an external pump, forcing the flow. In the tube (chimney), the flow was driven by the variation of the fluid density as a result of the temperature differences, so it was used for calculating h_o. The models for calculating $h_{o,}$ for both S3CH-X and S4CH-X are presented in Appendix C2.

Ajele[11] and Taherian[8] found that the heat exchanger hydraulic diameter, D_{hx} as the characteristic length presented in equation [4-38] was the most appropriate length scale for vertical SCHX natural convection heat exchangers

$$D_{hx} = \frac{4\,A_{c,f}H}{A_P} \quad [4\text{-}38]$$

Where $A_{c,f}$ is the cross sectional area perpendicular to the flow on the shell side, H is the shell height and A_P is the wetted surface area on the shell side of the heat exchanger, and it is given by the sum of the total outside surface area of the coils and the total inner surface area of the shell.

A_P and $A_{c,f}$ are defined in equation [4-39] and [4-40] respectively

$$A_p = A_o + A_S = \pi\, D_o L + \pi\, D_S H \quad [4\text{-}39]$$

Where D_o is the outer diameter of the tube and L is the total length of the tubes (sum of the tube lengths for the three coils or the four coils). D_S is the shell diameter

$$A_{c,f} = \frac{\pi\left({D_S}^2 - {D_{eq}}^2\right)}{4} \quad [4\text{-}40]$$

Where D_{eq} is the equivalent diameter and can be used as a measure of combined diameter of all coils. D_{eq} can be defined in equation [4-41] to combine all the coils together and produce an imaginary solid ring with its cross sectional area and that equal to the sum of the cross sectional area of the all coils.

$$D_{eq} = \sqrt{\sum_{j=1}^{N}\left({D_{c,o}}^2 - {D_{c,i}}^2\right)_j} \quad [4\text{-}41]$$

Where N is the number of coils, $D_{c,o}$ is the outer diameter of the coil and $D_{c,i}$ is the inner diameter.

Ajele[11] developed a correlation for the shell side Nusselt number presented in equation [4-42]

With Rayleigh number (see equation [4-43]).

$$Nu_{Dhx} = 0.53\frac{\left[Ra_{Dhx}\left(\frac{H}{L}\right)\right]^{0.33}}{S'} \quad [4\text{-}42]$$

$$Ra_L = \frac{g\beta\Delta TL^3}{\vartheta\alpha} = \frac{g\beta(T_{m,w} - T_\infty)L^3}{\vartheta\alpha} \quad [4\text{-}43]$$

Where S' is the dimensionless flow apace and it is a parameter defined by Ajele [11] for multiple coils with equivalent diameter D_{eq} within a shell diameter $D_{s,o}$.

$$S' = \frac{D_{s,o} - D_{eq}}{D_{eq}} \quad [4\text{-}44]$$

In equation [4-43] the temperature difference is defined as the difference between the bulk fluid and the adjacent wall. ($T_{m,w}$) is the mean temperature of the water inside the heat exchanger and (T_∞) is the water temperature at the inlet to the heat exchanger.

The heat transfer rate in equation [4-4] was used to calculate the heat transfer coefficient on the shell side, h_o, and the *UA*-value as stated in equations [4-45] and [4-6] respectively. ($T_{m,s}$) in equation [4-45] is the mean coil surface temperature.

$$h_o = \frac{q}{A\left(T_{m,s} - T_{m,w}\right)} \quad [4\text{-}45]$$

CHAPTER 5

RESULT AND DISCUSSION

Reliable results are obtained by calculating at least at two performance parameters of the heat exchanger, the pressure drop and the overall heat transfer coefficient. Two heat exchangers were analyzed and compared. The performance of the heat exchangers is expressed in terms of the overall heat transfer coefficient-area product (*UA*-value) and pressure drop. Using water and glycol as the working fluid on the tube side of both heat exchangers, four models were compared with the experimental data and plotted to predict the *UA*-values for both glycol and water for both the shell-and-3coil and shell-and-4coil heat exchangers.

5.1 Shell-and-coil heat exchanger performance results

5.1.1 Shell-and-3coil heat exchanger (S3CHX-W)

Figure 5.1 shows the relationship between the heat exchanger heat transfer rate, *q-hx*, and the *UA*-value for the shell-and-3coil heat exchanger using water as the working fluid on the tube side (S3CHX-W**)**. These values represent two tests. The *UA*-value for all heat exchangers using either glycol or water on the tube side are plotted at the same electrical wattage (500, 1000, 1500, 2000, 2500 and 3000 W), except for test #3 for the shell-and-4coil heat exchanger using glycol as the working fluid on the tube side (S4CHX-G), *q-hx* was 592 W, due to an error. However, due to losses the heat exchanger heat transfer rates are slightly different from one test to another.

The heat transfer rates for the two tests were (423, 912, 1382, 1870, 2351 and 2802 W) and (449, 910, 1376, 1869, 2328 and 2795 W) for test #1 and test #2 respectively.

For the two tests for the (S3CHX-W) the *UA*-value increases with increasing heat exchanger heat transfer rate. Both water (in the tube side) and storage tank temperatures increase slightly with an increase in the heat transfer rates. There is a small variation between test #1 and test #2 at low heat transfer rate because the flow meter was not reading accurately (hard to control it) at low mass flow rate. Consequently, the heat exchanger *UA*-value, a function of the mass flow rate and temperatures, increases.

The *UA*-value for the first S3CHX-W, test was 123 W/K at 423 W and 275 W/K at 2802 W. For the second test the *UA*-value was 109 W/K at 449 W and 277 W/K at 2795 W.

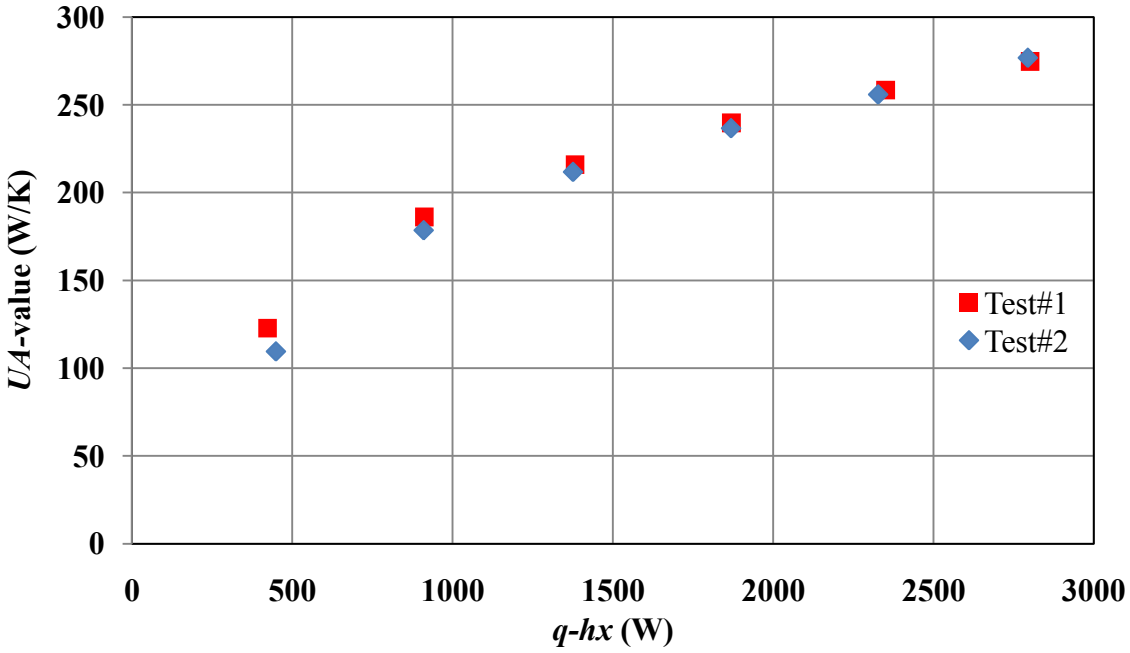

Figure 5.1. *UA*-value vs *q-hx* (S3CHX-W)

The water flow rate on the tube side was plotted with the pressure drop across the heat exchanger for the S3CHX-W as shown in Figure 5.2 for the two tests. Apart from the data shown in Table 5.1 for test #1 and Table 5.2 for test #2 the higher pressure drop on the tube side accrued at a high flow rate for both tests and the pressure drop was determined to be a function of temperature.

Table 5.1 Summary of the pressure measurements for Test #1-(S3CHX-W)

Actual heat transfer rate	Mass flow rate (LPM)	Low pressure (kPa)	High pressure (kPa)	ΔP
423	1.2	5.1	14.4	9.3
912	1.4	8.6	22.3	13.7
1382	1.6	11.4	28.4	17.0
1870	1.8	14.5	32.7	18.2
2351	2.0	15.5	34.5	19.0
2802	2.1	16.3	36.1	19.8

Table 5.2 Summary of the pressure measurements for Test #2-(S3CHX-W)

Actual heat transfer rate	Mass flow rate (LPM)	Low pressure (kPa)	High pressure (kPa)	ΔP
449	1.2	5.2	14.5	9.3
910	1.6	9.0	23.4	14.5
1376	1.8	12.4	30.3	17.9
1869	2.0	14.5	34.5	20.0
2328	2.1	15.9	36.5	20.7
2795	2.2	17.2	37.9	20.7

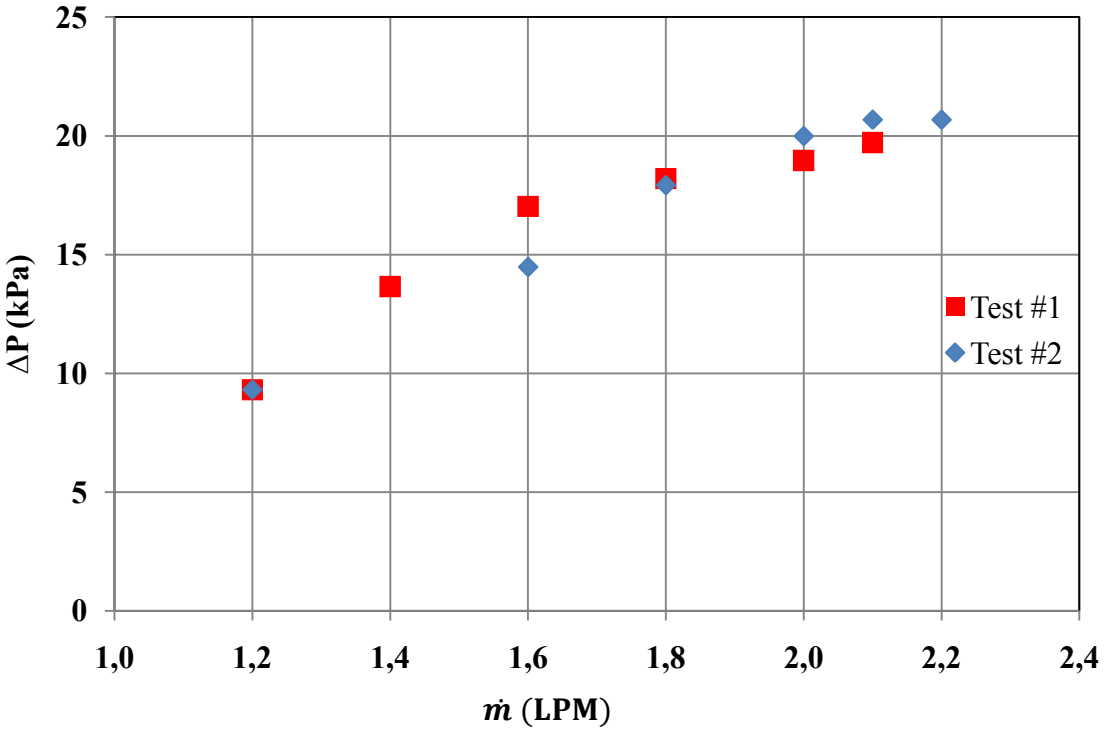

Figure 5.2 Pressure drop (S3CHX-W) vs. mass flow rate

5.1.2 Shell-and-4coil heat exchanger (S4CHX-W)

The *UA*-value was plotted against the heat exchanger heat rate for (S4CHX-W) in Figure 5.3., The *UA*-value of the heat exchanger increases for both tests with increasing heat rate, indicating that natural convection has a strong influence on the shell side heat transfer. However, other parameters have an influence on the *UA*-value, such as the thermal resistance of conduction through the coil walls (which was assumed to be negligible), the temperature distribution inside the tank and the temperature inlet and outlet for shell and tube sides. An example is that the *UA*-value at 2345 W was 289 W/K in Test #1 while the *UA*-value at 2334 W was 292 W/K, as shown in the Figure 5.3. This was higher than the expected value (based on Test #1 and because the inlet and the outlet temperatures were slightly different and that referred to the Log Mean Temperature Difference, (ΔT_{lm}) between the two tests, 8.1°C and 7.9°C for Test #1 and Test #2 respectively.

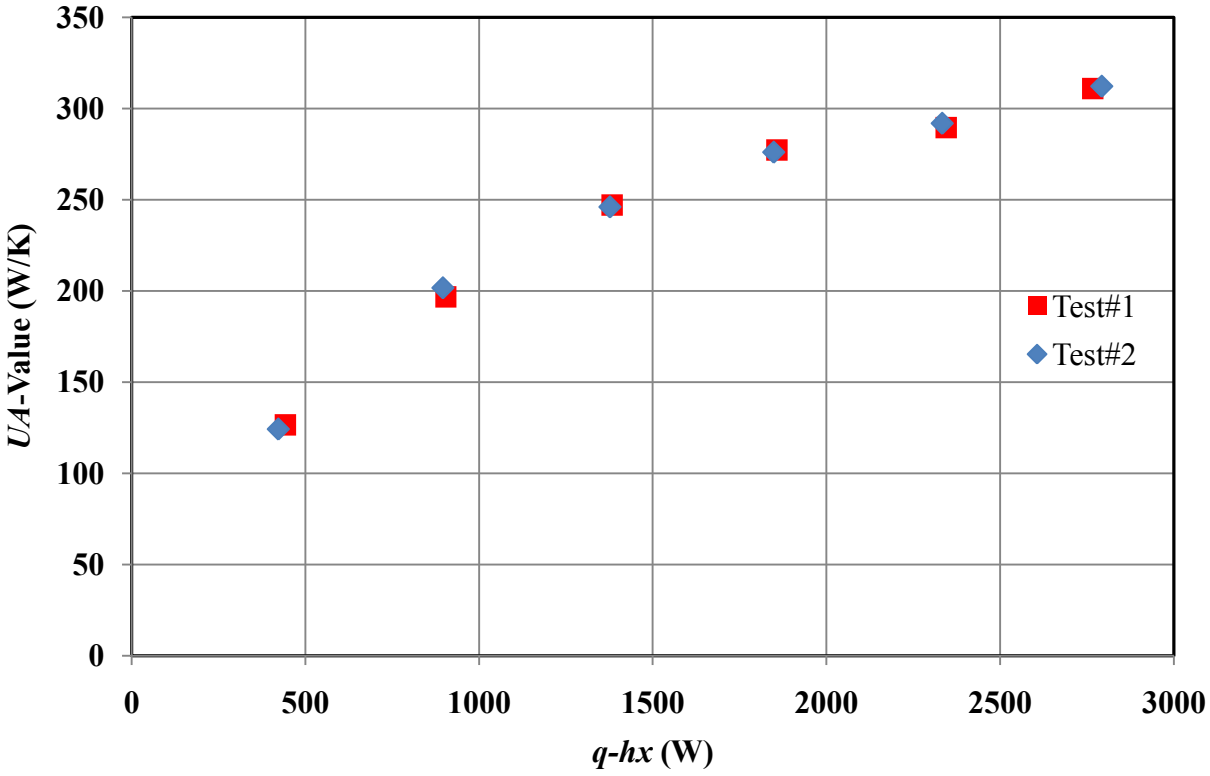

Figure 5.3 *UA* vs. *q-hx* (S4CHX-W)

The water flow rate on the tube side has been plotted with the pressure drop across the heat exchanger for the (S4CHX-W) as shown in Figure 5.4 for the two tests. Apart from the data shown in Table 5.3 for Test #1 and Table 5.4 for Test #2, the higher pressure drop accrued at high flow rates for both tests and the pressure drop was determined to be a function of temperature. Figure 5.4 depicts the effects of mass flow rate on the pressure drop for S4CHX-W. Mass flow rate increases by about the same value for both tests but not the same heat transfer rate as shown in Tables 5.3 for Test #1 and Table 5.4 for Test #2. For both tests, the pressure drop decreased with an increase in the average tube temperature inlet and outlet. For example, at the last two data points for Test #1 the temperature at 2345 W and 0.56 LPM was 49°C, the pressure drop was 10.3 kPa and in the same test at 2767 W and 0.57 LPM (which is not much difference between the two sets of values) the temperature was 59°C the pressure drop dropped to 9.7 kPa.

Table 5.3 Summary of the pressure measurements for Test #1-(S4CHX-W)

Actual heat transfer rate (W)	Mass flow rate (LPM)	Low pressure (kPa)	High pressure (kPa)	ΔP
443	1.2	9.5	14.8	5.3
905	1.6	11.7	19.3	7.6
1383	1.8	14.6	24.0	9.4
1858	2.0	16.4	26.7	10.3
2345	2.1	17.7	27.9	10.2
2767	2.2	18.8	28.4	9.7

Table 5.4 Summary of the pressure measurements for Test #2-(S4CHX-W)

Actual heat transfer rate (W)	Mass flow rate (LPM)	Low pressure (kPa)	High pressure (kPa)	ΔP
402	1.1	6.1	9.0	2.8
888	1.6	10.3	17.2	7.0
1371	1.8	13.1	22.1	9.0
1840	2.0	15.6	25.5	9.9
2323	2.1	17.2	27.3	10.1
2820	2.2	18.6	28.6	10.0

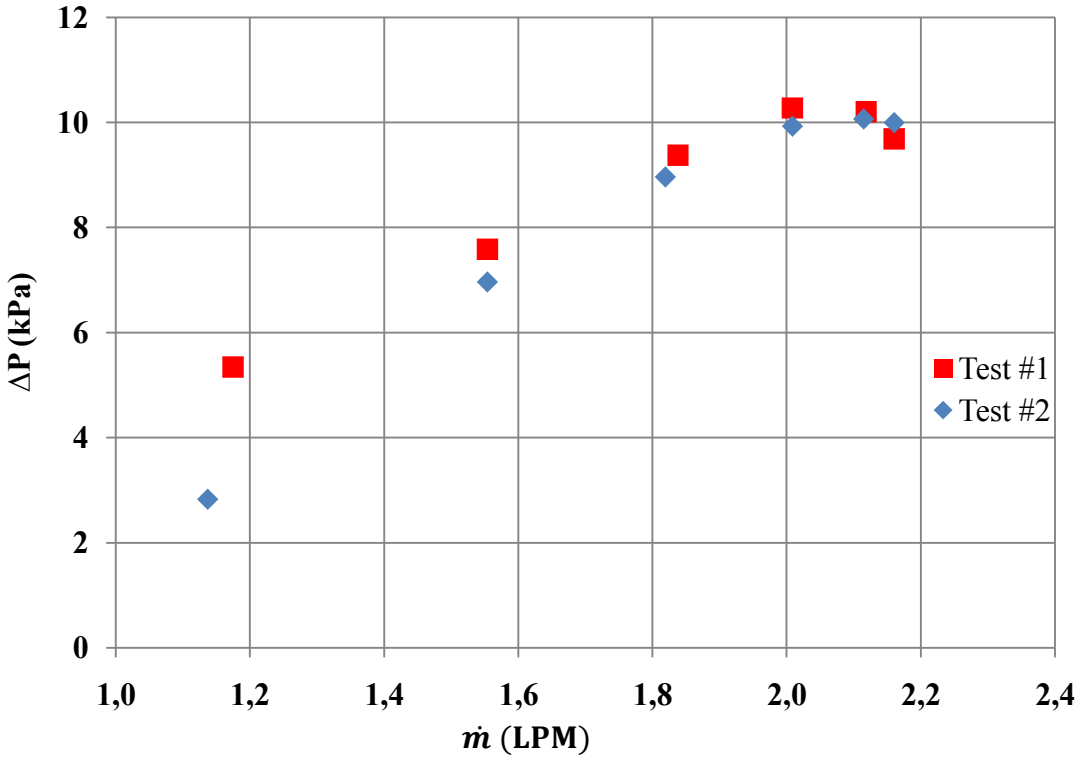

Figure 5.4 Pressure drop (S4CHX-W) vs. mass flow rate

Figure 5.5 illustrates the pressure drops for both heat exchangers, S3CHX-W and S4CHX-W for the first test for both heat exchangers. At the same flow rate the pressure drop in the S3CHX-W is higher because the cross-sectional area for flow with the S4CHX is greater than the cross-sectional area for flow with the S3CHX. The flow rate divided to 4 coils for S4CHX, but for the S3CHX only divided to 3 coils.

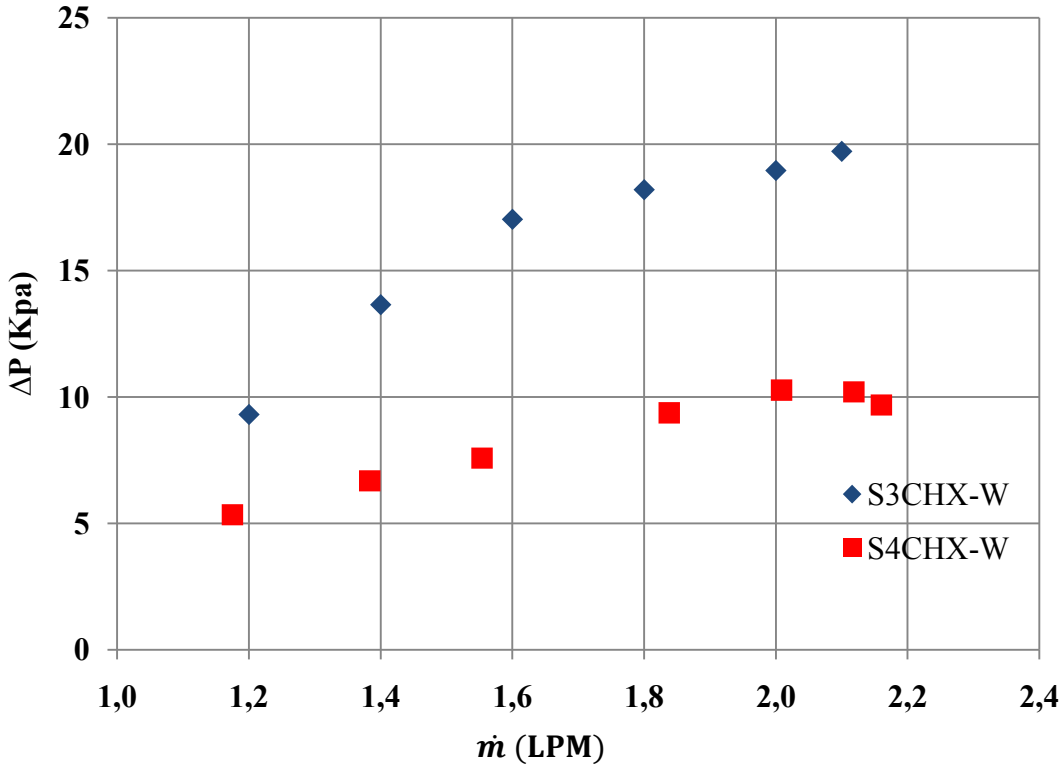

Figure 5.5 Pressure drop for S3CHX-W and S4CHX-W

5.1.3 Comparing the *UA*-values for S3CHX-W and S4CHX-W

The *UA*-value of the heat exchanger has been plotted with the heat transfer rate for both S3CHX-W and S4CHX-W in Figure 5.6. The average *UA*-values of the two tests are represented by the squares while the red line represents the logarithmic trend line of the average of the *UA*-values of the two tests for the S3CHX-W. Likewise, the diamonds represent the average *UA*-values of the two tests and the line with these diamonds represents the trend line of these values for the S4CHX-W.

The *UA*-values for the S4CHX-W was always higher than the *UA*-values of that S3CHX-W at the same heat transfer rate, which is reasonable because the heat transfer area in the shell-and-4coil heat exchanger is greater than that of the shell-and-3coil heat exchanger. The area of the S3CHX was 0.39 m^2; the area of the S4CHX was 0.59 m^2. For example at

a heat transfer rate of 2740 W the *UA*-values were 268 W/K and 301 W/K for S3CHX-W and S4CHX-W, and the overall heat transfer coefficients were 687 and 510 W/m^2·K respectively. The S4CHX has 52 % more surface area than the S3CHX, however, *UA* for the S4CHX is only 13 % greater than *UA* for the S3CHX.

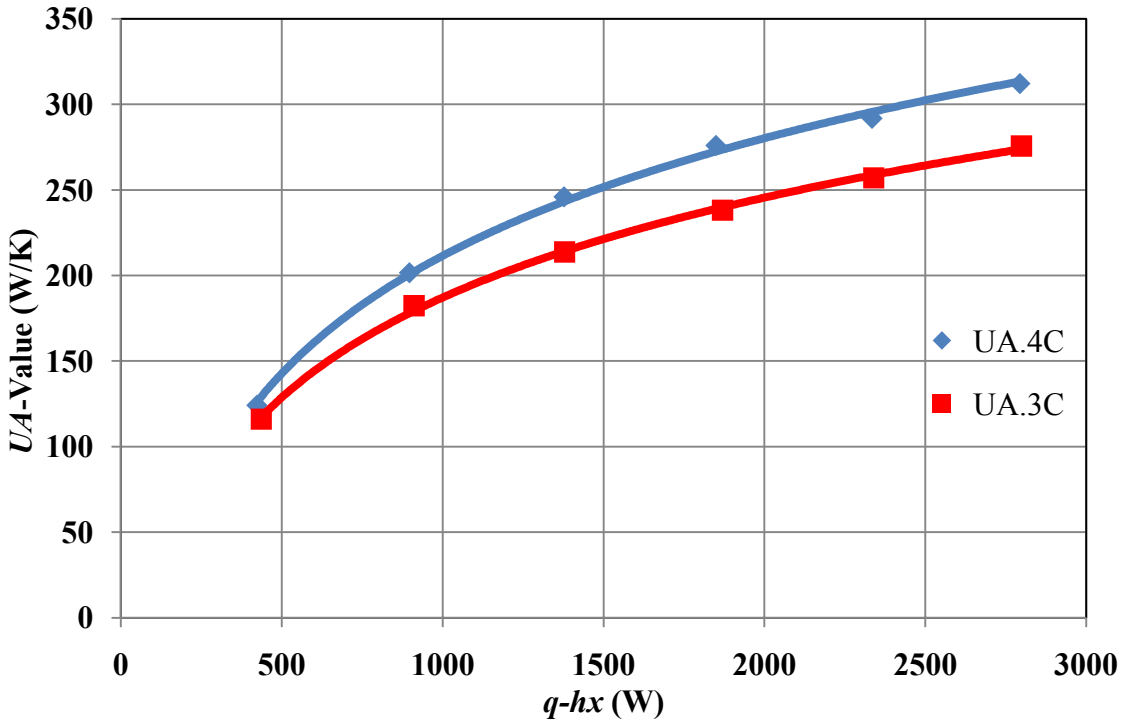

Figure 5.6 *UA*-values for S3CHX-W and S4CHX-W

5.1.4 Shell-and-3coil heat exchanger, S3CHX-G

Figure 5.7 shows the results obtained from testing the shell-and-3coil heat exchanger using glycol as the working fluid on the tube side (S3CHX-G), which represents the situation in most solar domestic hot water systems employed in regions where freezing condition areas. Four tests were plotted in one graph to illustrate the results. These tests were conducted using the same procedures employed with the S3CHX-W. At the same heat transfer rate the *UA*-values are not the same because the average glycol temperatures are different from one test to another. Figure 5.8 illustrates the glycol average temperature

with the *UA*-values for the four tests. As the glycol temperature increases the *UA*-value also increases. For example in Test #1 at 430 W the *UA*-value was 72 W/K and the glycol average temperature was 32°C. For Test #2 at 348 W the *UA*-value was 83 W/K and the glycol average temperature was 45°C, even though the heat transfer rate was 82 W lower in Test #2 than Test #1.

However, the *UA*-value was higher in Test #2 than Test #1 by 19% and that referred to the different glycol average temperature from Test #2 and Test #1 where the glycol average temperature was 35% higher than that of Test #2. For the same heat transfer rate and a very close average temperature range of glycol the *UA*-values are close for all tests.

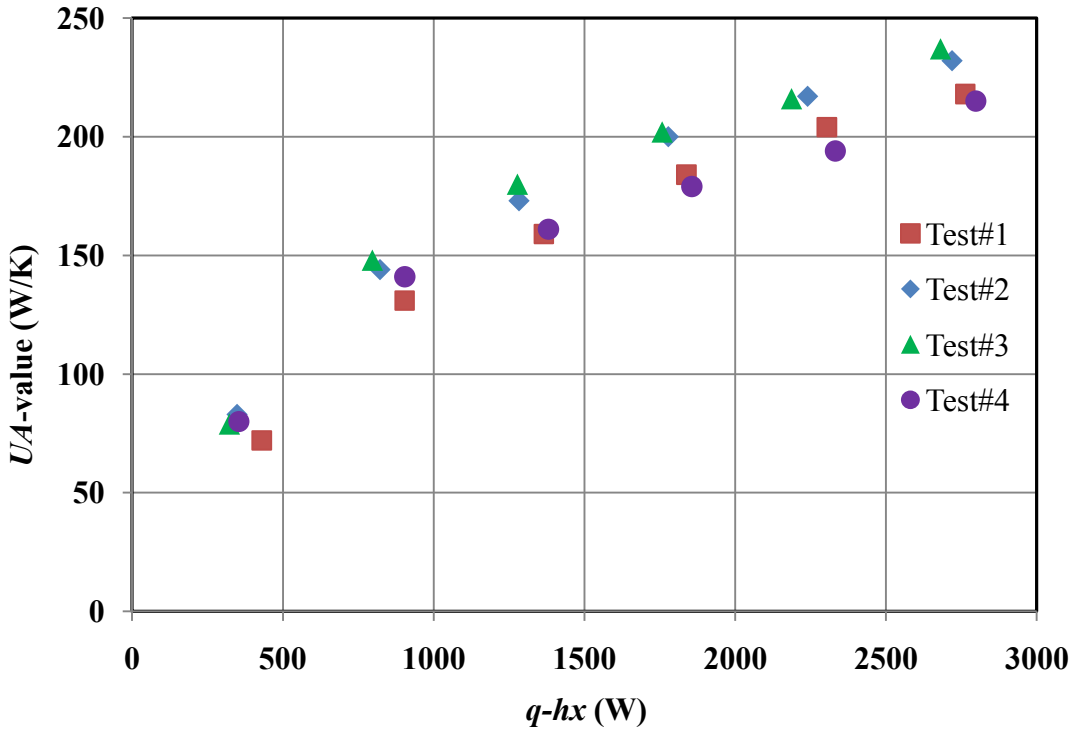

Figure 5.7 *UA*-value vs *q-hx* (S3CHX-G)

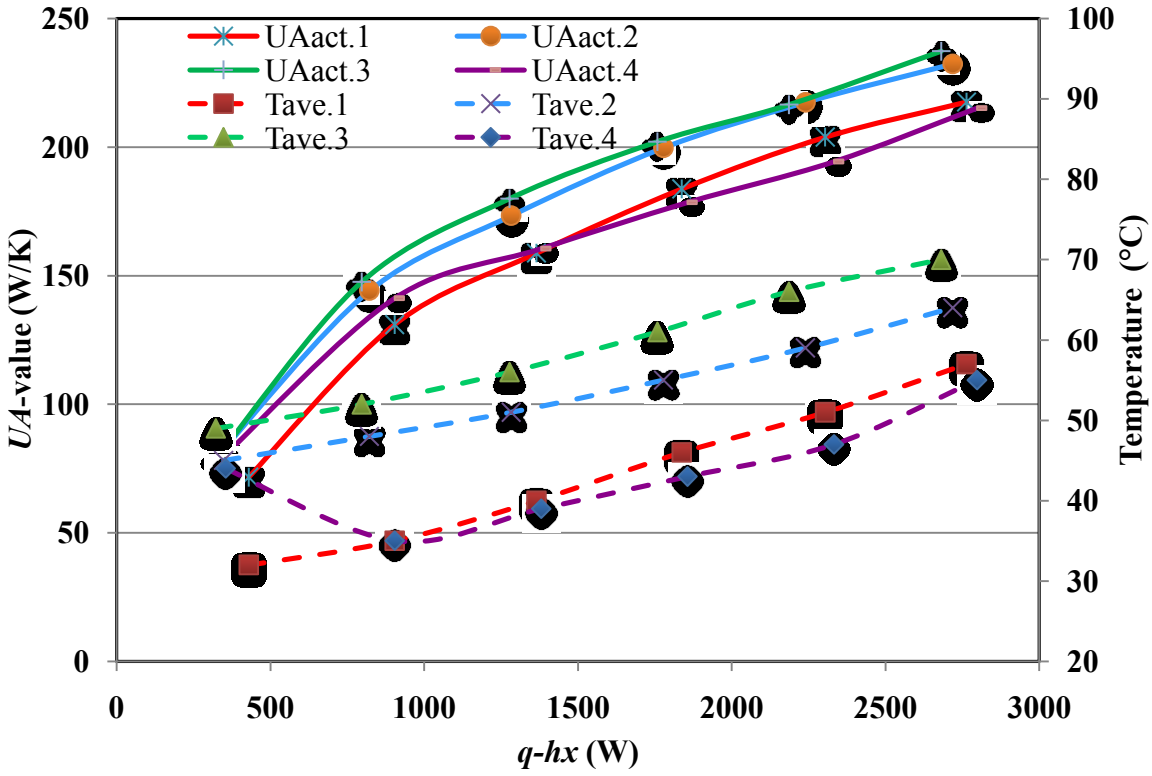

Figure 5.8 *UA*-value and average temperatures with *q-hx* (S3CHX-G)

Figure 5.9 shows the effect of glycol flow rate on the pressure drop on the tube side of the heat exchanger for two tests for the S3CHX-G. The pressure drop increases with an increasing flow rate. However, when the fluid became hot (at high heat transfer rates) the pressure increased slightly as flow rate increased until about 23.4 kPa and 1.70 LPM respectively for Test #2, and when the pressure dropped due to a rapid increase of the average temperature, the mean viscosity also went down. Table 5.5 and Table 5.6 represent Test #1 and Test #2 respectively. These tables show the summary of the measured parameters (heat transfer rate, average temperature, mass flow rate, low pressure, high pressure and pressure drop).

Table 5.5 Summary of the measured parameters for Test #1-(S3CHX-G)

Actual heat transfer rate (W)	Mass flow rate (LPM)	Average temperature (°C)	Low pressure (kPa)	High pressure (kPa)	Pressure drop (kPa)
669	0.87	32.0	29.6	42.1	12.5
1003	1.28	35.0	30.3	46.9	16.6
1458	1.59	40.0	33.1	53.1	20.0
1899	1.76	46.0	35.2	60.7	25.5
2266	1.87	51.0	41.4	68.3	26.9
2720	1.91	57.0	49.0	76.5	27.5

Table 5.6 Summary of the measured parameters for Test #2-(S3CHX-G)

Actual heat transfer rate (W)	Mass flow rate (LPM)	Average temperature (°C)	Low pressure (kPa)	High pressure (kPa)	Pressure drop (kPa)
372	0.87	45.0	40.0	53.1	13.1
822	1.28	48.0	37.2	56.5	19.3
1375	1.57	51.0	40.0	60.7	20.7
1993	1.76	55.0	42.7	66.9	24.1
2506	1.87	59.0	49.0	73.1	24.1
2988	1.91	64.0	57.2	82.7	25.5

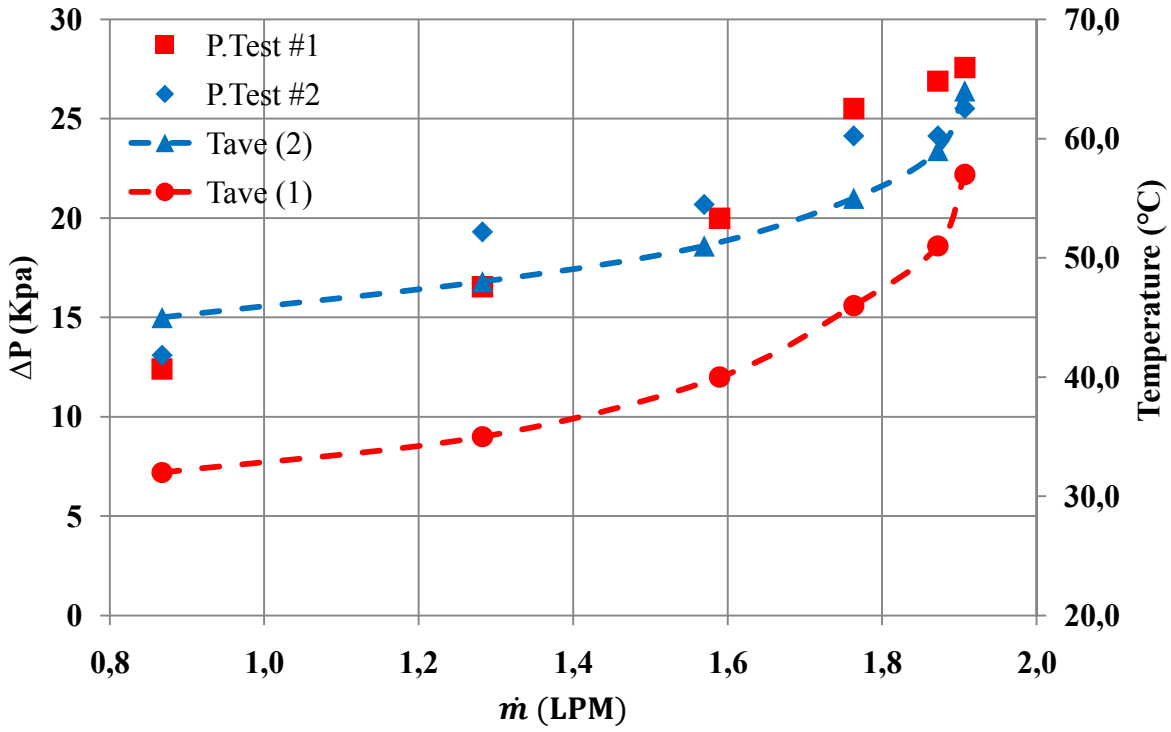

Figure 5.9 Pressure drop and temperature-(S3CHX-G) vs. mass flow rate

5.1.5 Shell-and-4Coil heat exchanger (S4CHX-G)

The results of this study indicate the *UA*-value changes significantly with variable operating conditions. The *UA*-value has been plotted with the heat exchanger heat rate for four tests using glycol as the working fluid on the tube side (Figure 5.10). With increasing heat rate, the *UA*-value of the heat exchanger increases for all tests, indicating that natural convection has a strong influence on the shell side heat transfer. In this study the results show that, with variable operating conditions, the *UA*-value changes significantly.

A further complication illustrated in Figure 5.10 is that for different tests the *UA*-value is not a unique function of the heat rate. This is due to differing temperature distributions in the tank and the heat exchanger. For example, at a heat rate of 1835 W, the *UA*-value for Test #4 was 2% higher than Test #1. For Test #4 the actual heat transfer rate was 551 W

which is much higher than the other tests because the electric watt was much higher (592 W), as mentioned at the beginning of this chapter.

Figure 5.10 shows also that Test #4 has a maximum *UA*-value of 264 W/K at a corresponding heat transfer rate of 2741 W, while Test #3 has a maximum heat transfer rate of 2845 W at a corresponding *UA*-value of 248 W/K, when compared with other tests.

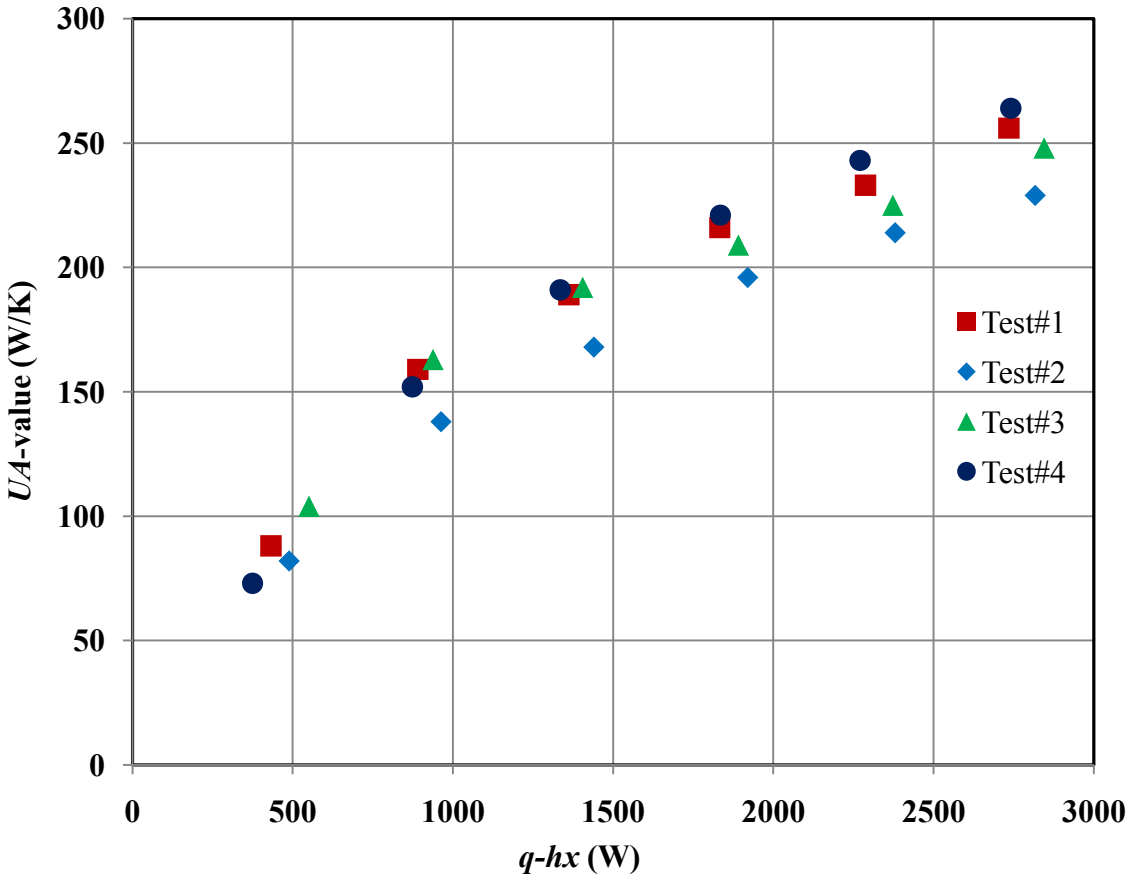

Figure 5.10 *UA*-value vs *q-hx* (S4CHX-G)

The effect of glycol flow rate on the pressure drop on the tube side of the heat exchanger for two different tests for the S4CHX-G is illustrated in Figure 5.11. Both the temperature and the pressure drop increase with increasing flow rates for both Test #1 and Test #2, until the values of the corresponding mass flow rate and pressure drop for Test#1 reaches 2 LPM and 15.0 kPa, while that of Test #2 reaches 2.1 LPM and 11.7 kPa. At these points for both tests the pressure drop decreased due to a rapid increase of the average temperature and corresponding decrease of the mean viscosity. Table 5.7 and Table 5.8 represents Test #1 and Test #2 respectively, which shows the summary of the measured parameters.

Table 5.7 Summary of the measured parameters for Test #1-(S4CHX-G)

Actual heat transfer rate (W)	**Mass flow rate (LPM)**	**Average temperature (°C)**	**Low pressure (kPa)**	**High pressure (kPa)**	**Pressure drop (kPa)**
669	1.2	32.0	29.0	33.4	4.4
1003	1.6	35.0	25.8	32.4	6.6
1458	1.8	40.0	28.3	37.9	9.6
1899	2.0	46.0	33.3	44.1	10.8
2266	2.1	51.0	40.0	51.7	11.7
2720	2.2	57.0	48.2	58.2	10.0

Table 5.8 Summary of the measured parameters for Test#2-(S4CHX-G)

Actual heat transfer rate (W)	Mass flow rate (LPM)	Average temperature (℃)	Low pressure (kPa)	High pressure (kPa)	Pressure drop (kPa)
372	1.2	45.0	11.7	19.0	7.3
822	1.6	48.0	15.0	25.9	10.9
1375	1.8	51.0	18.6	31.0	12.4
1993	2.0	55.0	19.3	34.5	15.2
2506	2.1	59.0	21.9	36.9	15.0
2988	2.2	64.0	21.4	35.5	14.1

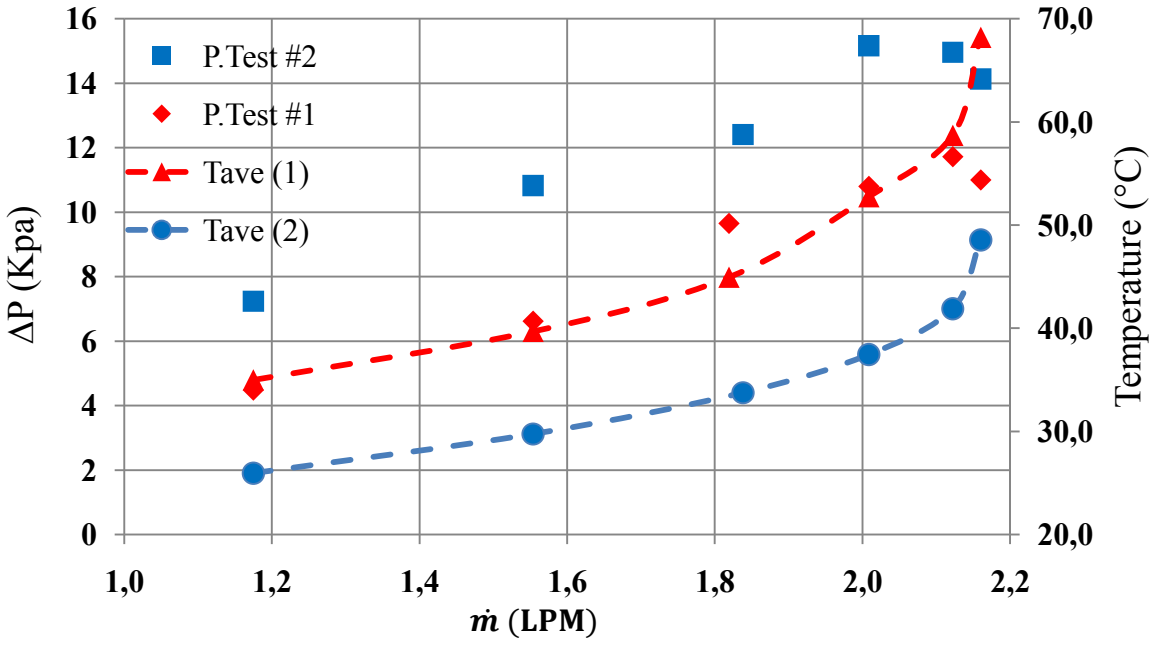

Figure 5.11 Pressure drop (S4CHX-G) vs. mass flow rate

5.1.6 Comparison between *UA*-values for S3CHX-G and S4CHX-G

Figure 5.12 illustrates the relationship between the average *UA*-values of the heat exchanger for the 4 tests with respect to the heat transfer rate (*q-hx*) for the S3CHX-G and S4CHX-G. The trend line with the diamonds represents the S3CHX-G and the trend line with the squares represents the S4CHX-G. The trend line used for this graph is a logarithmic trend line (log) because it was the best trend line for fitting the data. As shown in Figure 5.12 the *UA*-values for the S4CHX-G are always higher than the *UA*-values of that S3CHX-G at the same heat transfer rate. For example, at a heat transfer rate of 2740 W, the *UA*-value was 222 W/K and 240 W/K for the S3CHX-G and the S4CHX-G, respectively. However, there is a negligible difference between the *UA*-values at heat transfer rates less than 1500 W.

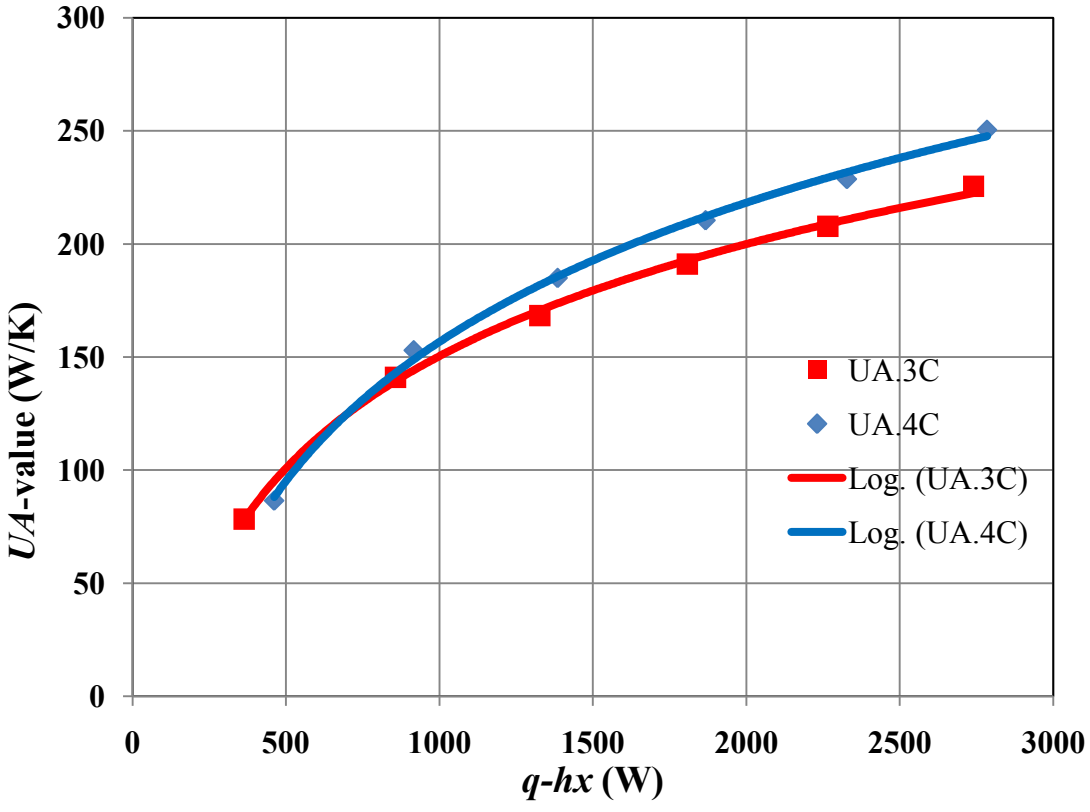

Figure 5.12 *UA*- values for S3CHX-G and S4CHX-G

5.1.7 Comparison between *UA*-values for S3CHX-W and S3CHX-G

The *UA*-values of the S3CHX-W for the 2 tests and S3CHX-G for the 4 tests with respect to the heat transfer rate (*q-hx*) are shown in Figure 5.13. The *UA*-value for the S3CHX-W is always higher than S3CHX-G at the same heat transfer rate, *q-hx*. For example, at a heat transfer rate of 1808 W the *UA*-value were 191 W/K and 242 W/K and, at 2740 W the *UA*-values were 225 W/K and 275 W/K for S3CHX-G and S3CHX-W, respectively. Water is simply a better heat transfer fluid than glycol, due to its higher thermal conductivity and lower viscosity.

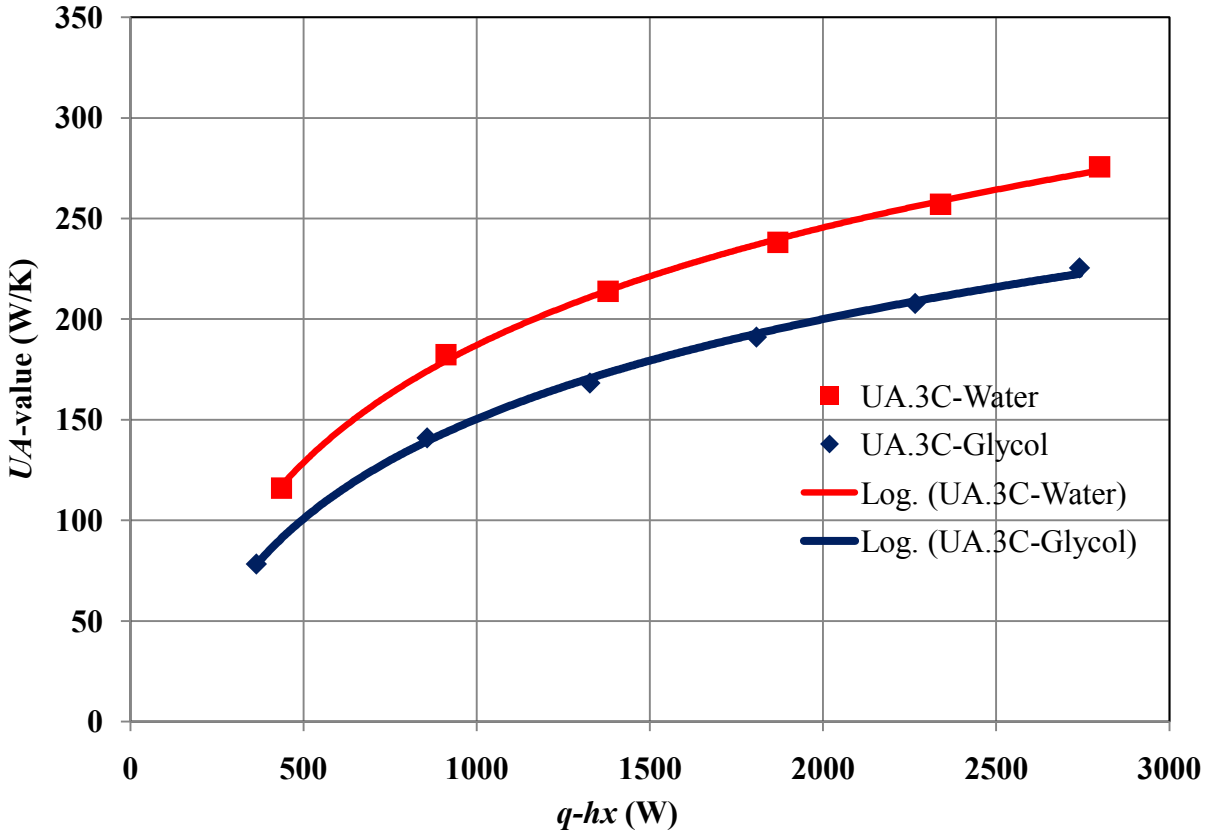

Figure 5.13 *UA*-values for S3CHX-W and S3CHX-G

5.1.8 Comparison between *UA*-values for S4CHX-W and S4CHX-G

Figure 5.14 illustrates the *UA*-values of the S4CHX-W for the 2 tests and S4CHX-G for the 4 tests with respect to the heat transfer rate (*q-hx*). As can be seen from Figure 5.14 the *UA*-values for the S4CHX-W are higher than the *UA*-values for S4CHX-G. The *UA*-values for S4CHX-G and S4CHX-W were 202 W/K and 216 W/K at 1808 W and; 247 W/K and 308 W/K at 2740 W, respectively. The reason for this decrement is the same for the S3CHX-W and S3CHX-G. The high *UA*-values for water are due to high values of h_i, associated with water flowing on the tube side. Water has a higher specific heat and thermal conductivity than propylene glycol. For example, at 35°C, the specific heat of water and glycol are 4177 J/kg·K and 3803 J/kg·K, respectively and thermal conductivities are 0.62 W/m·K and 0.41 W/m·K respectively. This leads to high Nusselt number. Table 5.9 shows the important thermal properties and dimensionless numbers for coil #1 for glycol and water at 35°C and 60°C as examples.

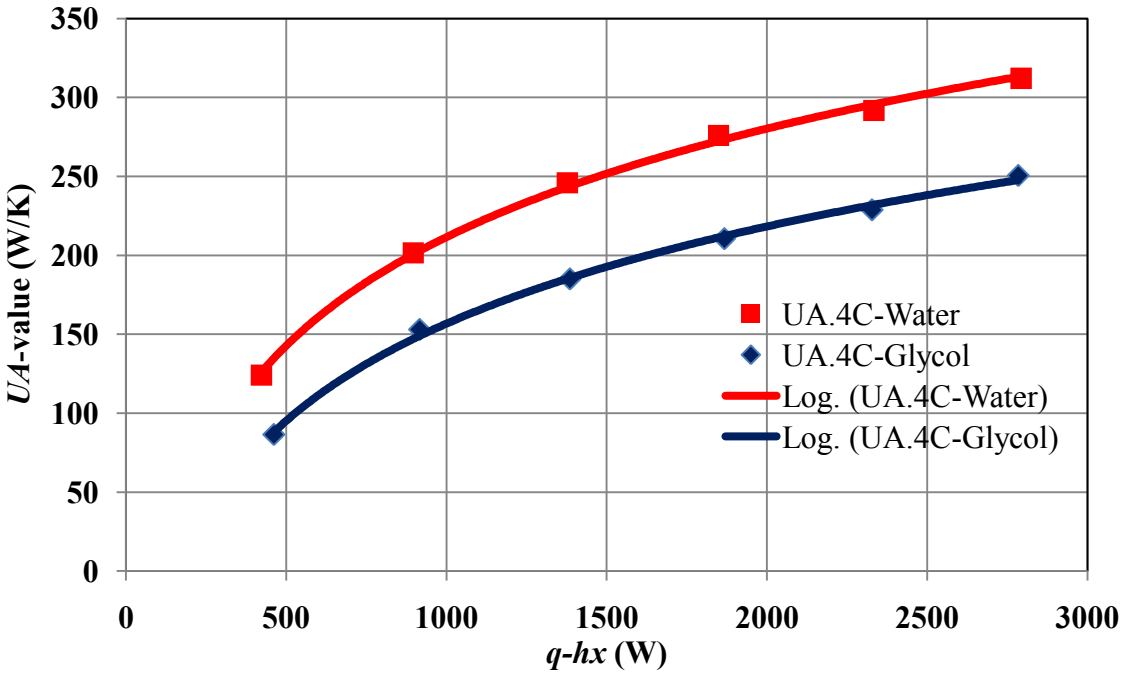

Figure 5.14 *UA*-values for S4CHX-W and S4CHX-G

Table 5.9 Physical properties for water and glycol at 30°C and 60 °C

Coil #1	**Water**		**Glycol**	
	35 °C	**60 °C**	**35 °C**	**60 °C**
Thermal conductivity k, W/m·K	0.62	0.65	0.41	0.42
Specific heat C_p , J/kg·K	4177	4181	3803	3857
Dynamic viscosity, μ, N·s/m^2	0.00079	0.00051	0.00317	0.00144
Kinematic viscosity, v, m/s^2	0.79	0.52	3.09	1.42
Prandtl number, Pr	5.37	3.28	29.58	13.26
Reynolds number, Re_{Di}	2796	7019	714	2483
Nusselt number, Nu_i	35.30	52.80	19.80	35.10
Heat transfer coefficient, h_i, W/m^2·K	5275	8245	1954	3569

5.2 Model Results

In order to determine values for the natural convection heat transfer coefficients and to predict the performance of the shell-and-coil heat exchanger in terms of heat exchanger *UA*-value for each arrangement, four models were developed. The four input variables needed for all models are: (i) temperature of the glycol at the inlet of the heat exchanger (T_{hi})**,** (ii) mass flow rate, $\dot{m}_g$ *i*f glycol was used or $\dot{m}_w$ if water was used as the working fluid on the tube side and mass flow rate on the shell side (iii) temperature of the water inlet to the heat exchanger on the shell side (T_{ci}) (iv) heat transfer rate, *q-hx*.

Based on this study and where applicable for the input, experimental results were used. The experimental correlations from the literature were used to calculate the heat transfer coefficient, after the tube surface and glycol exit temperatures were guessed initially. Also, the rate of heat through the heat exchanger, *q-hx*, and the *UA*-value were found after the heat transfer coefficients were known. Finally, a new heat transfer coefficients were calculated and compared based on the knowledge of *q-hx* and the *UA*-value.

5.2.1 Performance Factor

The performance factor is associated with heat transfer outside the tube (shell side). *UA*-values from the computer program were predicted values based on performance factors which were determined using the experimental data. Random values were not use in the model, but in order to obtain the results from the model, experimental values were used and the performance factor for each coil was adjusted to obtain the heat transfer for each coil as measured (h_o). This gave the *UA*-values predicted, based on the experimentally determined performance factor for each coil. In order to achieve convergence, this process was repeated. Appendix C shows a diagram explaining the methodology employed. Copies of the four models are also provided in Appendix C.

The performance factor (*PF*) was defined as the ratio of the outside heat transfer coefficient $h_{o,meas}$measured for the experiment to the outside heat transfer coefficients $h_{o,calc}$ calculated for the model.

This is represented mathematically as

$$PF = \frac{h_{o,meas}}{h_{o,calc}} \qquad [5\text{-}1]$$

$h_{o,meas}$ is the measured heat transfer coefficient that inferred by experimentally determined *UA*-value, and h_i which is based on Manlapaz correlation [33]

$h_{o,\ meas}$ was determined from equation [4-8]

$$h_{o,meas} = \left\{A_o \left(\frac{1}{UA} - \frac{1}{h_i A_i}\right)\right\}^{-1} \qquad [5\text{-}2]$$

Where,

UA is the overall heat transfer coefficient area-product determined using equation [4-6]

h_i is the heat transfer coefficient on the tube side, based on the Manlapaz correlation as stated in equation [4-28].

A_i and A_o are the surface areas inside and outside the tubes respectively.

$h_{o,calc}$ is calculated using equation [4-33], which is based on the assumption of forced water flow through the heat exchanger.

5.2.2 Model-1 (S3CHX-W)

Table 5.10 and Table 5.11 present the measured and predicted *UA*-values for (S3CHX-W) for Test #1 and Test #2 respectively. These tables also show the input values of the mass flow rate on the shell side ($\dot{m}_c$) and on the tube side ($\dot{m}_h$) and the temperature of the water inlet to the heat exchanger on the shell side ($T_{c,i}$) and temperature of the water at the inlet of the heat exchanger ($T_{hx,i}$).

Table 5.10 Model-1 predictions for S3CHX-W-Test #1

$q\text{-}hx_{EXP}$	$q\text{-}hx_{TH}$	UA_{EXP}	UA_{PR}	T_{hi}	T_{ci}	$\dot{m}_h$	$\dot{m}_c$
423	427	123	161	36	24	0.160	1.336
912	915	186	200	38	23	0.081	0.049
1382	1386	216	219	43	24	0.107	0.083
1870	1864	240	236	49	25	0.123	0.094
2351	2359	258	246	53	25	0.129	0.103
2802	2796	275	216	61	29	0.146	0.110

Table 5.11 Model-1 predictions for S3CHX-W-Test #2

$q\text{-}hx_{EXP}$	$q\text{-}hx_{TH}$	UA_{EXP}	UA_{TH}	T_{hi}	T_{ci}	$\dot{m}_h$	$\dot{m}_c$
449	454	109	146	33	19	0.059	0.044
910	911	178	190	38	22	0.104	0.069
1376	1374	212	212	43	22	0.123	0.084
1869	1871	237	232	38	24	0.135	0.097
2328	2338	256	244	53	25	0.142	0.107
2795	2804	277	262	62	30	0.147	0.115

Figure 5.15 describes the model predictions for the shell-and-3coil heat exchanger (S3CHX-W) performance. The measured values represent the average of the values for Test #1 and Test #2 and the predicted values were obtained for the model after the average values were used in the model.

From the graph it can be seen that at a higher heat transfer rate of range 1379 W-3000 W, the model was more accurate in predicting the *UA*-value of the S3CHX-W.

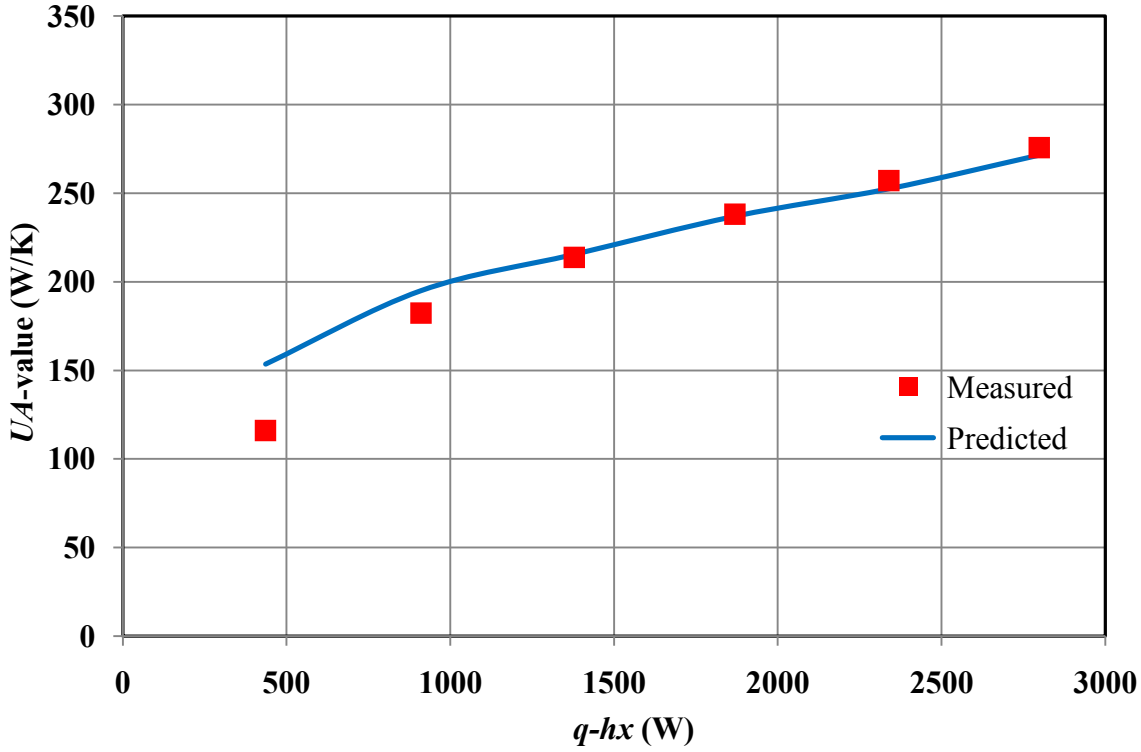

Figure 5.15 Model-1 predictions for (S3CHX-W) performance

Figure 5.16, 5.17 and 5.18 show the performance factors for S3CHX-W for Test #1, Test #2 and the average of Test #1 and Test #2, respectively. In each case the performance factor was obtained for Coil #1 (PF.C1), Coil #2 (PF.C2) and Coil #3 (PF.C3). For Test #1 and Test #2, the performance factors for Coil#3 are the same (0.53) and the low value due to the small clearance between the coil and the shell of the heat exchanger, which results in low heat transfer. Likewise, for Test #1 and Test #2, the Coil #2 has the same performance factor of 0.66.

The only difference recorded was with Coil #1, where the performance factor for Test #1 was in the range of 0.68 to 0.72, while that of Test #2 was a constant value of 0.70 (shown in Figure 5.17), which is the average value of the performance factor for both Test #1 and Test #2 for each coil. Within the range of the precision of the measurements, 0.68 and 0.72 are basically the same

Table 5.12 Performance factors for (S3CHX-W)-Test #1

q-hx	***qhx1$_{EXP}$***	***qhx2$_{EXP}$***	***qhx3$_{EXP}$***	***PF.C1***	***PF.C2***	***PF.C3***
423	117	152	155	0.68	0.66	0.53
912	272	325	315	0.70	0.66	0.53
1382	410	499	474	0.70	0.66	0.53
1870	564	665	642	0.72	0.66	0.53
2351	691	853	808	0.70	0.66	0.53
2802	826	1007	969	0.70	0.66	0.53

Table 5.13 Performance factors for (S3CHX-W)-Test #2

q-hx	***qhx1$_{EXP}$***	***qhx2$_{EXP}$***	***qhx3$_{EXP}$***	***PF.C1***	***PF.C2***	***PF.C3***
449	136	158	155	0.70	0.66	0.53
910	265	329	316	0.70	0.66	0.53
1376	401	498	476	0.70	0.66	0.53
1869	546	677	647	0.70	0.66	0.53
2328	681	841	806	0.70	0.66	0.53
2795	819	1012	963	0.70	0.66	0.53

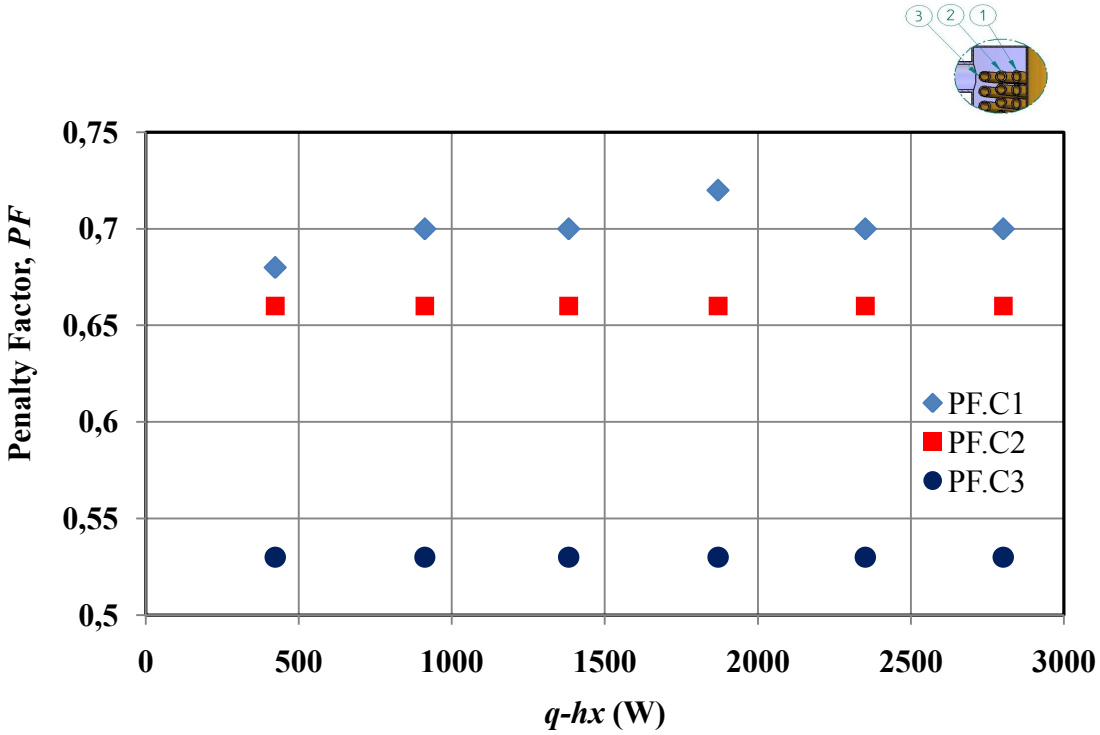

Figure 5.16 Performance factors for (S3CHX-W)-Test#1

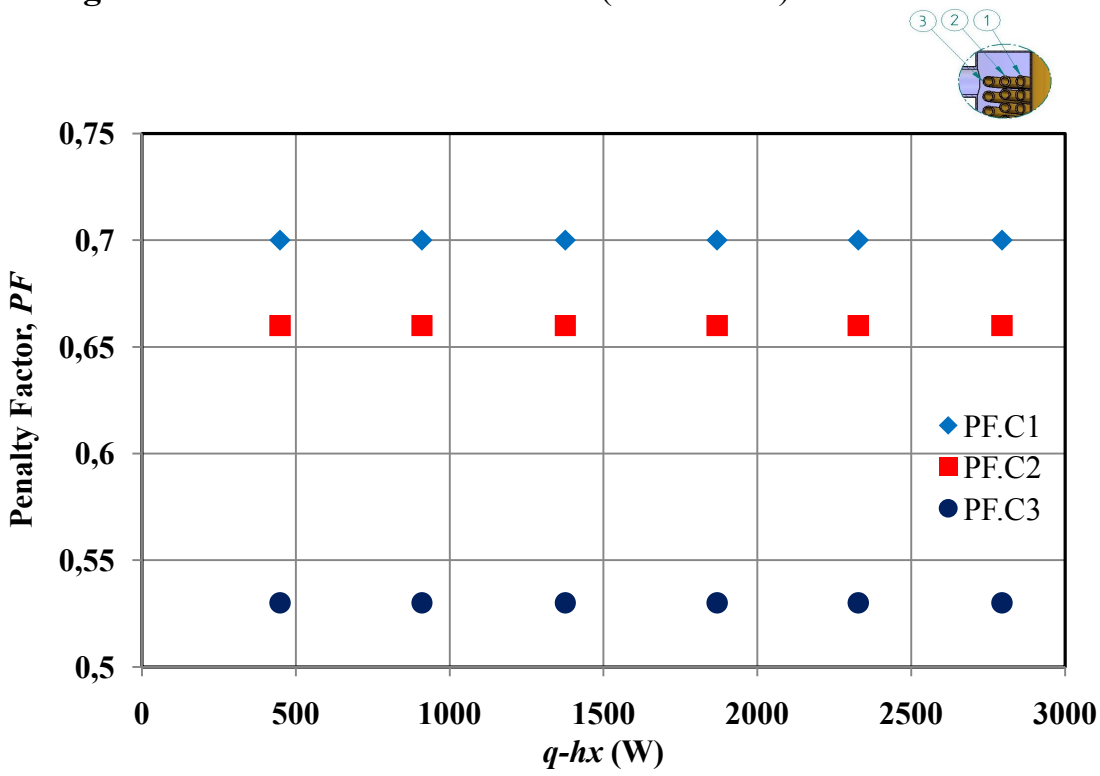

Figure 5.17 Performance factors for (S3CHX-W)-Test#2

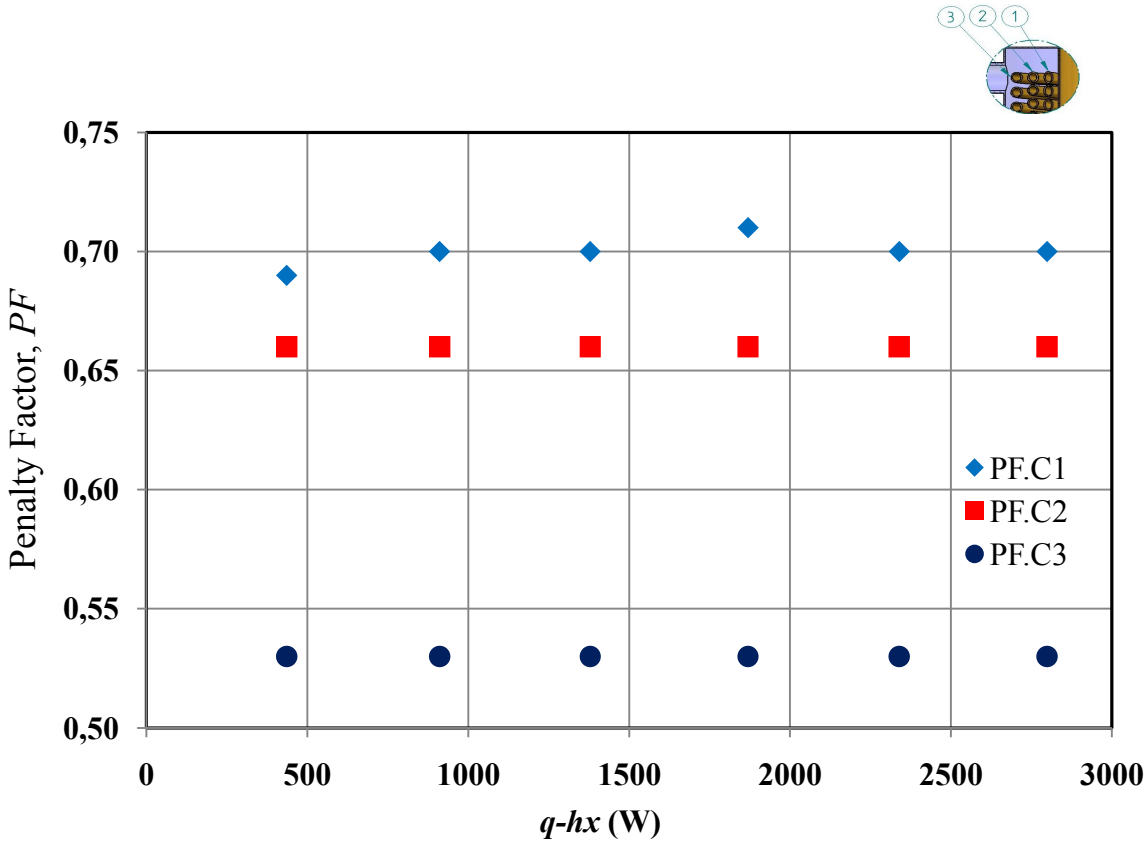

Figure 5.18 Average performance factors for S3CHX-W for Test #1 and Test #2

5.2.3 Model-2 (S4CHX-W)

Model-2 is similar to Model-1, with the same parameters and same properties of water, the only difference being that Model-2 (modeled for the (S4CHX-W)) is based on the number of coils and shell diameters.

As can be seen from Table 5.14 and Table 5.15 , the predicted *UA*-values (UA_{PR}) were lower than the experimental *UA*-values (UA_{EXP}) for both tests conducted in range of 402-1371W (heat transfer rates). For Test #1 the UA_{PR} were 167, 205 and 258 W/K at 443, 905 and 1383 W respectively while at the same heat transfer rates the UA_{EXP} were 127, 197 and 247 W respectively. Similarly, for Test #2 the UA_{PR} were 140, 236 and 264 W/K

at 402, 888 and 1371 W respectively and that of UA_{EXP} were 122, 206 and 245 W respectively.

Table 5.14 Model-2 predictions for S4CHX-W-Test #1

$q\text{-}hx_{EXP}$	$q\text{-}hx_{TH}$	UA_{EXP}	UA_{PR}	T_{hi}	T_{ci}	$\dot{m}_h$	$\dot{m}_c$
443	442	127	167	37	25	0.054	0.040
905	898	197	205	42	26	0.097	0.062
1383	1382	247	258	47	27	0.117	0.074
1858	1861	277	277	52	27	0.131	0.083
2345	2345	289	291	57	27	0.132	0.087
2767	2771	311	312	64	32	0.136	0.092

Table 5.15 Model-2 predictions for S4CHX-W-Test #2

$q\text{-}hx_{EXP}$	$q\text{-}hx_{TH}$	UA_{EXP}	UA_{PR}	T_{hi}	T_{ci}	$\dot{m}_h$	$\dot{m}_c$
402	402	122	140	41	29	0.052	0.036
888	888	206	236	45	29	0.098	0.064
1371	1370	245	264	49	30	0.115	0.077
1840	1840	275	280	54	30	0.126	0.087
2323	2323	294	299	58	31	0.132	0.094
2820	2821	313	316	63	32	0.136	0.101

Figure 5.19 describes the model predictions for the (S4CHX-W) performance. The measured values represent the average of the values for Test #1 and Test #2 and the predicted values were obtained for the model after the average values were used in the model. The model was accurate in predicting the *UA*-value of the S4CHX-W at higher heat transfer rates, as stated in Table 5.14 and Table 5.15, since the predicted values were obtained by taken the average values for the two tests. The reason for the over-predicting is that the inlet mass flow rates to the heat exchanger on the tube side

$\dot{m}_h$ were over estimated, or in other words the mass flow rates at these heat transfer rates were very low.

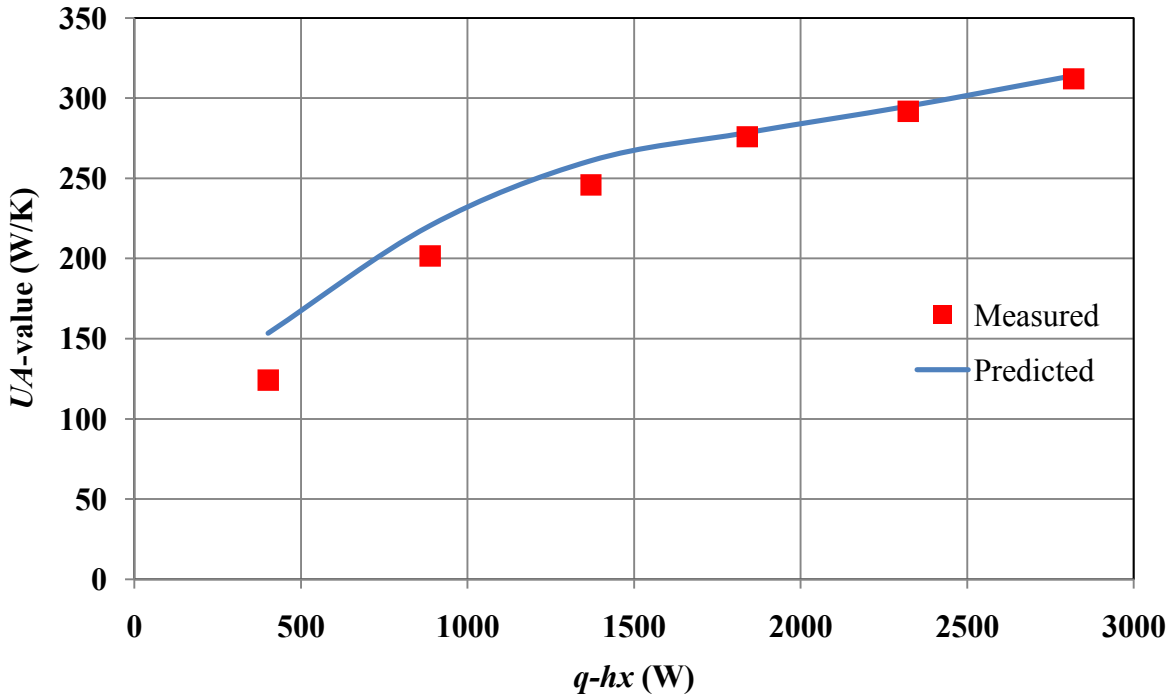

Figure 5.19 Model-2 predictions for (S4CHX-W) performance

The performance factors for S4CHX-W for Test #1, Test #2 and the average of Test #1 and Test #2 are reported in Figure 5.20, 5.21 and 5.22 respectively. In each case the performance factor was obtained for Coil #1 (PF.C1), Coil #2 (PF.C2), Coil #3 (PF.C3) and Coil #4 (PF.C4). For Test #1 and Test #2, the performance factors for Coil #1 were nearly the same for all heat transfer measurements which were 0.70, for Coil #2, Coil #3 and Coil #4 and the performance factor were 0.64, 0.55 and 0.53 respectively as presented in Table 5.15 and Table 5.16 (for Test #1 and Test #2). The performance factors are higher or lower than expected because the coils could be close to each other, or even might be touching each other, and that may limit the flow rate between these coils. Considering that Coil #4 is close to the shell; has the lowest performance factor when compared to other coils and this is due to the small clearance between the coil and the

shell. Table 5.16 and Table 5.17 also show the heat transfer inside each coil that was obtained for each test: Coil #1 ($qhx1_{EXP}$) Coil #2 ($qhx2_{EXP}$) Coil #3 ($qhx3_{EXP}$) and Coil #4 ($qhx4_{EXP}$).

Table 5.16 Performance factors for (S4CHX-W)-Test #1

q-hx	***qhx1$_{EXP}$***	***qhx2$_{EXP}$***	***qhx3$_{EXP}$***	***qhx4$_{EXP}$***	***PF.C1***	***PF.C2***	***PF.C3***	***PF.C4***
443	141	161	166	154	0.70	0.64	0.55	0.53
905	201	240	244	231	0.70	0.64	0.56	0.53
1383	299	374	355	346	0.70	0.64	0.55	0.53
1858	418	495	486	468	0.70	0.64	0.55	0.53
2345	532	662	616	581	0.70	0.65	0.55	0.52
2767	675	728	706	674	0.72	0.64	0.55	0.53

Table 5.17 Performance factors for (S4CHX-W)-Test #2

q-hx	***qhx1$_{EXP}$***	***qhx2$_{EXP}$***	***qhx3$_{EXP}$***	***qhx4$_{EXP}$***	***PF.C1***	***PF.C2***	***PF.C3***	***PF.C4***
402	129	144	146	136	0.7	0.64	0.55	0.54
888	197	250	228	217	0.7	0.64	0.55	0.53
1371	304	366	356	341	0.7	0.63	0.55	0.53
1840	428	493	478	458	0.71	0.63	0.55	0.52
2323	524	651	595	570	0.7	0.64	0.55	0.53
2820	670	743	723	680	0.72	0.63	0.55	0.52

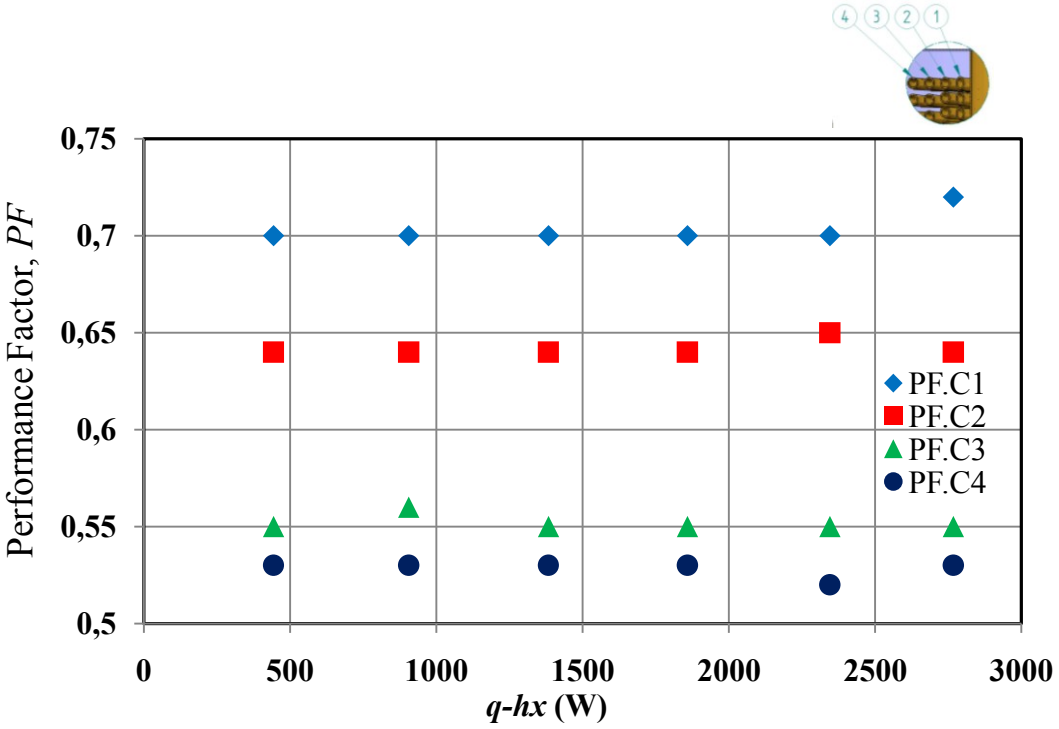

Figure 5.20 Performance factors for (S4CHX-W)-Test #1

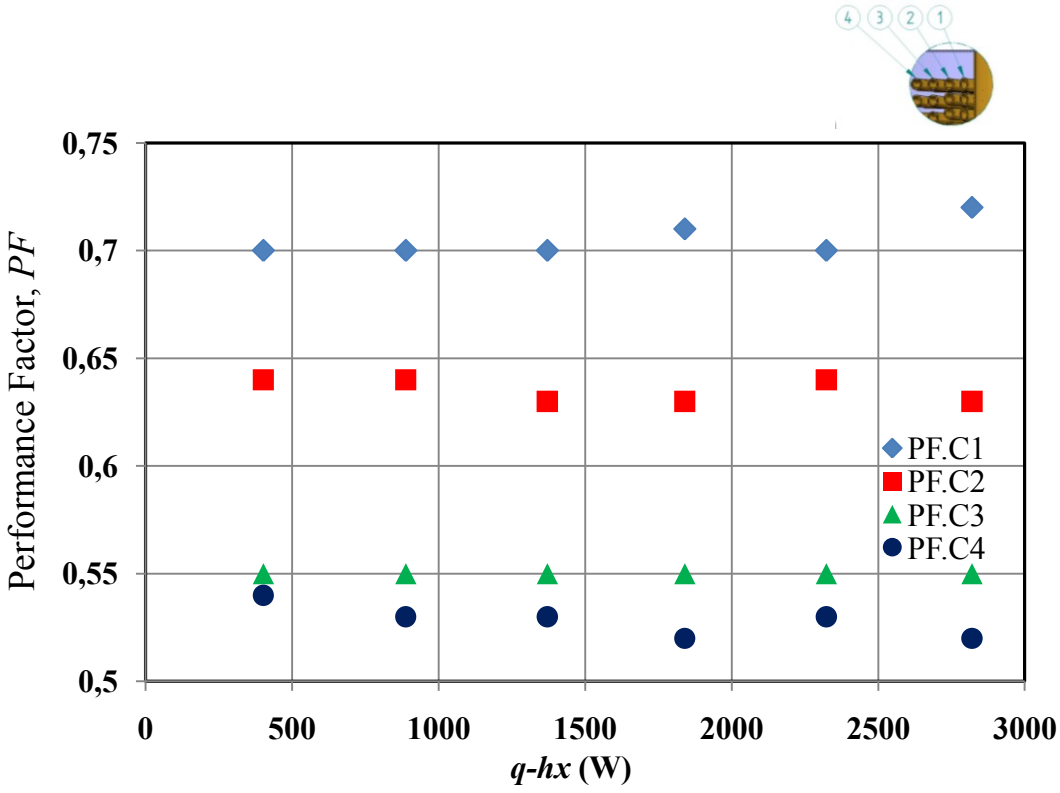

Figure 5.21 Performance factors for (S4CHX-W)-Test #2

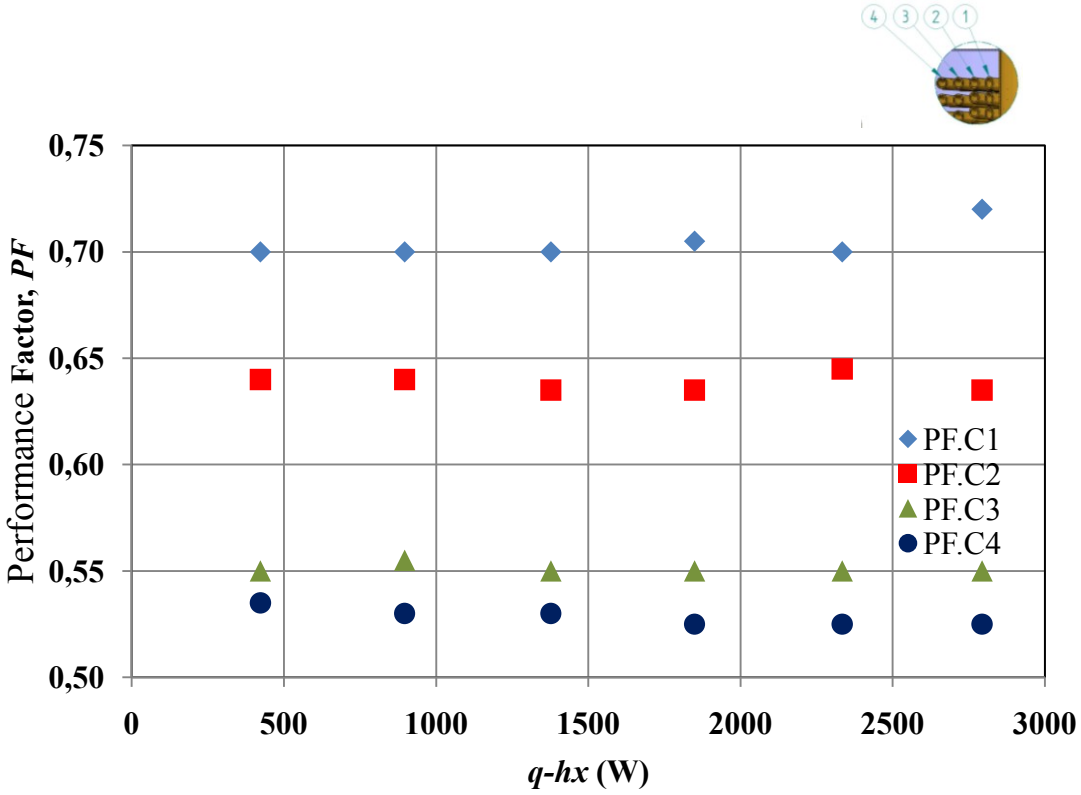

Figure 5.22 Average performance factors for S4CHX-W, Test#1 and Test #2

5.2.4 Model-3 (S3CHX-G)

Model-3 is identical in structure to Model-1. For Model-3, Model-1 was modified to use the properties of glycol instead of water on the tube side. As can be seen from Table 5.18, Table 5.19, Table 5.20 and Table 5.21 the *UA*-values are lower than those predicted at range of 323 W to 1381 W for all tests. Predicted *UA*-value for Test #1 at 2304 W was 204 W/K and the experimental *UA*-value was the same 204 W/K, and for Test #4 at 2332 W was 194 W/K which is the same *UA*-value from the experiment at the same heat transfer rate. The lower predicted *UA*-values when compared with the experimental *UA*-values were because the mass flow rates were very low. Moreover, the natural convection heat transfer coefficients can be attributed to the higher thermal resistance imposed by thicker boundary layers around the inside surface area of the shell which could obstruct the circulation of water around the tube. Figure 5.23 compares the measured and predicted *UA*-values for S3CHX-G

Table 5.18 Model-3 predictions for S3CHX-G-Test #1

$q\text{-}hx_{EXP}$	$q\text{-}hx_{TH}$	UA_{EXP}	UA_{PR}	T_{hi}	T_{ci}	$\dot{m}_h$	$\dot{m}_c$
430	430	72	124	37.2	20.7	0.055	0.057
904	908	131	145	40.5	20.9	0.081	0.066
1365	1365	159	164	47	22	0.100	0.073
1838	1837	184	188	54	26	0.111	0.089
2304	2306	204	204	60.9	29	0.117	0.101
2763	2769	218	216	68	32	0.120	0.108

Table 5.19 Model-3 predictions for S3CHX-G-Test #2

$q\text{-}hx_{EXP}$	$q\text{-}hx_{TH}$	UA_{EXP}	UA_{PR}	T_{hi}	T_{ci}	$\dot{m}_h$	$\dot{m}_c$
348	337	83	94	49	33	0.042	0.022
822	820	144	153	53	33.6	0.070	0.042
1283	1287	173	174	58	34	0.092	0.061
1778	1780	200	198	63	36	0.106	0.078
2240	2234	217	212	69	38	0.115	0.092
2719	2723	232	223	75	40.5	0.118	0.102

Table 5.20 Model-3 predictions for S3CHX-G-Test #3

$q\text{-}hx_{EXP}$	$q\text{-}hx_{TH}$	UA_{EXP}	UA_{PR}	T_{hi}	T_{ci}	$\dot{m}_h$	$\dot{m}_c$
323	321	79	131	53	38	0.055	0.032
797	801	148	156	57	39	0.081	0.053
1278	1279	180	190	63	41	0.099	0.077
1758	1761	202	211	69	44	0.111	0.097
2187	2186	216	224	75	46	0.118	0.107
2681	2678	237	235	81	48	0.120	0.111

Table 5.21 Model-3 predictions for S3CHX-G-Test #4

$q\text{-}hx_{EXP}$	$q\text{-}hx_{TH}$	UA_{EXP}	UA_{PR}	T_{hi}	T_{ci}	$\dot{m}_h$	$\dot{m}_c$
354	342	80	179	47	32	0.070	0.034
904	905	141	147	40	22	0.096	0.068
1381	1387	161	167	45	22	0.114	0.083
1856	1864	179	184	50	23	0.125	0.088
2332	2337	194	194	56	23	0.132	0.091
2798	2788	215	216	65	29	0.136	0.099

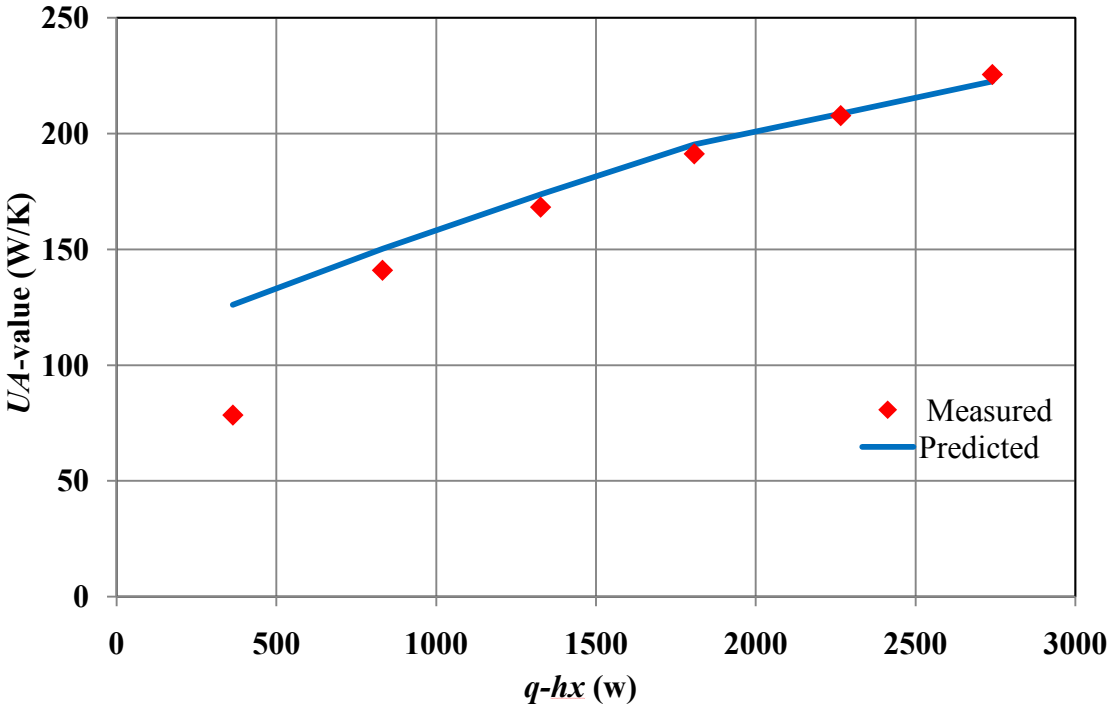

Figure 5.23 Model-3 predictions for (S3CHX-G) performance

Table 5.22, Table 5.23, Table 5.24 and Table 5.25 show the performance factors for each coil in Test #1, Test #2, Test #3 and Test #4, respectively, for the S3CHX-G. These tables also show the heat transfer rate for each coil obtained from the experiment. The five figures, showing the performance factors for the 4 tests and the average are presented. Figure 5.24 shows the performance factors for Test #1; for the inner most coil the performance factor was 0.70, but at 1365 and 1838 W it was 0.69, which is a little lower while at 2763 W it was a little higher at 0.71. For coil #2 the performance factor was 0.66, but at 904 W it was 0.65 and at 1365 and 2763 W it was 0.67. For the outer most (coil #3), it was 0.53. Figure 5.25 represents the performance factors for the second test (Test #2). For the innermost coil the performance factor was the same as Test #1. For coil #2 it was a little different than that of Test #1; which was about 0.67 except for 348 and 1778 W that was 0.66. Figures 5.26 and 5.27 illustrate the performance factors for Test #3 and Test #4 respectively, for both tests the plenty factors were the same, in a range of 0.69-

0.71 for coil #1 and 0.65-0.67 for coil #2, and 0.52-0.54 for coil #3. Figure 5.28 represents the average of the performance factors for the 4 tests, and the graph shows that the performance factor was 0.7 for coil #1, 0.66 for coil #2 and 0.53 for coil #3, which are the same values as obtained for the tests with water as the tube-side liquid.

Table 5.22 Performance factors for (S3CHX-G)-Test #1

q-hx	***qhx1$_{EXP}$***	***qhx2$_{EXP}$***	***qhx3$_{EXP}$***	***PF.C1***	***PF.C2***	***PF.C3***
430	140	145	145	0.70	0.66	0.53
904	280	316	307	0.70	0.65	0.53
1365	398	499	469	0.69	0.67	0.53
1838	548	653	637	0.69	0.66	0.53
2304	700	806	797	0.70	0.66	0.53
2763	854	960	949	0.71	0.67	0.53

Table 5.23 Performance factors for (S3CHX-G)-Test #2

q-hx	***qhx1$_{EXP}$***	***qhx2$_{EXP}$***	***qhx3$_{EXP}$***	***PF.C1***	***PF.C2***	***PF.C3***
348	100	121	127	0.70	0.66	0.53
822	230	294	298	0.69	0.67	0.54
1283	364	469	448	0.69	0.67	0.53
1778	535	625	619	0.70	0.66	0.53
2240	677	801	763	0.70	0.67	0.52
2719	837	965	918	0.71	0.67	0.52

Table 5.24 Performance factors for (S3CHX-G)-Test #3

q-hx	***qhx1$_{EXP}$***	***qhx2$_{EXP}$***	***qhx3$_{EXP}$***	***PF.C1***	***PF.C2***	***PF.C3***
323	91	116	116	0.70	0.66	0.53
797	234	280	283	0.69	0.66	0.53
1278	387	448	441	0.70	0.66	0.53
1758	553	628	578	0.69	0.66	0.52
2187	690	755	742	0.71	0.65	0.52
2681	838	913	927	0.71	0.65	0.53

Table 5.25 Performance factors for (S3CHX-G)-Test #4

q-hx	***qhx1$_{EXP}$***	***qhx2$_{EXP}$***	***qhx3$_{EXP}$***	***PF.C1***	***PF.C2***	***PF.C3***
354	96	129	130	0.69	0.66	0.54
904	264	326	313	0.70	0.66	0.53
1381	402	495	484	0.69	0.66	0.53
1856	536	664	655	0.69	0.66	0.53
2332	664	847	820	0.68	0.67	0.53
2798	829	998	970	0.70	0.67	0.53

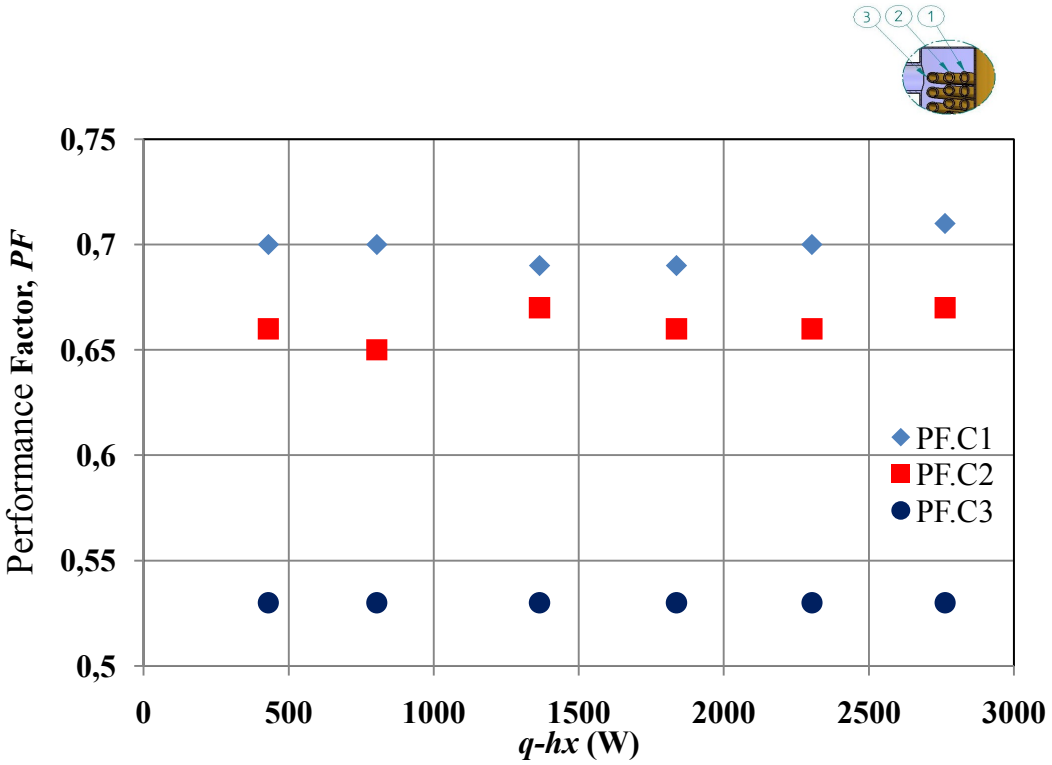

Figure 5.24 Performance factors for (S3CHX-G)-Test #1

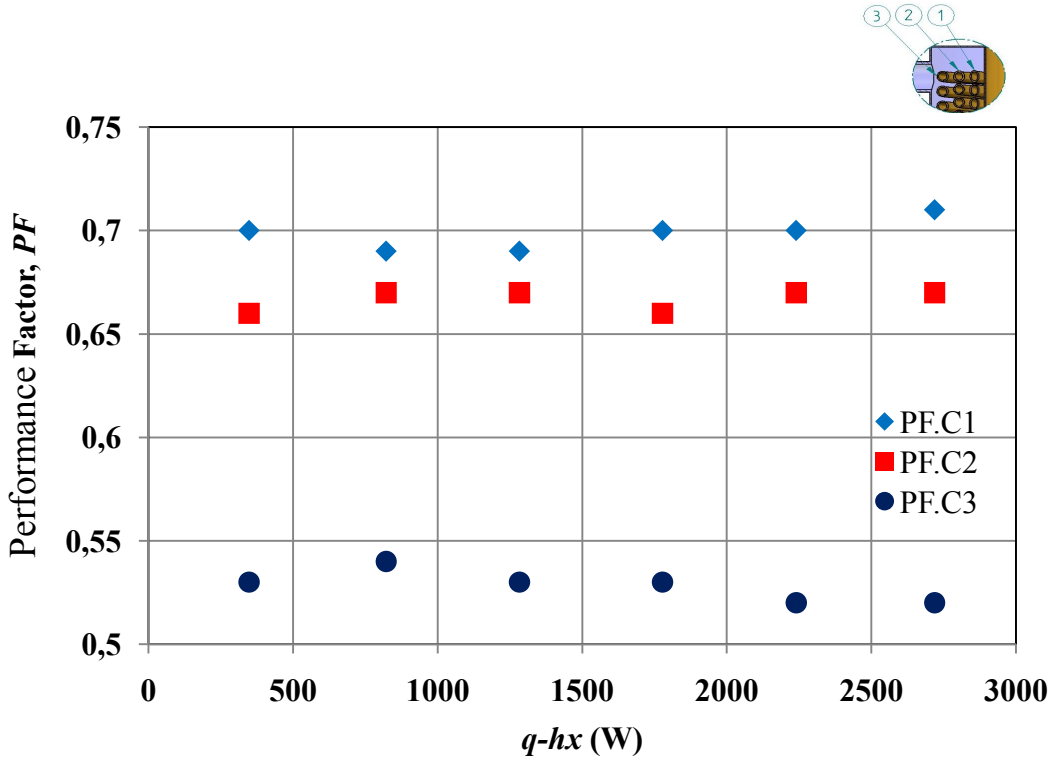

Figure 5.25 Performance factors for (S3CHX-G)-Test #2

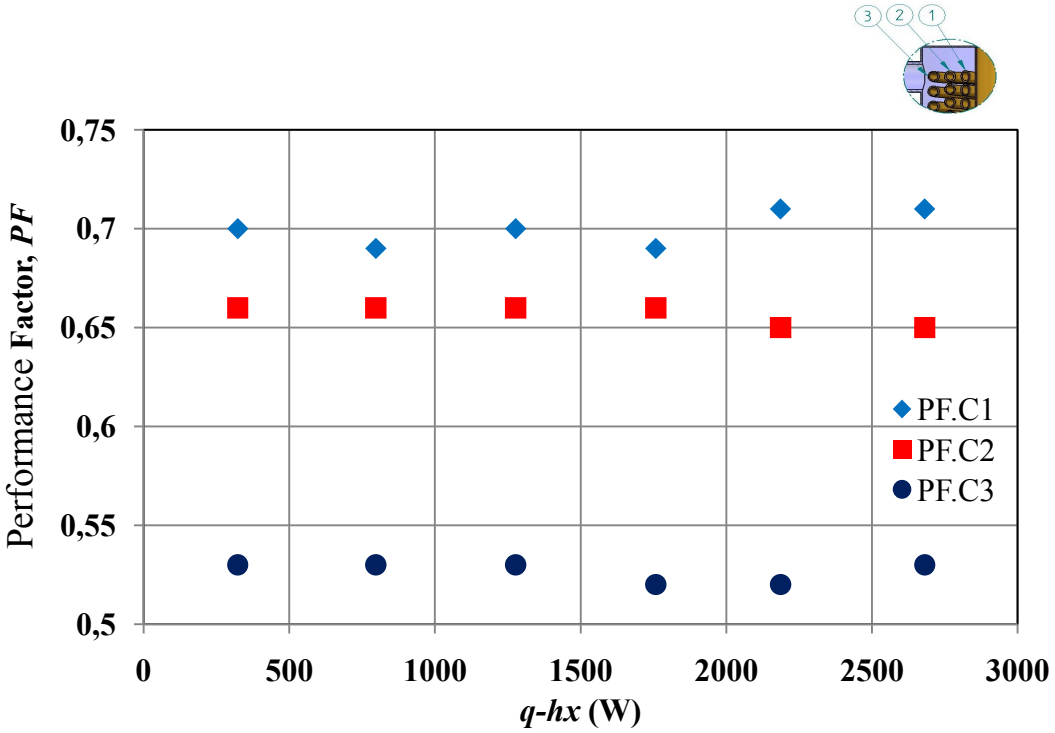

Figure 5.26 Performance factors for (S3CHX-G)-Test #3

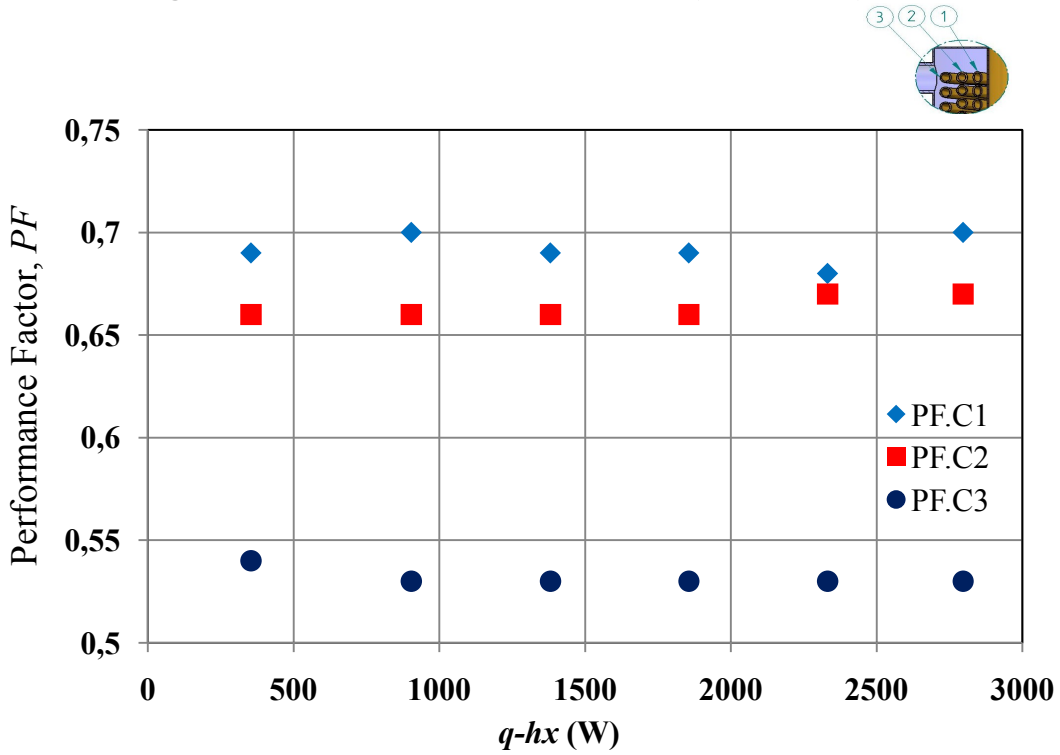

Figure 5.27 Performance factors for (S3CHX-G)-Test #4

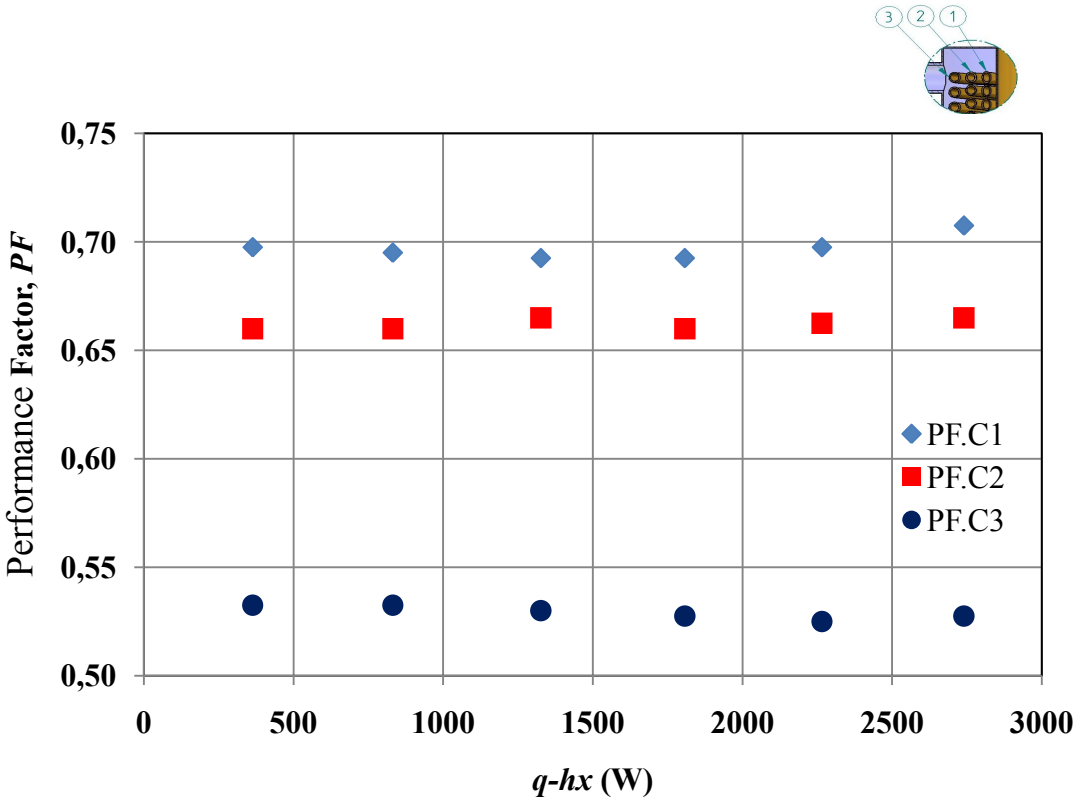

Figure 5.28 Performance factors for (S3CHX-G)- Average 4 Tests

5.2.5 Model-4 (S4CHX-G)

Model-4 and Model-2 have the same set up except that water was used as the fluid for Model-2 on the tube side and glycol was used for Model-4. The *UA*-values that were calculated from the experimental data and the predicted from the model for each test show in Table 5.26, Table 5.27, Table 5.28 and Table 5.29 for Test #1, Test #2, Test #3 and Test #4, respectively. All tests show that at higher flow rates the model is more accurate for the predicted *UA*-values. The tables also show the glycol inlet temperature ($T_{hx,i}$), inlet mass flow rate to the coils (*mdh***)**, the inlet water temperature to the shell (T_{ci}) and the inlet mass flow rates to the shell (*mdcw*). As can be seen from these tables these parameters have a great influence on the predicted UA_{PR}.

The predicted values in Figure 5.29 were obtained by taking the average values for the four tests. Both the predicted UA_{PR} values and the experiment UA_{EXP} values versus the heat transfer rate $q\text{-}hx_{EXP}$ were plotted in the same graph. The figure shows a reasonable agreement between the experimental result and the model in terms of the *UA*-values, especially at a high heat transfer rate for the same reason stated in the previous model.

Table 5.26 Model-4 predictions for S4CHX-G-Test #1

$q\text{-}hx_{EXP}$	$q\text{-}hx_{TH}$	UA_{EXP}	UA_{PR}	T_{hi}	T_{ci}	$\dot{m}_h$	$\dot{m}_c$
432	430	88	100	41	25	0.039	0.031
891	890	159	180	45	26	0.078	0.052
1362	1366	189	190	51	27	0.095	0.065
1833	1835	216	229	59	31	0.109	0.078
2288	2281	233	249	67	35	0.116	0.083
2735	2735	256	256	76	40	0.122	0.088

Table 5.27 Model-4 predictions for S4CHX-G-Test#2

$q\text{-}hx_{EXP}$	$q\text{-}hx_{TH}$	UA_{EXP}	UA_{PR}	T_{hi}	T_{ci}	$\dot{m}_h$	$\dot{m}_c$
489	489	82	124	32	14	0.035	0.031
963	962	138	158	35	14	0.074	0.047
1440	1440	168	170	41	14	0.089	0.060
1920	1920	196	199	46	14	0.103	0.068
2380	2379	214	215	52	15	0.109	0.074
2817	2817	229	234	58	19	0.113	0.081

Table 5.28 Model-4 predictions for S4CHX-G-Test#3

$q\text{-}hx_{EXP}$	$q\text{-}hx_{TH}$	UA_{EXP}	UA_{PR}	T_{hi}	T_{ci}	$\dot{m}_h$	$\dot{m}_c$
551	549	104	140	35	19	0.058	0.036
938	944	163	170	38	19	0.091	0.056
1405	1405	192	194	43	19	0.108	0.067
1891	1891	209	214	49	20	0.117	0.074
2373	2379	225	230	54	20	0.129	0.079
2845	2846	248	250	60	23	0.138	0.086

Table 5.29 Model-4 predictions for S4CHX-G-Test#4

$q\text{-}hx_{EXP}$	$q\text{-}hx_{TH}$	UA_{EXP}	UA_{PR}	T_{hi}	T_{ci}	$\dot{m}_h$	$\dot{m}_c$
375	385	73	160	45	26	0.067	0.025
874	878	152	189	49	28	0.094	0.042
1335	1335	191	216	54	29	0.112	0.058
1835	1835	221	228	58	32	0.125	0.070
2271	2269	243	257	66	35	0.132	0.082
2741	2743	264	275	73	40	0.135	0.090

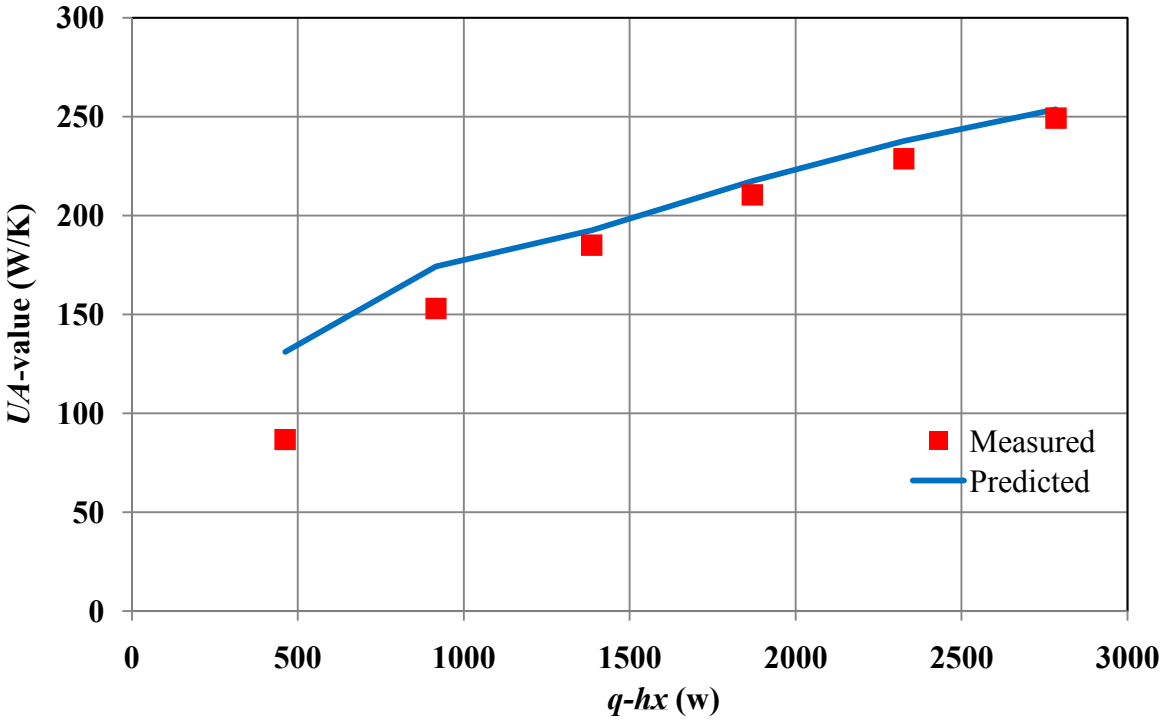

Figure 5.29 Model-4 predictions for (S4CHX-G) performance

Table 5.30, Table 5.31, Table 5.32 and Table 5.33 show the performance factors for each coil in Test #1, Test #2, Test #3 and Test #4, respectively, for the model of S4CHX-G. These tables also show the heat transfer rates for each coil that were obtained from the experiment. For all tests, the heat transfer rates are slightly different from one test to another. However, the performance factors are roughly the same for each coil for all tests. Coil #1 was 0.70, coil #2 was 0.64, coil #3 was 0.55 and for coil #4 was 0.53. These are the same values as obtained for the coils with water on the tube side. The performance factors were also plotted versus the heat transfer heat exchanger for each test. Figure 5.30 shows this for Test #1 and at 2735 W the performance factor for coil #1 was 0.72, coil #3 was 0.54 and coil #4 was 0.52. This is slightly different from other performance factors at different heat transfer rate, which indicates for at least two performance factors that different coils effect the performance factor for the others. This can also be seen for the

other tests in the following figures: Figure 5.31 for Test #2, Figure 5.32 for Test #3 and Figure 5.33 for Test #4. The average performance factor for S4CHX-G are plotted in Figure 5.31, which represents the average of the performance factors for the 4 tests, 0.7, 0.64, 0.55 and 0.53 for coil #1, coil #2, coil #3 and coil #4 respectively.

Table 5.30 Performance factors for (S4CHX-G)-Test #1

q-hx	***qhx1$_{EXP}$***	***qhx2$_{EXP}$***	***qhx3$_{EXP}$***	***qhx4$_{EXP}$***	***PF.C1***	***PF.C2***	***PF.C3***	***PF.C4***
432	187	221	214	203	0.70	0.64	0.55	0.53
891	261	290	300	284	0.70	0.64	0.55	0.53
1362	375	424	437	426	0.70	0.64	0.55	0.53
1833	482	539	569	548	0.70	0.64	0.55	0.53
2288	590	666	690	663	0.70	0.64	0.55	0.52
2735	706	779	794	761	0.72	0.64	0.54	0.52

Table 5.31 Performance factors for (S4CHX-G)-Test #2

q-hx	***qhx1$_{EXP}$***	***qhx2$_{EXP}$***	***qhx3$_{EXP}$***	***qhx4$_{EXP}$***	***PF.C1***	***PF.C2***	***PF.C3***	***PF.C4***
489	228	270	267	250	0.69	0.64	0.55	0.54
963	290	345	339	336	0.69	0.64	0.55	0.53
1440	427	487	497	480	0.69	0.63	0.56	0.53
1920	544	613	640	611	0.69	0.63	0.56	0.53
2380	665	755	786	745	0.68	0.64	0.55	0.53
2817	770	875	906	867	0.69	0.63	0.56	0.53

Table 5.32 Performance factors for (S4CHX-G)-Test #3

q-hx	$qhx1_{EXP}$	$qhx2_{EXP}$	$qhx3_{EXP}$	$qhx4_{EXP}$	***PF.C1***	***PF.C2***	***PF.C3***	***PF.C4***
551	156	189	193	191	0.70	0.64	0.55	0.54
938	226	255	271	261	0.70	0.64	0.55	0.53
1405	337	382	406	385	0.70	0.63	0.56	0.53
1891	443	518	538	522	0.69	0.63	0.56	0.53
2373	548	615	616	648	0.70	0.63	0.55	0.54
2845	626	732	736	722	0.70	0.64	0.55	0.53

Table 5.33 Performance factors for (S4CHX-G)-Test #4

q-hx	$qhx1_{EXP}$	$qhx2_{EXP}$	$qhx3_{EXP}$	$qhx4_{EXP}$	***PF.C1***	***PF.C2***	***PF.C3***	***PF.C4***
375	125	114	120	128	0.72	0.62	0.54	0.53
874	181	212	237	240	0.70	0.63	0.56	0.54
1335	277	328	361	354	0.69	0.63	0.55	0.53
1835	379	457	475	470	0.69	0.63	0.56	0.54
2271	494	565	594	573	0.70	0.63	0.56	0.53
2741	587	684	681	667	0.70	0.64	0.55	0.53

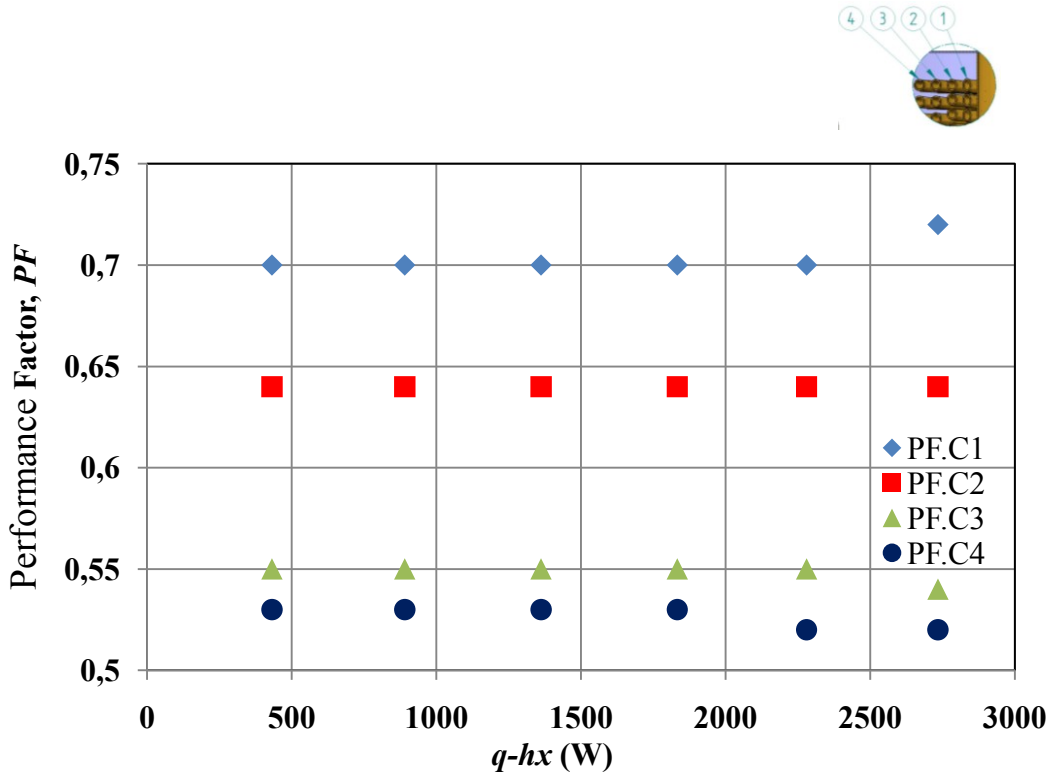

Figure 5.30 Performance factors for (S4CHX-G)-Test #1

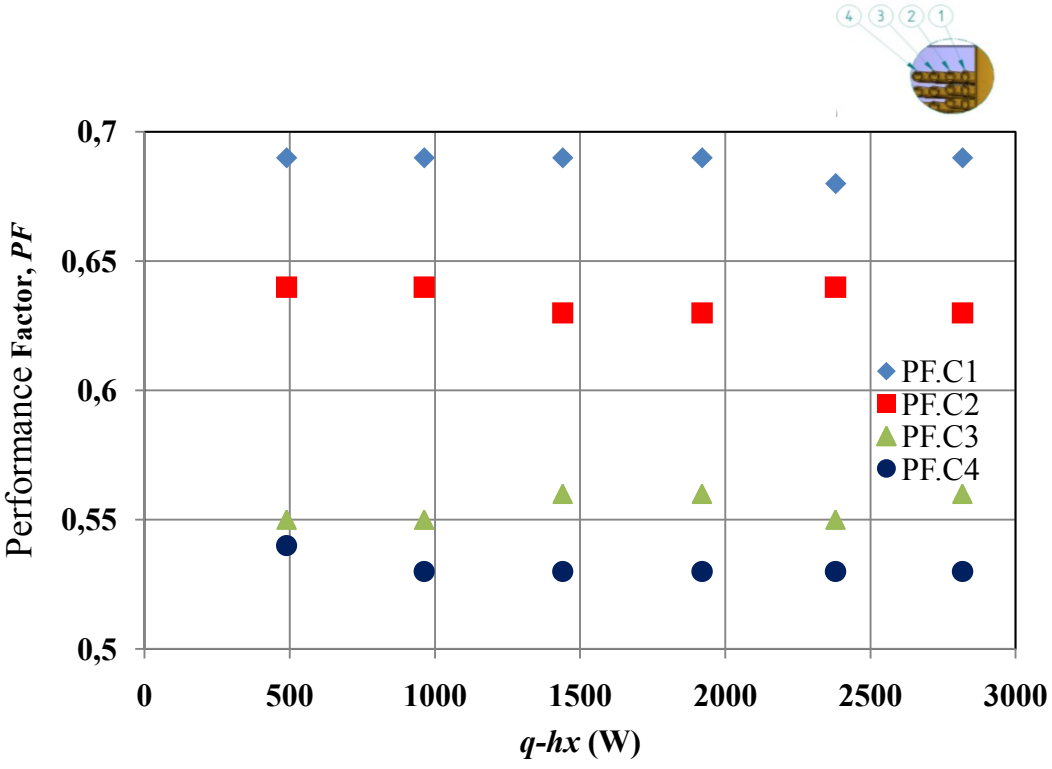

Figure 5.31 Performance factors for (S4CHX-G)-Test #2

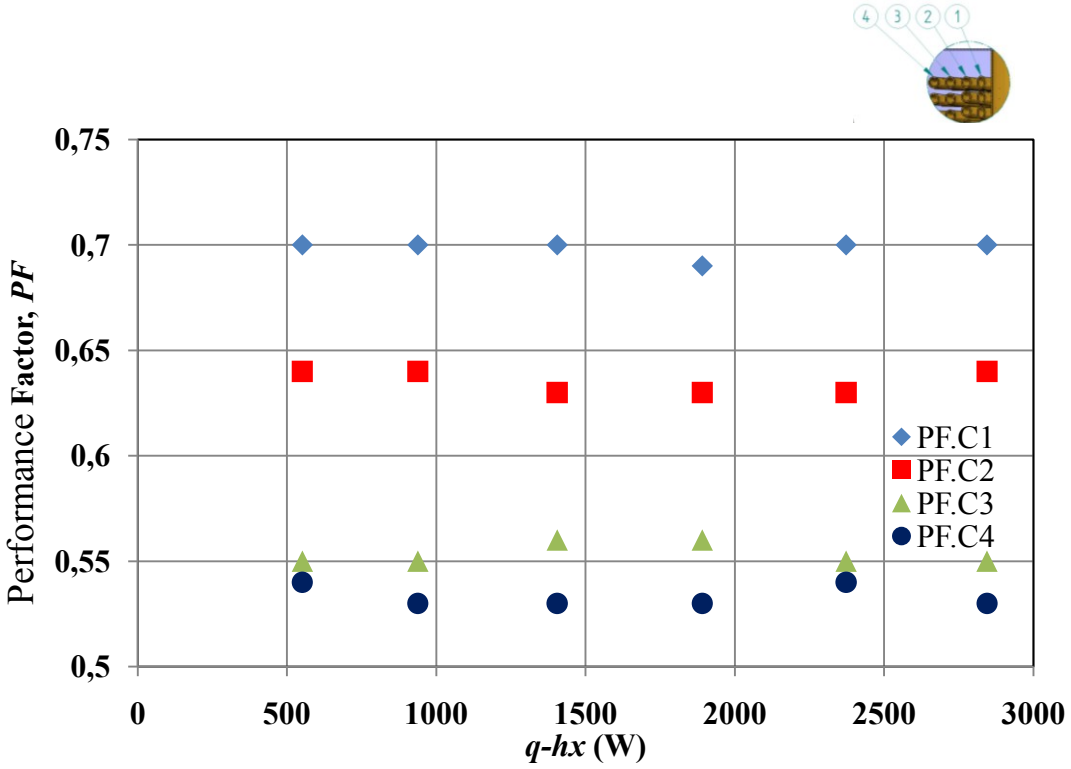

Figure 5.32 Performance factors for (S4CHX-G)-Test #3

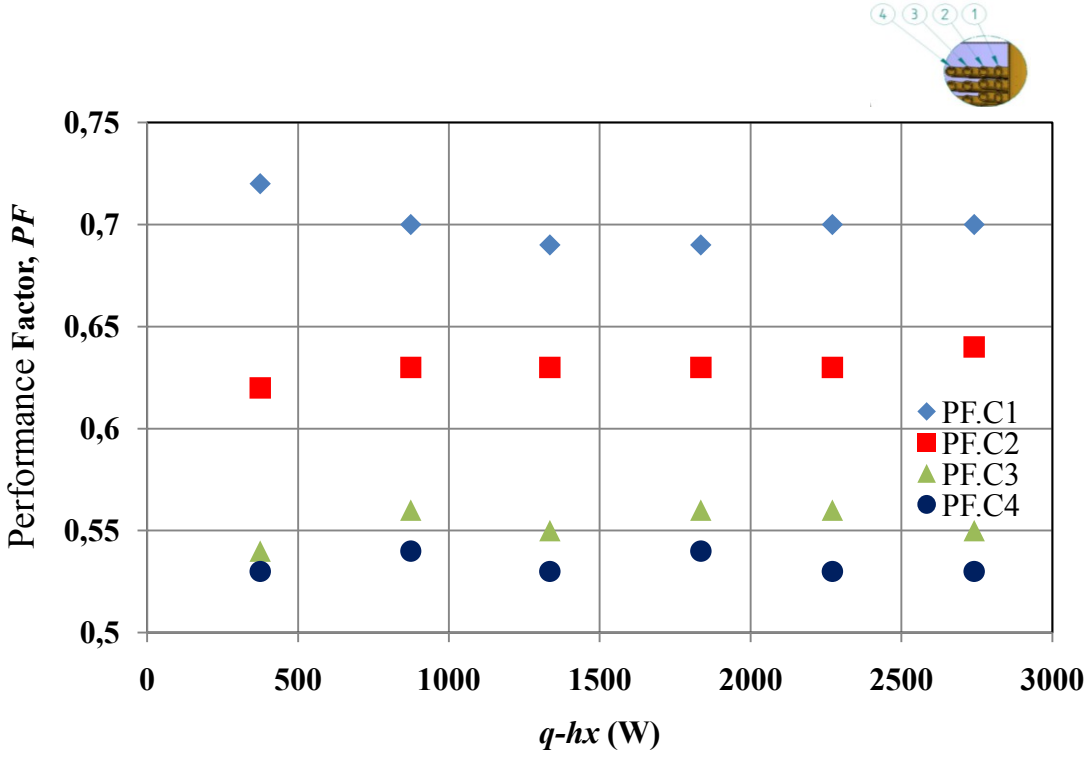

Figure 5.33 Performance factors for (S4CHX-G)-Test #4

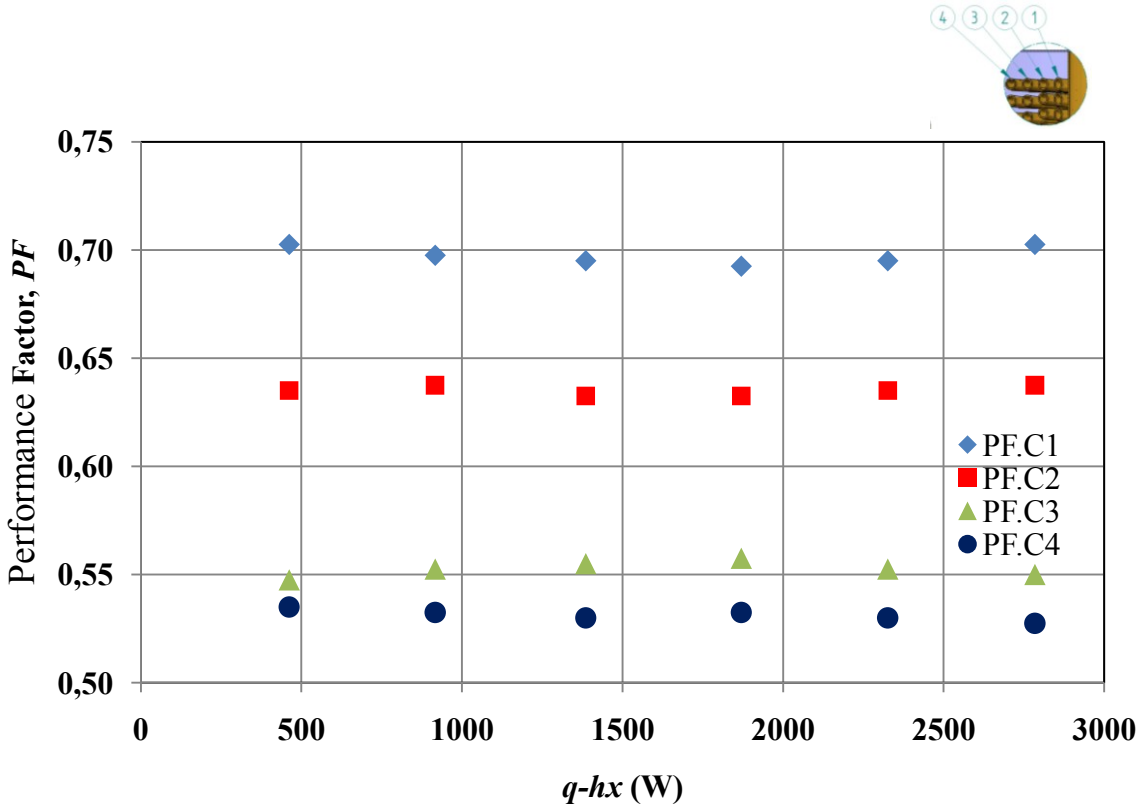

Figure 5.34 Performance factors for (S4CHX-G)-average 4Tests

Table 5.34 illustrates the average of the performance factors for S3CHX and S4CHX. The performance factor for S3CHX-W and S3CHX-G were 0.70, 0.66 and 0.53 for coil #1, coil #2 and coil #3 respectively, and for S4CHX-W and S4CHX-G were 0.70, 0.64, 0.55 and 0.53 for coil #1, coil #2, coil #3 and coil #4 respectively. The sum of the gaps between coil #1/#2 and coil #2/#3 is smaller than the sum of the gaps between coil# 4/#3 and coil #3/#2. However, the performance factor for coil #3 is lower than the performance factor for coil #2 for S4CHX and this is because the flow through the small gap results in higher velocity when compared to the flow in the big gaps.

Table 5.34 Performance factors for S3CHX and S4CHX

	Coil #1	Coil #2	Coil #3	Coil #4
S3CHX	0.70	0.66	0.53	N/A
S4CHX	0.70	0.64	0.55	0.53

CHAPTER 6

CONCLUSIONS

6.1 Summary

The performance of several external shell-and-coil heat exchangers was investigated experimentally and theoretically. As Shell-and-3coil heat exchanger and a shell-and-4coil heat exchanger were tested and compared. Two electrical heaters were used to simulate the solar collectors in a real SDHW system. The fluids used as working fluid in the tube side were water and a 38% solution propylene glycol. The results from the experimental studies were compared with the theoretical models and the general conclusions related to the experimental setup and testing procedure used is as follows:

I. The thermal performance of the heat exchangers (*UA*-value) was observed to be a function of the glycol or water flow rate on the tube side, and the temperature inlet and outlet for both sides of the heat exchangers.

II. In order to obtain higher *UA*-values, the heat transfer coefficients on the shell side (h_o) were consistently smaller on the natural convection side, which indicates that efforts should be concentrated on improving the h_o values. On the outside and inside the tube, the overall heat transfer coefficient-area product (*UA*-value) of the heat exchangers was a function of both the area and heat transfer coefficients.

6.2 Specific Conclusions

Two different external shell-and-coil heat exchangers were built and tested, and their thermal performance were compared in terms of the *UA*-value. The collected data from the experiments were used as input for four models constructed to predict the *UA*-value based on performance factors for each coil. The following are the conclusions drawn from both the experimental results and the model predictions:

1) S3CHX-W and S4CHX-W: the overall heat transfer coefficient-area product (*UA*-value) varied between 45 and 276 W/K for the S3CHX-W, and 84 and 312 W/K for the S4CHX-W.

2) S3CHX-G and S4CHX-G: The overall heat transfer coefficient-area product (*UA*-value) for S3CHX-G, and S4CHX-G varied between 38 and 225 W/K and, 63 and 251 W/K respectively.

3) At the same heat transfer rate, *q-hx*, *UA*-values was always higher for both heat exchangers when water was used as working fluid on the tube side as when compared to glycol. This was because water is a better heat transfer than glycol (the specific heat capacity, C_p ,of water is higher than for glycol) and the thermal conductivity of water is higher

4) The *UA*-value of S4CHX-W was always higher than that of S3CHX-W at the same heat transfer rate. Similarly, the *UA*-value of S4CHX-G was also higher than S3CHX-G; however, the difference was not much between the two heat exchangers for both glycol and water when used as working fluid on the tube side. S4CHX *UA*-values were always higher because it has a larger surface area. This is illustrated in figure 5.5 for S3CHX-W and S4CHX-W, and figure 5.11 for S3CHX-G and S4CHX-G.

5) The performance factor did not depend on glycol versus water and heat rate.
6) The S3CHX is suggested to be used instead of S4CHX due to the performance in terms of the cost.
7) The actual *UA*-values for both heat exchangers and both water and glycol on the tube side are expected to be lower than those predicted, considering the additional thermal resistances created between consecutive coil turns.
8) The *UA*-value profiles were of the logarithmic form for both heat exchangers.
9) The effect of increasing the heat transfer rate was to increase the slope of the axial temperature profiles.
10) The thermal performance of each coil in all the heat exchangers was found to be below that predicted by application of the relevant heat transfer correlations.
11) For both glycol and water, and both heat exchangers, the performance factors for the inner most and outer most coils were 0.70 and 0.53, respectively. The outermost coil (#3/#4) had the lowest performance factor due to small clearance between the shell and the coil also for the same reason between the coil #1 and coil #3 and, coil #3 and coil #4, thus the flow was obstructed, resulting in lower heat transfer.
12) The performance factor for coil #3 is lower than the performance factor for coil #2 for S4CHX and this is because the flow in the small gap results in a higher velocity when compared to the flow in the large gaps
13) The S4CHX has 52 % more surface area than the S3CHX, however, *UA* for the S4CHX is only 13 % greater than *UA* for the S3CHX.
14) The performance factor did not depend on glycol versus water and did not depend on heat rate, 0.53, 0.66 and 0.7 for S3CHX and 0.53, 0.55, 0.64, 0.7 for S4CHX and was constant from test to the other.
15) Comparison was made with results of other authors that used helical coil heat exchangers, and it was seen to increase the heat transfer coefficient when compared to a similarly dimensioned straight tube heat exchanger.

16) The degradation of the thermal performance of the shell-and-3coil was offset by benefits, such as reduction in mass, volume, labor cost and the final cost. Table B.3 shows the total mass and the cost for S3CHX and S4CHX.

6.3 Recommendations for future work

The spaces between each coil and the shell should be studied because of its effect on the heat exchanger performance and also to allow water to flow freely around the coils. Having a rod going down from the top to the bottom at three locations to keep coil #1 centered with coil #2 and another three rods keeping coil #2 centered with coil #3 and another set keeping coil #3 centered with the shell for S3CHX. This procedure can be repeated for S4CHX.

REFERENCES

[1] Salimpour, M. R. (2008, 11). Heat transfer characteristics of a temperature-dependent-property fluid in shell and coiled tube heat exchangers. *Int. Commun. Heat Mass Transfer 35(9),* pp. 1190-1195.

[2] Taherian, H.(1998). "Natural convection heat transfer in heat exchangers with vertical helical coils." Ph.D. thesis, Dalhousie University, Halifax, Nova Sc otia.

[3] H. Shokouhmand, M. R. Salimpour and M. A. Akhavan-Behabadi. (2008, 1). Experimental investigation of shell and coiled tube heat exchangers using wilson plots. *Int. Commun. Heat Mass Transfer 35(1),* pp. 84-92.

[4] V. Kumar, M. Mridha, A. K. Gupta and K. D. P. Nigam. (2007, 5). Coiled flow inverter as a heat exchanger. *Chemical Engineering Science 62(9),* pp. 2386-2396.

[5] Bergelt, T. K., Brunger, A. P., and Hollands, K. G.(1993), "Optimum hydraulic resistance for natural convection SDHW heat exchanger loops.

[6] Srinivasan,V., Christensen, R., "full-scale, testing, and analysis of an innovative natural-convection-driven heat-recouvery heat exchangerfor space-condtioning applications," *Heat Transfer Engineering,* vol. 15, pp. 44-54, 1994.

[7] White, L. M., Allen, P.L., Van Rossum, N.J.(1990), "Development of a new SDHW heat exchanger," 16th Annual conference of the solar energy society of heat-recouvery canada,

[8] D. Richmond. (1989). Numerical solution of an open cavity, natural convection heat exchanger. *Journal of Heat Transfer 111(1),* pp. 80.

[9] M. Parent. (1990), Natural convection heat exchangers in solar water heating systems. theory and experiment. *Solar Energy 45(1),* pp. 43.

[10] Ajele, O. J (1995) "Natural convection heat transfer from enclosed helical coils". Unpublished Ph.D. thesis, Technical University of Nova Scotia, Halifax, Nova Scotia 1995.

[11] Avina, J. (1995), "The modeling of a natural convection heat exchanger in a solar domestic hot water system". Master's thesis, University of Wisconsin-Madison, Madison, U.S.A.

[12] Salimpour, M. R.. (2009, 1). Heat transfer coefficients of shell and coiled tube heat exchangers. *Exp. Therm. Fluid Sci. 33(2),* pp. 203-207.

[13] S. Furbo, E. Andersen, S. Knudsen, N. K. Vejen and L. J. Shah. (2005, 2). Smart solar tanks for small solar domestic hot water systems. *Solar Energy 78(2),* pp. 269-279.

[14] M. Bojic, S. Kalogirou and K. Petronijevic. (2002, 11). Simulation of a solar domestic water heating system using a time marching model. *Renewable Energy 27(3),* pp. 441-452.

[15] Hollands, K.G.T and Brunger, A.P. "Optimum flow rates in solar water heating systems with a counterflow exchanger," vol. 48,No.1,pp,15-19, pp. 15, 1991.

[16] Gertzos, K. P. S. E. Pnevmatikakis and Caouris, Y. G. (2008, 11). Experimental and numerical study of heat transfer phenomena, inside a flat-plate integrated collector storage solar water heater (ICSSWH), with indirect heat withdrawal. *Energy Conversion and Management 49(11),* pp. 3104-3115.

[17] Rao,N.M., Maiti,B. and K. Das,P. (2008) Stability behavior of a natural circulation loop with end heat exchanger. *127(August 2008),*

[18] Prabhanjan, D. G. T. J. Rennie and Vijaya Raghavan, G. S. (2004, 4). Natural convection heat transfer from helical coiled tubes. *International Journal of Thermal Sciences 43(4),* pp. 359-365.

[19] Macleod, B.K (1998) "Evaluation of components in solar water heaters with photovoltaic powered pumps".Unpublished Master's thesis, Dalhousie University, Halifax, Nova Scotia.

[20] Xin, R. (1996, Natural convection heat transfer from helicoidal pipes. *J. Thermophys. Heat Transfer 10(2),* pp. 297.

[21] Fraser, K. F. Hollands, K. G. T. and Brunger, A. P. (1995, 8). An empirical model for natural convection heat exchangers in SDHW systems. *Solar Energy 55(2),* pp. 75-84.

[22] Ali, M.. (1994) Experimental investigation of natural convection from vertical helical coiled tubes. *Int. J. Heat Mass Transfer 37(4),* pp. 665.

[23] Conté, I. and Peng, X. F.. (2009, 6). Numerical and experimental investigations of heat transfer performance of rectangular coil heat exchangers. *Appl. Therm. Eng. 29(8-9),* pp. 1799-1808.

[24] Jayakumar, J. S. Mahajani, S. M. Mandal, J. C. Vijayan, P. K. and Bhoi, R. (2008, 3). Experimental and CFD estimation of heat transfer in helically coiled heat exchangers. *Chem. Eng. Res. Design 86(3),* pp. 221-232.

[25] Gupta, P. K. Kush, P. K. and Tiwari, A. (2007, 6). Design and optimization of coil finned-tube heat exchangers for cryogenic applications. *Cryogenics 47(5-6),* pp. 322-332.

[26] Coronel, P.(2008) Heat transfer coefficient in helical heat exchangers under turbulent flow conditions. *International Journal of Food Engineering 4(1),*

[27] Hosseini, R. Hosseini-Ghaffar, A. and Soltani, M. (2007, 4). Experimental determination of shell side heat transfer coefficient and pressure drop for an oil cooler shell-and-tube heat exchanger with three different tube bundles. *Appl. Therm. Eng. 27(5-6),* pp. 1001-1008.

[28] Fernando, P. Palm, B. Ameel, T. Lundqvist, P. and Granryd, E. (2008, 6). A minichannel aluminium tube heat exchanger – part I: Evaluation of single-phase heat transfer coefficients by the wilson plot method. *Int. J. Refrig. 31(4),* pp. 669-680.

[29] Naphon, P. (2007, 3). Thermal performance and pressure drop of the helical-coil heat exchangers with and without helically crimped fins. *Int. Commun. Heat Mass Transfer 34(3),* pp. 321-330.

[30] Prabhanjan, D. G. Raghavan, G. S. V. and Rennie, T. J. (2002, 2). Comparison of heat transfer rates between a straight tube heat exchanger and a helically coiled heat exchanger. *Int. Commun. Heat Mass Transfer 29(2),* pp. 185-191.

[31] Camacho-Duke, J.A.(2002) "Experimental study of low flow immersion heat exchangers. (Master's thesis, Dalhousie University,2002).

[32] Incropera, F. P.,& DeWitt, D.P.(2007). *Fundamentals of Heat and Mass Transfer* (6th ed.). New York: Wiley.

[33] Manlapaz, R. L., & Churchill, S. W. (1980) Fully Developed Laminar Flow in A Helically Coiled Tube of Finite Pitch. *Chem. Eng. Commun. 7(1-3),* pp. 57.

APPENDIX A

EXPERIMENTAL SETUP

1. VARIAC AND AUTO TRANSFORMER SPECIFICATION

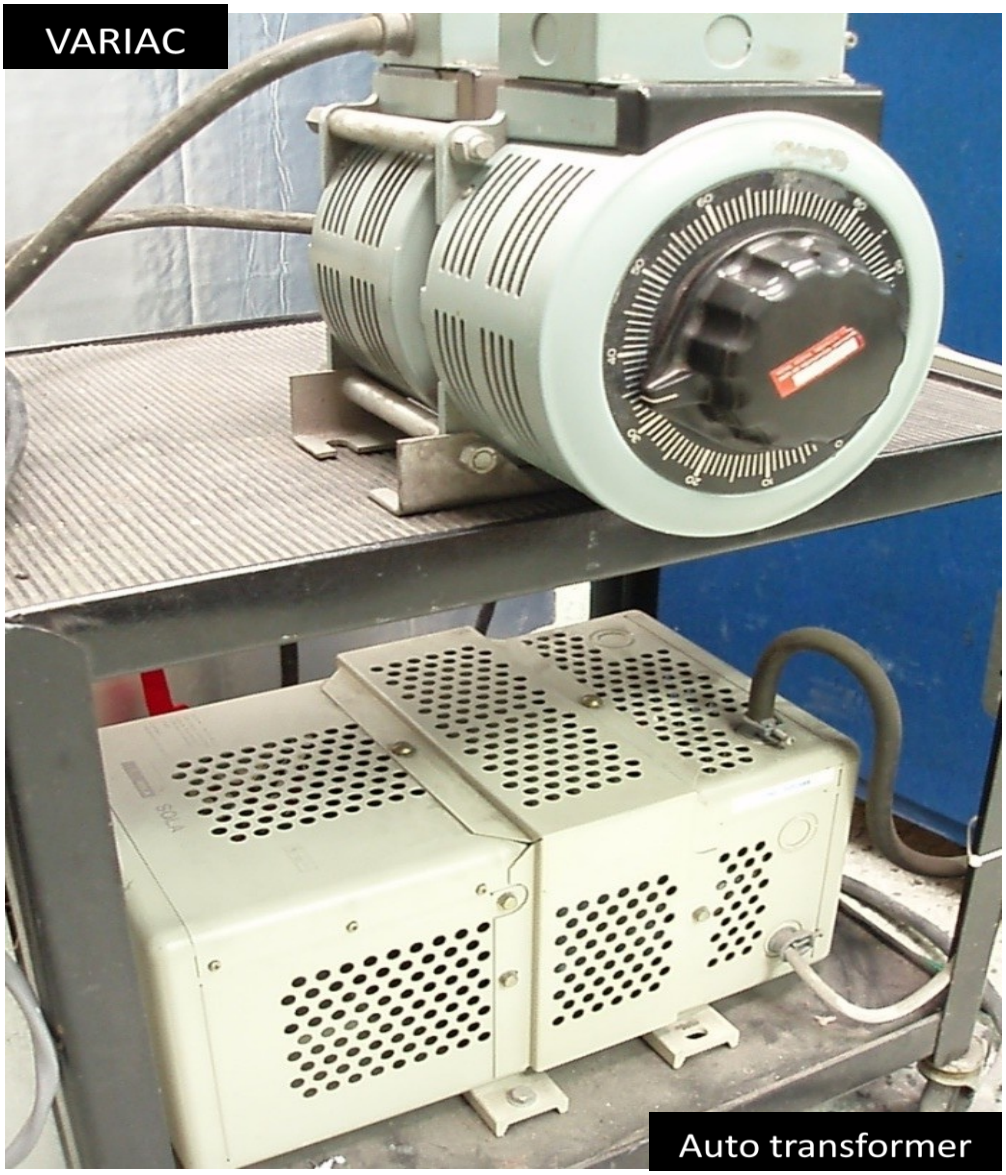

Figure A.1. Variac and auto transformer

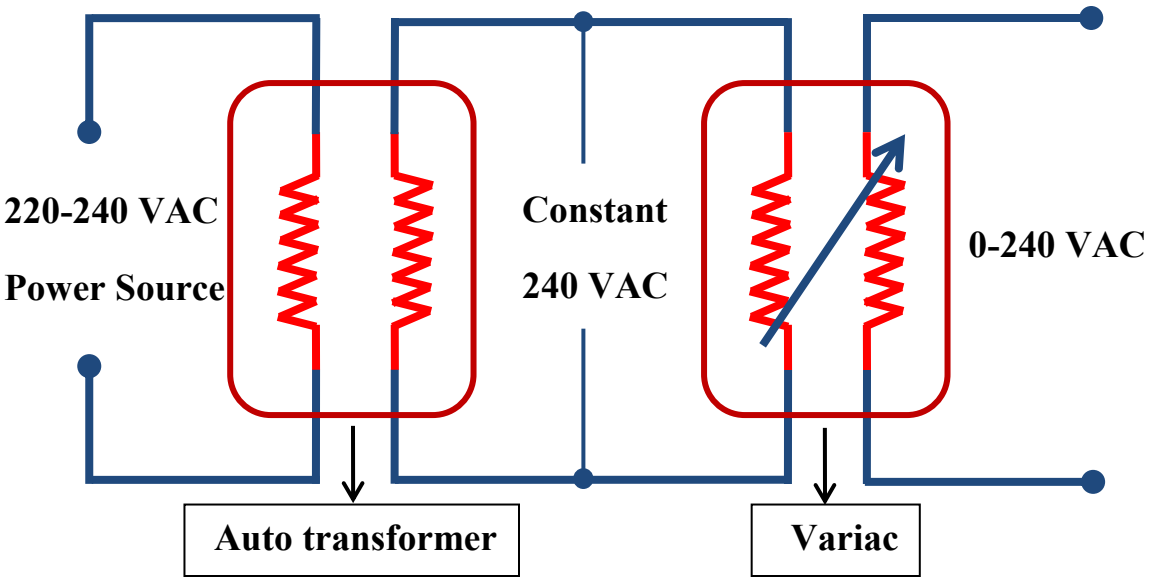

Figure A.2. Electrical circuit for the variac and auto transformer

Table A.1. Specifications of the auto transformer

VA	Voltage Input	Voltage Output	Height (inch)	Width (inch)	Depth (inch)	Ship Weight (lbs)
3000	120, 208, 240, 480	120.240	19	13	10	142

Table A.2. Specifications of the Variac

VA	Voltage Input (Volt)	Voltage Output (Volt)	Frequency (Hz)	Current (Amps)
3100	240	0-140	50/60	22

2. EXPERIMENTAL APPARATUS

Figure A.3. Experimental setup

APPENDIX B

THERMO PHYSICAL PROPERTIES OF 38/62 PROPYLENE GLYCOL AND WATER

B.1. Propylene Glycol

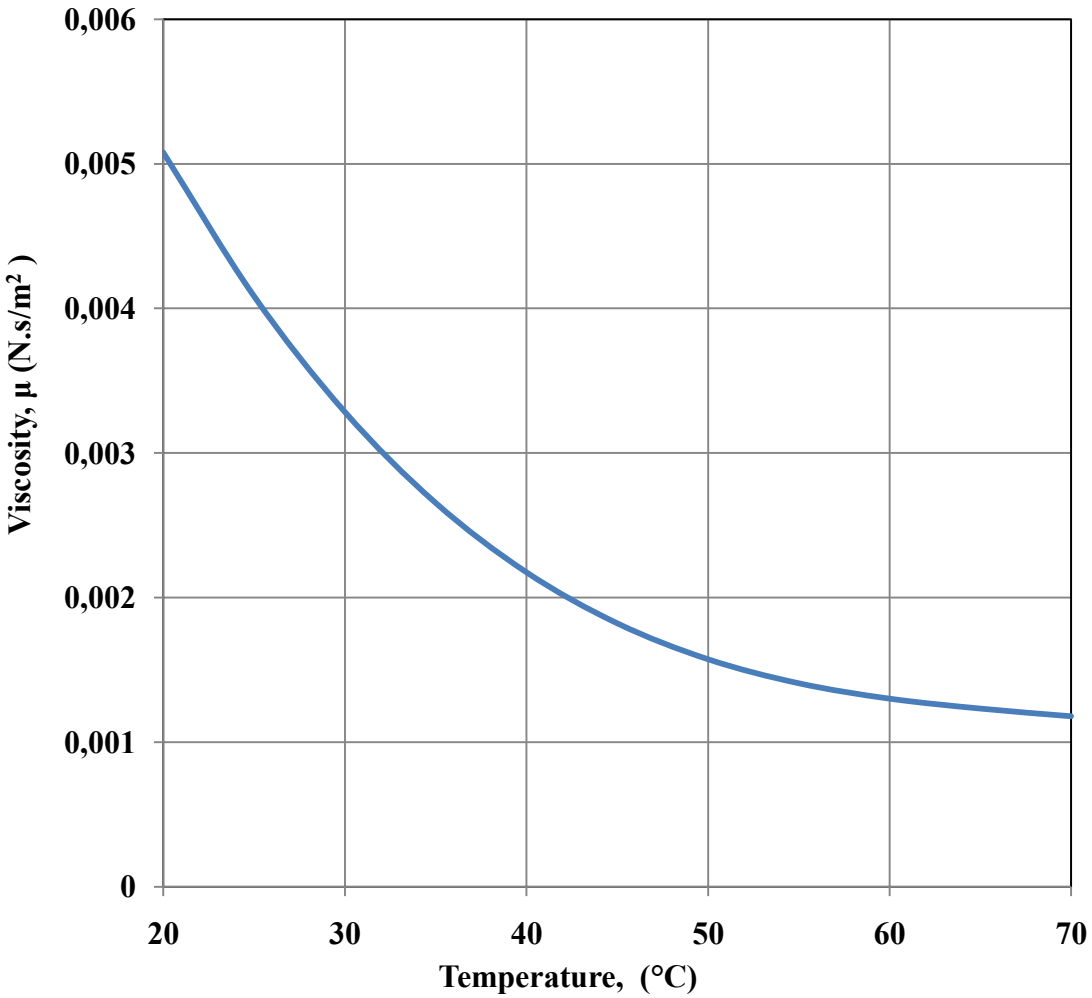

Figure B.1 (A) Dynamic viscosity of propylene glycol

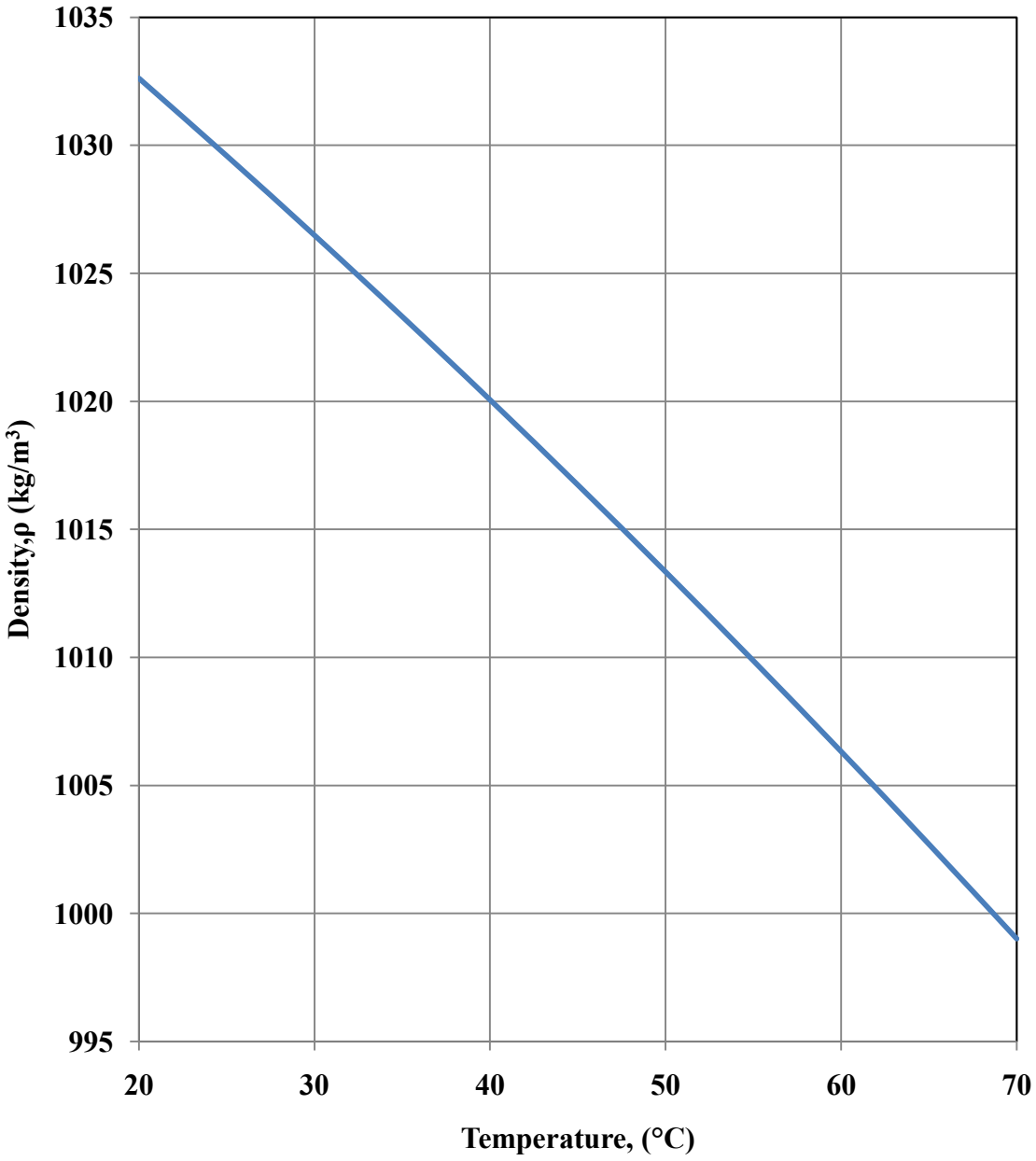

Figure B.1 (B) Density of propylene glycol

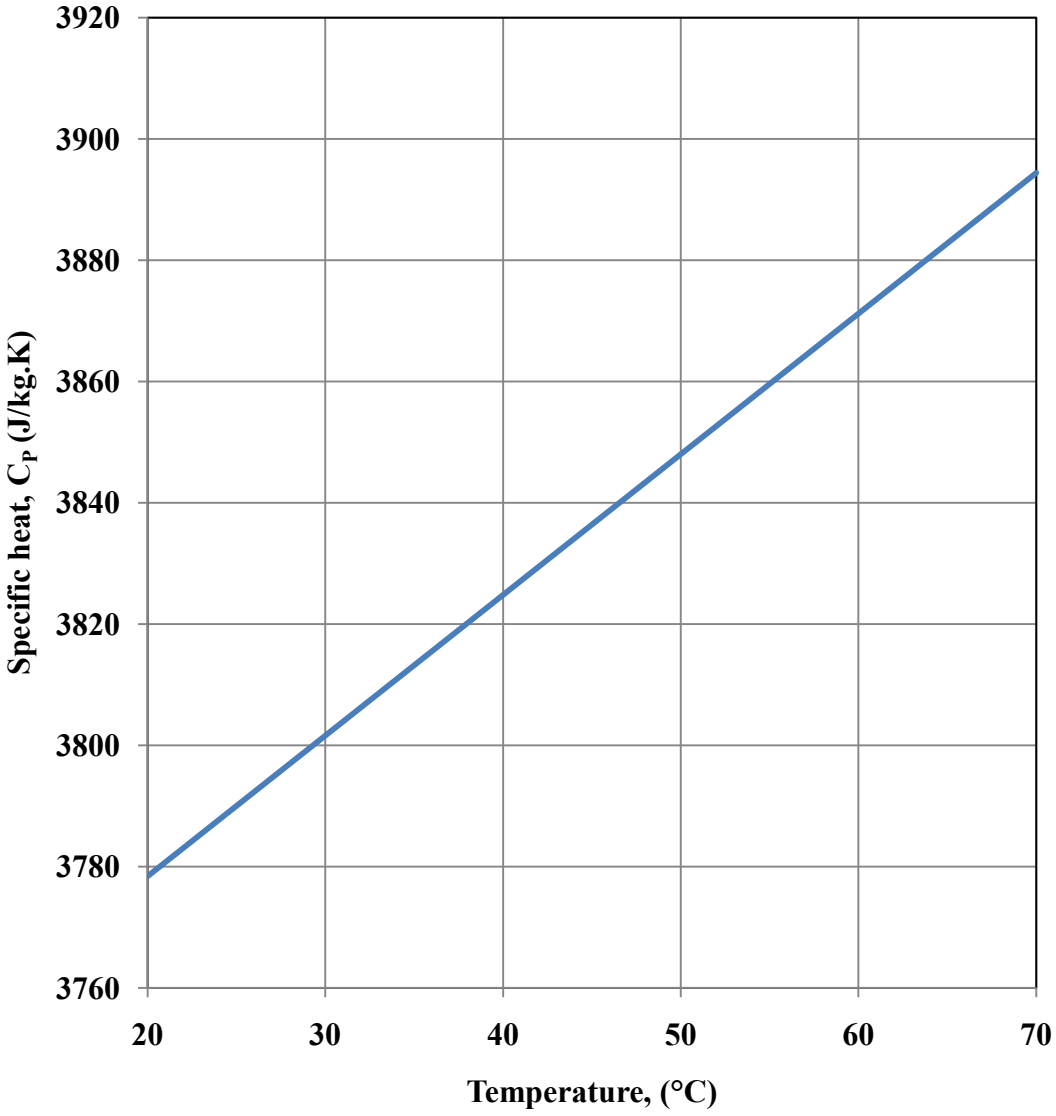

Figure B.1 (C) Specific heat of propylene glycol

Table B.1 Test #1 for S4CHX-G

q	q_{elec}	$DTLM_{ave}$	Δq	$qhx4c_{ave}$	$qhx4c_{act}$	$UA2_{ave}$	UA_{act}	R	$mdot$	$mdot_{act}$	GPM_{act}
500	505	4.9	73	825	432	168	88	0.53	0.0196	0.0103	0.163
1000	983	5.6	92	1136	891	201	159	0.79	0.0259	0.0205	0.324
1500	1485	7.2	123	1663	1362	229	189	0.82	0.0303	0.0250	0.396
2000	2000	8.5	167	2135	1833	252	216	0.86	0.0335	0.0287	0.454
2500	2493	9.8	205	2611	2288	266	233	0.88	0.0350	0.0307	0.486
3000	2990	10.7	256	3052	2735	286	256	0.89	0.0360	0.0322	0.510

Table B.2 Test #2 for S4CHX-G

q	q_{elec}	$DTLM_{ave}$	Δq	$qhx4c_{ave}$	$qhx4c_{act}$	$UA2_{ave}$	UA_{act}	R	$mdot$	$mdot_{act}$	GPM_{act}
500	499	6.0	10	992	489	171	82	0.48	0.0196	0.0093	0.148
1000	992	7.0	29	1309	963	184	138	0.75	0.0259	0.0194	0.307
1500	1494	8.6	54	1892	1440	220	168	0.76	0.0306	0.0234	0.370
2000	1999	9.8	79	2408	1920	242	196	0.81	0.0335	0.0271	0.428
2500	2484	11.1	104	2952	2380	263	214	0.81	0.0354	0.0288	0.455
3000	2959	12.3	142	3418	2817	278	229	0.82	0.0360	0.0297	0.470

Table B.3 Mass and Cost (≈$ 20/kg) of the Heat Exchangers

	S4CHX	**S3CHX**	**Difference**
Coil #1	0.538 kg	0.538 kg	0
Coil #2	0.806 kg	0.806 kg	0
Coil #3	0.986 kg	0.986 kg	0
Coil #4	1.254 kg	N/A	1.254 kg
Shell & reservoir	3.226 kg	1.792 kg	1.434 kg
Plates	0.268 kg	0.186 kg	0.082 kg
Total Mass	7.078 kg	4.308 kg	2.770 kg
Total Cost	141.56 $	86.16 $	55.4 $

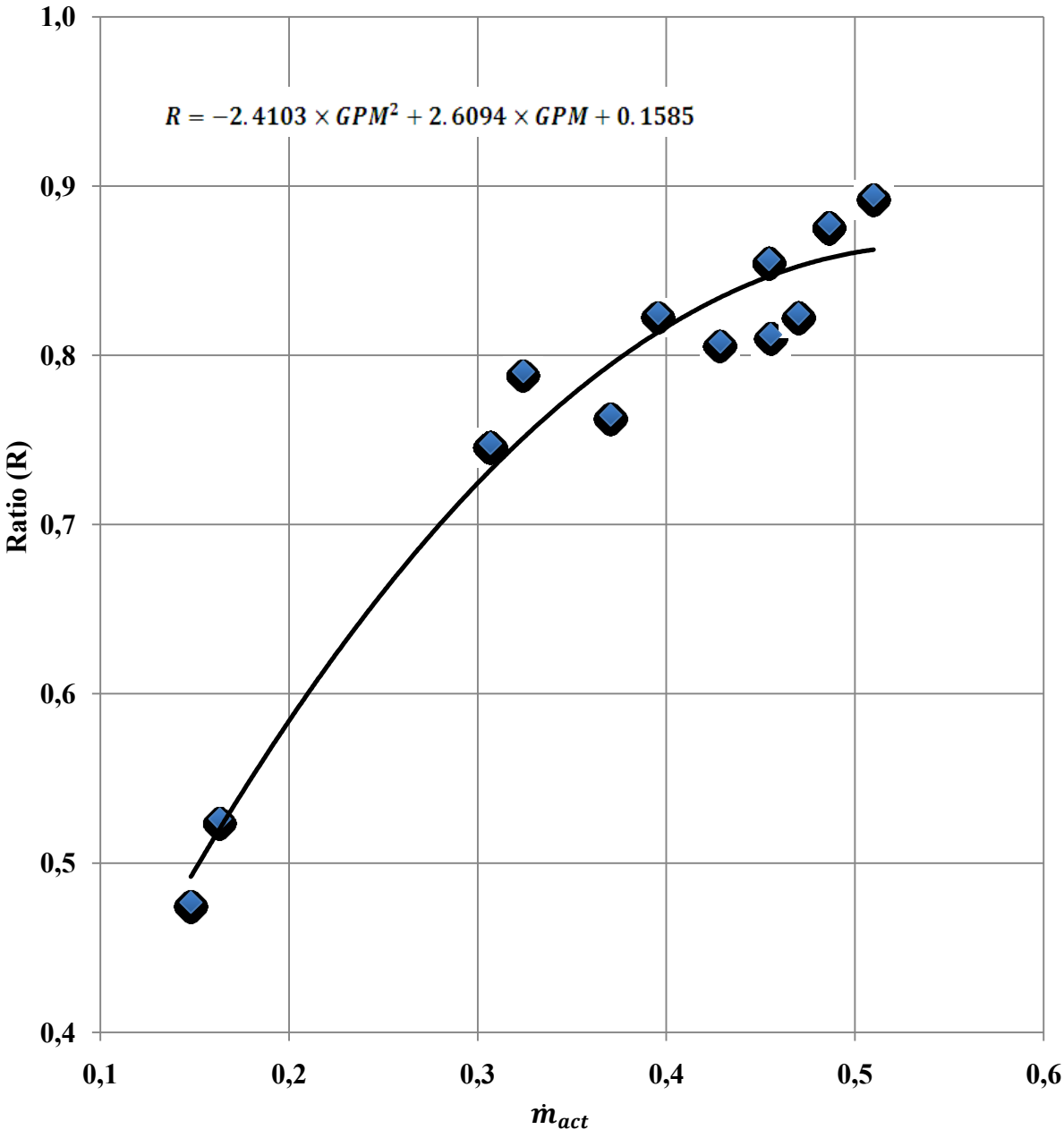

Figure B.1 (D) Calibration curve for the Propylene glycol

B.2. Water

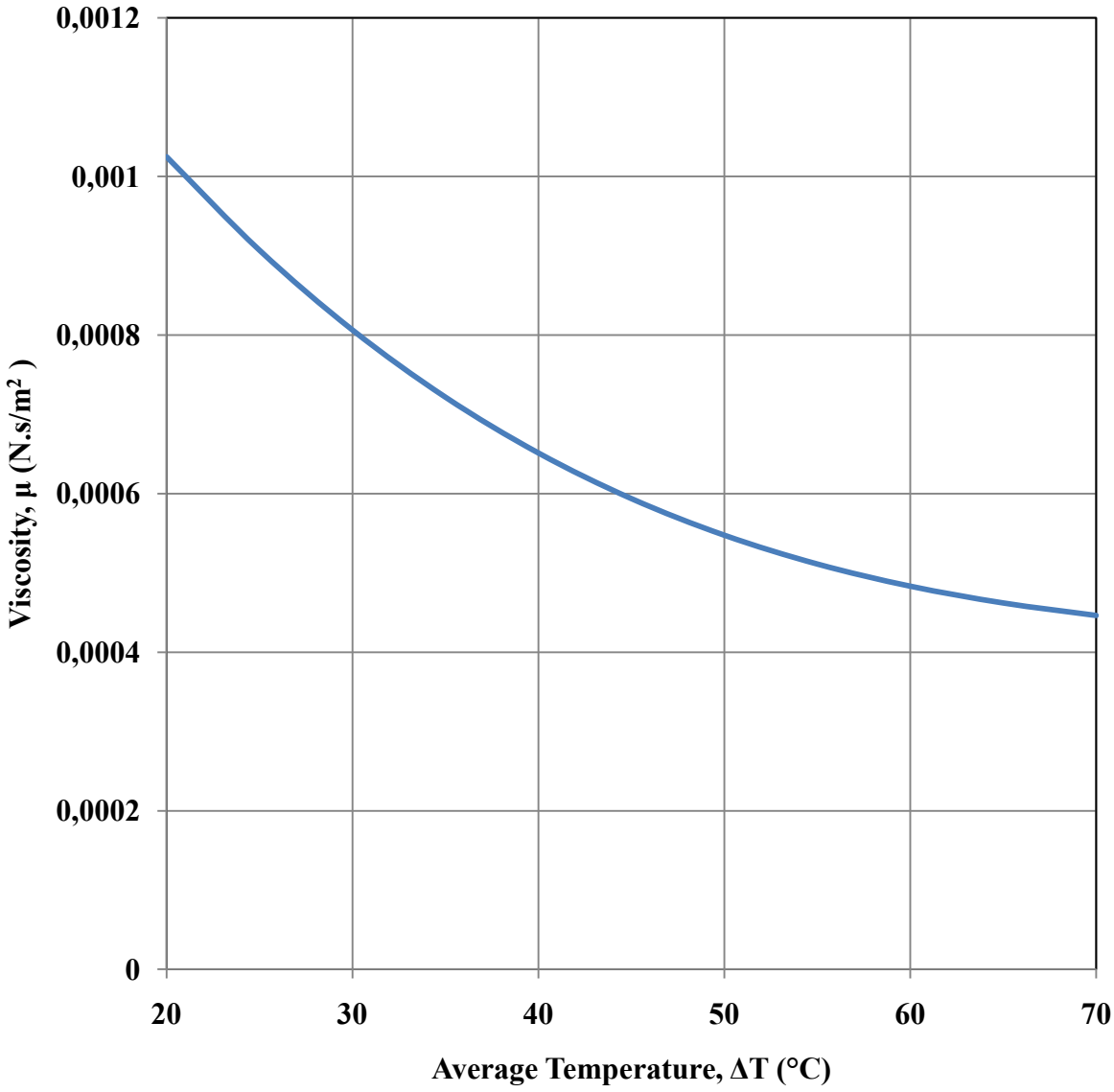

Figure B.2 (A) Dynamic viscosity of water

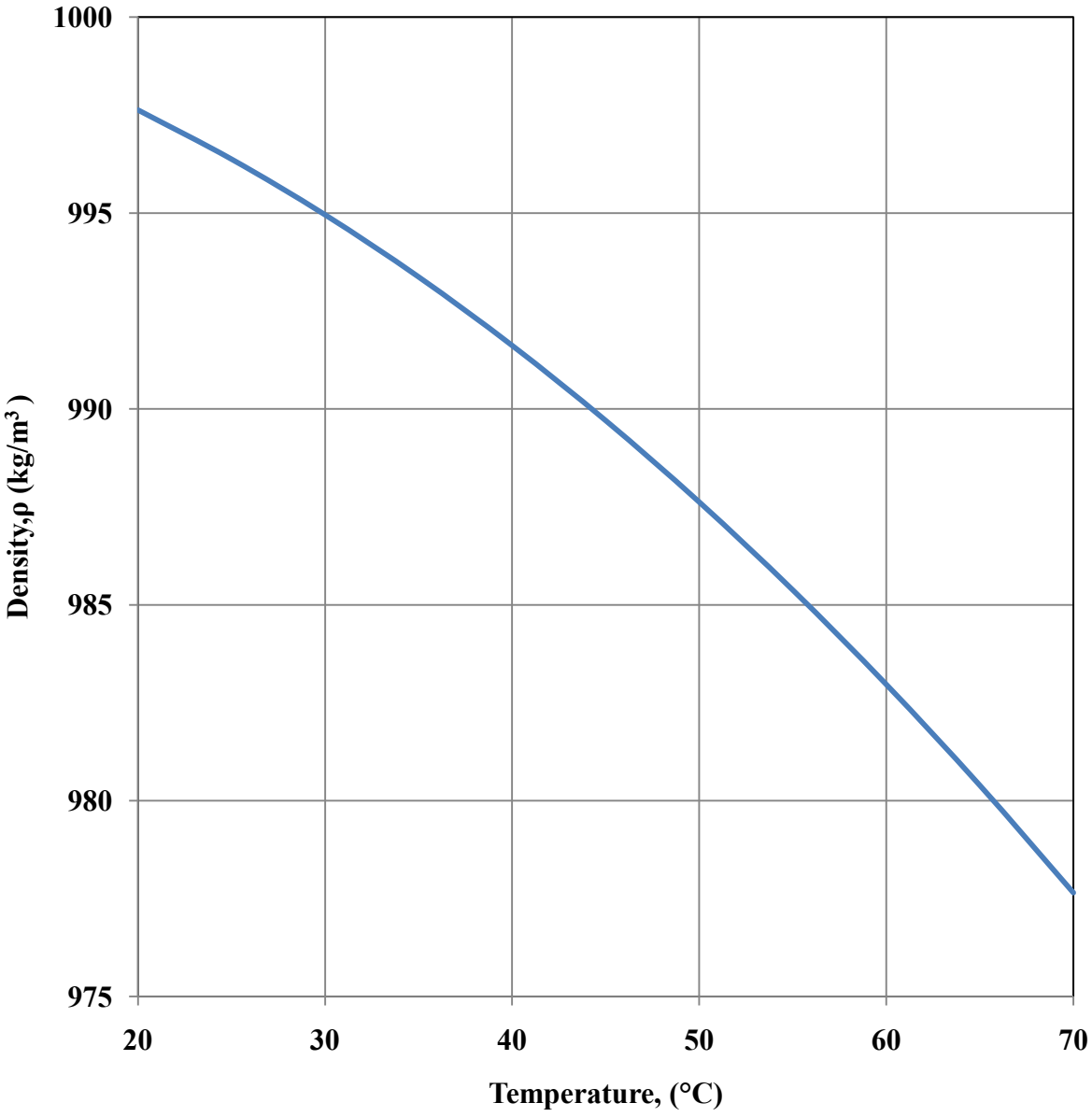

Figure B.2 (B) Density of water

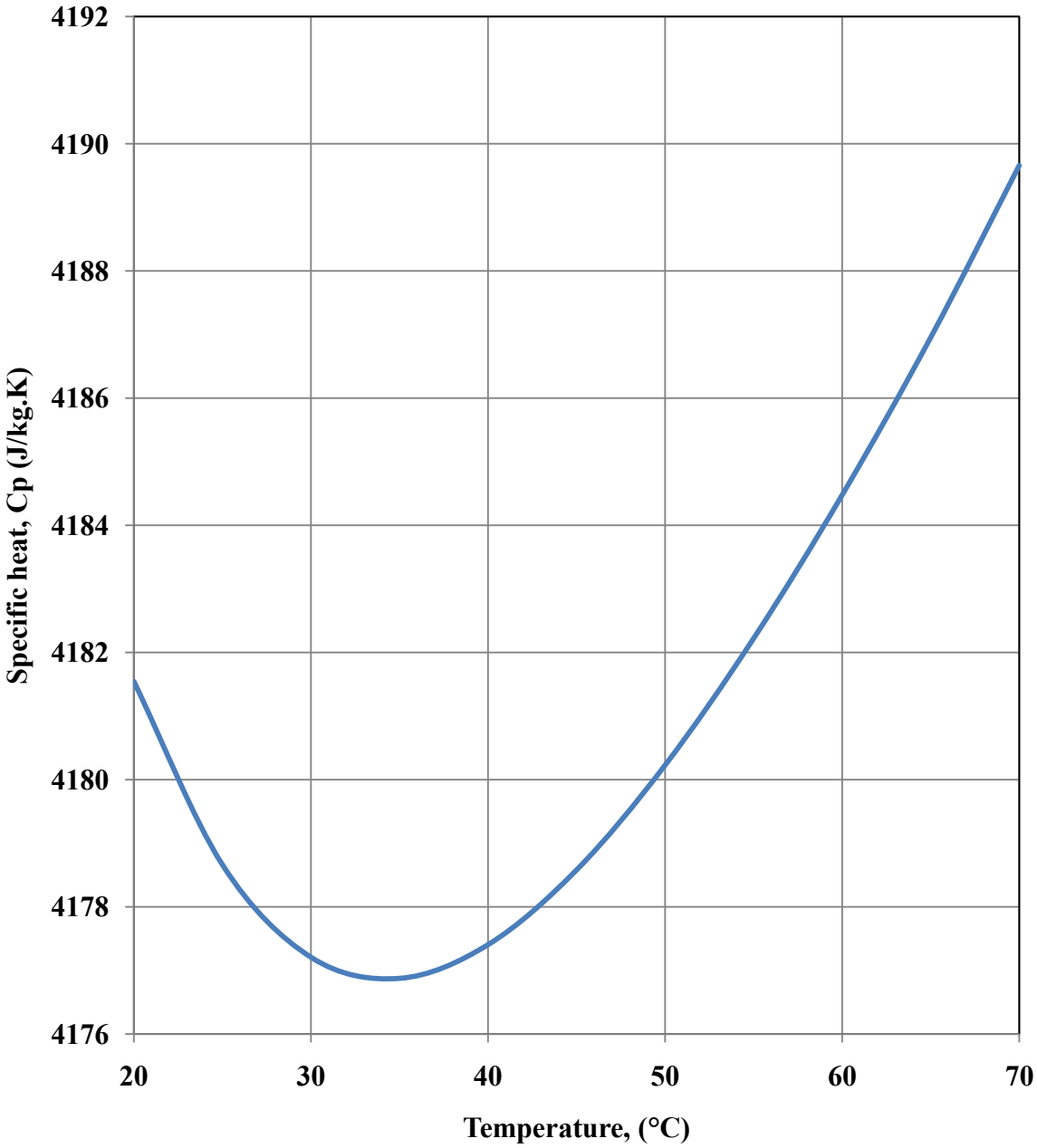

Figure B.2 (C) Specific heat of water

APPENDIX C

MODELS

C.1. General Structure of the Models

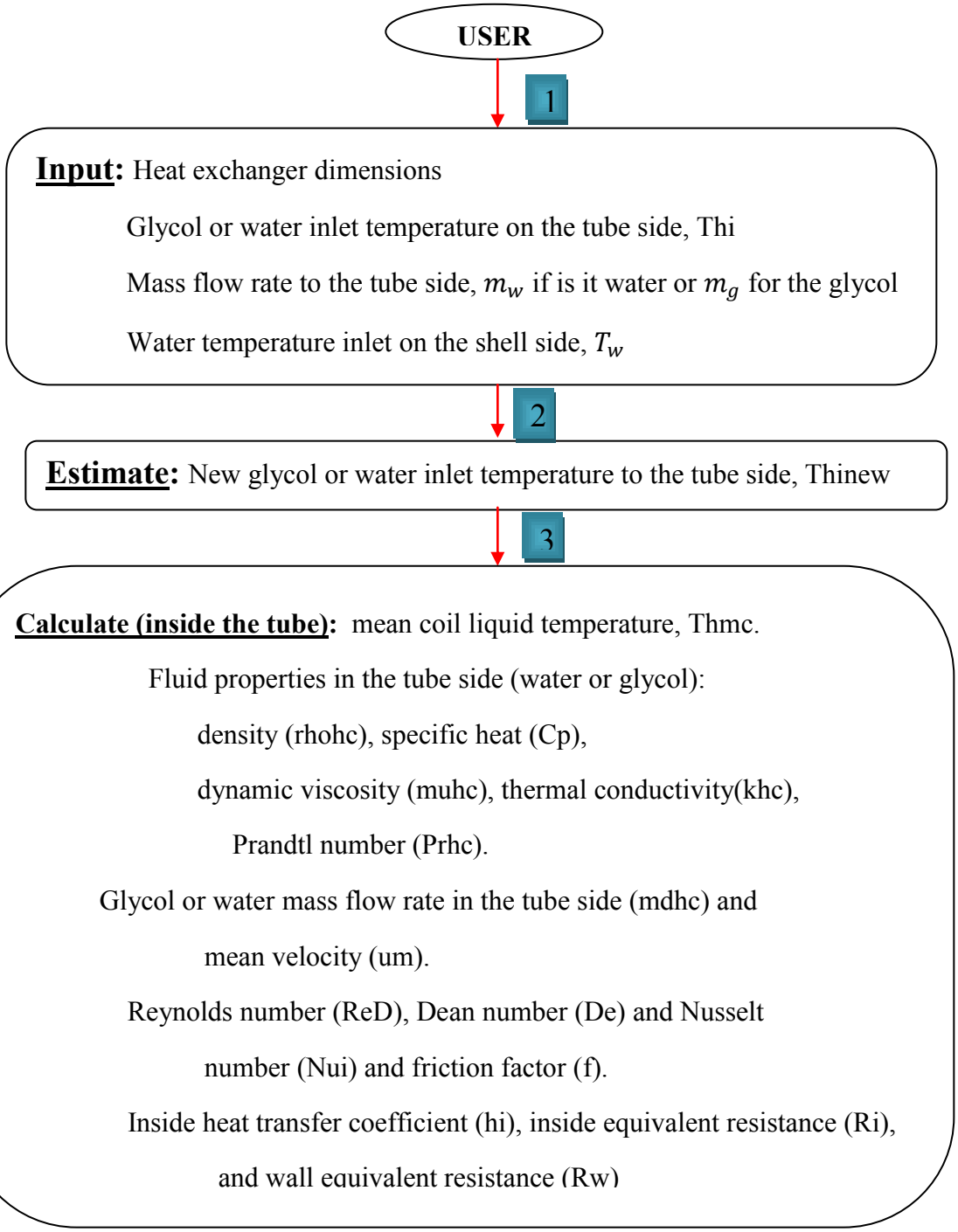

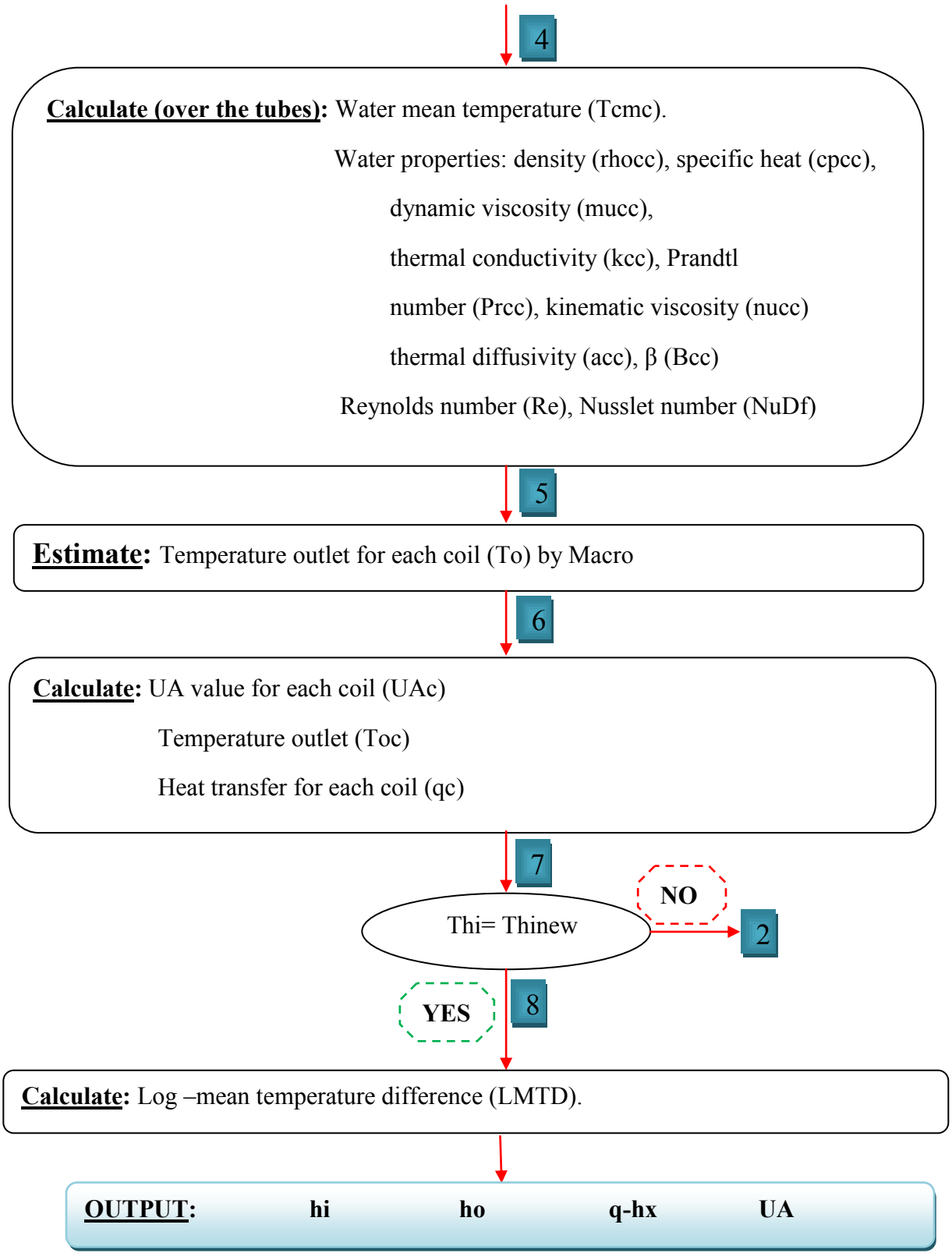
4
Calculate (over the tubes): Water mean temperature (Tcmc).
Water properties: density (rhocc), specific heat (cpcc),
dynamic viscosity (mucc),
thermal conductivity (kcc), Prandtl
number (Prcc), kinematic viscosity (nucc)
thermal diffusivity (acc), β (Bcc)
Reynolds number (Re), Nusslet number (NuDf)
5
Estimate: Temperature outlet for each coil (To) by Macro
6
Calculate: UA value for each coil (UAc)
Temperature outlet (Toc)
Heat transfer for each coil (qc)
7
Thi= Thinew
NO
2
YES
8
Calculate: Log –mean temperature difference (LMTD).
OUTPUT: hi ho q-hx UA

C.2 Copies of Models

Model-1

Please open the macro program: HX4.macro

Modified on Feb. 16, 2008 by PLA input data

Data in bold is input information that is required.

q	2304	W			
Thm	52.0	C			
Tmw	39.9	C			
coil liquid (w or g	w				*50.4*
mdh	0.0310	kg/s	0.49 USGPM	1.86 L/m	
mdc	0.0264	kg/s	0.42 USGPM	1.58 L/m	
cph	4,181	J/kg.K	based on Thm		
cpc	4,177	J/kg.K	based on Tmw		
balanced mdc	0.0310	kg/s			
(mcp)c/(mcp)h	85%				
kt (Cu)	400	W/m.K			
m	0	exponent in Ajele's eq'n			
Ds, shell diamete	77.00	mm	3.031 in		
H, shell height	0.406	m	15.98 in		
		(based on height of coil #1)			

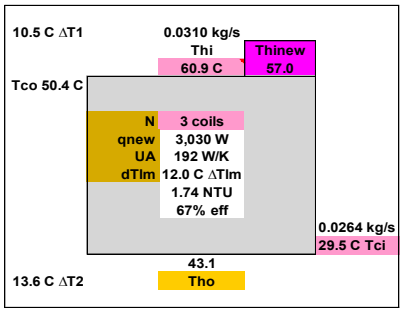

	Coil #	1	2	3	
Do (in)	tube outer dia., in	0.250	0.250	0.250	tube outer diameter, before bending
Do	tube outer dia., mm	6.35	6.35	6.35	
tw	wall thickness, mm	0.76	0.76	0.76	0.030 inch
Di	tube inner dia., mm	4.83	4.83	4.83	tube inner diameter, before bending
a	Major axis, outer, n	7.51	6.74	6.72	Dele's measurements; [(a2+b2)/2]^0.5 below
b	Minor axis, outer, r	4.87	5.68	6.00	6.33 6.23 6.37
ain	Major axis, inner, n	5.99	5.22	5.20	a-2*tw
bin	Minor axis, inner, n	3.35	4.16	4.48	b-2*tw
Ac	Area of X-sect., mm	15.75	17.04	18.28	π ain*bin/4
nrcp	Ratio of turns	1.00	1.05	0.92	as built
nrc	Ratio of turns	1.00	1.00	1.00	for testing purposes
nrca	Ratio of turns	1.00	0.84	0.68	for constant Ti-To
coil factor, cnf: 0 = nrcp, 1 = nrc		0			
nc	number of turns	43	45	39	INT(nrc*NC1) NC1=35 - production model
Space between tubes, SL (mm)		1.93	2.28	3.69	
Space between tubes, SL (in)		0.076	0.090	0.145	1 given; 2,3: (H-nc*a)/nc
Coil pitch		1.26	1.34	1.55	
Dhi	hyd. diameter, mm	4.13	4.60	4.80	(ain*bin)/((ain^2+bin^2)/2)^0.5
Dc	coil mean dia., mm	31.6	48.6	67.6	
Dco	coil outer dia., mm	36.5	54.3	73.6	Dc+b
Dci	coil inner dia., mm	26.7	42.9	61.6	Dc-b
Space between coils (mm)		3.2	3.7	1.7	
Dco^2 - Dci^2		616	1,104	1,622	
Awf	area for flow, mm2	627	532	746	1,905 mm2
Deq	57.8	S	0.332		

Aot
0.387 m2

Calculation of hi, the inside heat transfer coefficient

Thmc	mean coil liquid tei	52.6	50.2	50.8	(Thi+To)/2
rhohc	Density, (kg/m3)	986	988	987	1044-0.5395T-(0.0384T)^2
cp	Specific heat, (J/kg	4,181	4,180	4,181	3732+2.32T
muhc	Viscosity, (N.s/m2)	0.00051	0.00053	0.00053	11437-428T+6.1T^2-0.0297T^3
khc	Ther. conductivity,	0.645	0.643	0.643	.379+.0013T-(0.000379T)^2+(0.00431T)^3
Prhc	Prandtl number	3.31	3.45	3.42	muhc*cp/khc
Lc	tube length, m	4.27	6.87	8.28	nc πDc; Length, Lt 19.42 m 64 ft 76.23 mm Di 0.0
pfc	% flow received	34.8	31.9	33.3	equal ΔP for each coil
pfnew	% flow received (n	34.8	31.9	33.3	equal ΔP for each coil
mdhc	flow rate, (kg/s)	0.0108	0.0099	0.0103	0.0310 kg/s
um	velocity, m/s	0.694	0.588	0.572	mdhc/(rhohc*Ac)
ReD	Reynolds #	5549	5036	5150	rhohc*Dhi*um/muhc
De	Dean #	2007	1549	1372	ReD*(Dhi/Dc)^0.5
f	friction factor	0.059	0.056	0.052	64/ReD*[1+(1+Dhi/Dc/3)^2*De/88.33]^0.5
ΔP (Pa)		14.38	14.38	14.38	f*Lc/Dhi*rhohc*um^2/2
ΔP (psi)		2.09	2.09	2.09	ΔPave 2.09 psi
X3f	constant	1.000	1.000	1.000	[1+1342/(De^2*Prhc)]^2
X4f	constant	1.348	1.333	1.337	1+1.15/Prhc
Nui	Nusselt #	47.0	41.6	39.1	[(4.36+4.64/X3f)^3+1.82*(De/X4f)^1.5]^0.333
hi	W/m2.K	7,339	5,809	5,243	Nui*khc/Dhi
Ai	m2	0.0647	0.1042	0.1256	πDi*Lc Ait (m2) 0.295
Ric	1/(hiAi)	0.00210	0.00165	0.00152	
hiAi (W/k)		475	605	659	hi(eq) = 5,904
Ri	equivalent R	0.00057			hiAi,total 1,739

Rwc	wall resistance	2.55E-05	1.59E-05	1.32E-05
Rw	equivalent R	5.61E-06		

But ton

Click on this button to re-calculate the values for "% flow received"

Coils in HX as per Oct.24, 2007
31
35 (=92 feet only)
40
39
Coils in Oakland HX
44
45
39
35
Coils in TDL HX, Nov5, 07
42
45
39
35

Calculation of ho based on forced water flow and proportioning water flow over the coils

Tcmc	°C	45.29	44.18	44.57	(Tmsoc+Tmw)/2	#VALUE!	
rhocc	Density, (kg/m3)	990	990	990	1001-0.1026T-0.0033T^2	Tcmc	
cpcc	Specific heat, (J/kg	4,179	4,178	4,178	4215-2.849T+(0.2688T)^2-(0.0901T)^3+(0.0414T)^4		
mucc	Viscosity, (N.s/m2)	0.000588	0.000600	0.000595	0.0017-0.0000429T+(0.000704T)^2-(0.00126T)^3		
kcc	Th. conductivity, (W	0.637	0.636	0.636	0.569+0.00183T-0.00000724T^2		
Prcc	Prandtl number	3.86	3.94	3.91	mucc*cpcc/kcc		
nucc	Viscosity, (m/s2)	0.594	0.606	0.601	mucc/rhocc * 1000000		
acc	Th. diffusivity, (m/s	0.154	0.154	0.154	kcc/(rhocc*cpcc)*1000000		
Bcc	Beta (1/K)	421	412	416	(-10.1+11.2T-0.037T^2)		
Water flow (kg/s)		0.0119	0.0112	0.0114	based on fraction of total q (qc/qh * mdc)	#VALUE!	
Water velocity (m/s)		0.0191	0.0213	0.0155	0.0345 mdc -calc		
Dho	hyd. diameter, mm	5.78	6.14	6.33	(a*b)/((a^2+b^2)/2)^0.5		
Reynolds#		169.9	201.1	150.9			
NuDf	Nusselt #	12.12	13.11	11.47	based on forced flow; single cylinder		
hocf	W/m2.K	1,336	1,357	1,153			
ratio		1.00	1.02	0.86			
1/(hoAo)		0.00879	0.00538	0.00525	1,265 ho-effective for forced flow		

3 inch copper tube
3.125 inches
79.38 Do -mm
0.062 t-wall
1.575 mm
3.15 2 t-wall

Calculation of ho for each coil, assuming natural convection only

dTcc	°C	21.14	18.91	19.70	Tmsoc-Tci	#VALUE!
dTccx	°C	10.70	8.47	9.25	Tmsoc-Tmw (use this ΔT)	#VALUE!
RaDcc	based on dTcc	184,218	190,516	220,099	g*Bcc*dTcc*Do^3/(nucc*acc)	
RaDccx	based on dTccx	93,209	85,293	103,394	g*Bcc*dTccx*Do^3/(nucc*acc)	
NuDcc	based on Radcc	7.08	7.16	7.52	0.125*RaDcc^0.333 (Morgan, turbulent, RaD>10 million)	
NuD	based on RaDcc	9.94	10.03	10.40	0.48*RaDcc^0.25 (Morgan, laminar)	
NuDx	based on Radccx	8.39	8.20	8.61	0.48*RaDccx^0.25 (Morgan, laminar)	
hoc	W/m2.K	925	849	865	NuDx*kcc/Do (Morgan turbulent)	
Roc2	1/(hoAo)	0.01270	0.00859	0.00700	872 ho-effective	
Ao	area, m2	0.0852	0.1371	0.1652	Aot (m2) 0.387	
DoAo		0.5408	0.8704	1.0492	6.35 Do-e (mm)	
0 - use one ho; 1 - use hoc		1	1226	Ajele's value		
ho or hoc (W/m2.K)		925	849	865	hoc - natural conv. for each coil	
correction factor for hoc		1.11	0.79	0.67	used to adjust ho to fit experimental data	
hocc	ho corrected	1,026	671	580		
Roc	1/(hoAo)	0.01144	0.01088	0.01044	710 ho-effective for natural convection	

NuDfff	penalty factor	0.71	0.66	0.53
NuDc	combined conv.	9.22	9.10	6.64
h-comb	combined conv.	1017	942	668
Rocc	combined conv.	0.01155	0.00774	0.00906

Calculate UA for each coil and qc for each coil

UAc	W/K	73.1	106.2	94.4	1/(Ric+Rwc+Roc) (or use Rocc)
To	from HX4.macro	44.3	39.6	40.6	
Toc	calculated	40.6	34.5	37.2	
Tonew	new values	42.8	37.5	39.6	x*To+(1-x)*Toc
qc	W - for the single c	916	1093	1021	3030 W qnew
q"	W/m2	10,755	7,975	6,179	heat flux

Bu
tto

Click on this button to re-calculate the values for "To".

Calculate the mean temp. of the outside surface of each coil (req'd for ho, nat conv.)

Tmsic	n inner surf. temp.	50.67	48.43	49.21	Thmc-qc*Ric		
Tmsi x Ai		3.28	5.05	6.18	49.26	Tmsi -ave	
Tmsoc	n outer surf. temp.	50.64	48.41	49.20	Tmsic-qc*R	49.42	Tmso-av
Tmsoc-Tmw		10.70	8.47	9.25		9.47	dT-av
(Tmsoc-Tmw)/dT-av		1.13	0.89	0.98			
Tmso x Ao		4.31	6.64	8.13	49.24	Tmso	*49.24*

Various methods for calculating ho (single value)

Tmw (C) *39.9*

Thermophysical properties of water evaluated at Tmw

kc	rhoc	cpc	alphac	muc	nuc	Prc	beta
0.631	992	4,177	1.52E-07	6.44E-04	6.49E-07	4.27	0.000378

Aot	As	Ap	Acf	Dhx	uw	ReDo	NuDo	ho	NuDo
0.387	0.098	0.486	0.00191	0.00637	0.0140	136.7	10.95	1087	11.59

		dT							
		19.7	Ajele						

Ajele correlation is for 1-4 coils only!

Ra(Dhx)	Ram	Ff	Nuo	ho	Ro	Ri
191,425	4,001	1.684	11.06	1226	0.00211	0.00057

RaDo	NuDo	Nuo	Nuo	1094
189,683	10.02	7.15	10.78	
ho=	995	710	1070	
	Morgan lam.	Morgan tur.	Churchill	

Ri+Rw+Ro	Thonew
0.00269	37.5

tube bank

NuDo
11.39

Zhukauskas

Hilpert (forced)

Churchill (forced)

NuDo	ho
7.60	752

Nu=0.48Ra*^0.33
Ajele (general)

Model-2

Please open the macro program: HX4.macro

Modified o Feb. 17, 2008 by PLA

Data in bold is required input.

qh	3,000	W		
prop. gly. (	50	%		
Thm	41.3	C		43.7
Tmw	29.4	C	USGPM	
mdh	0.0330	kg/s	0.524	1.98 L/m
mdc	0.0250	kg/s	0.397	1.50 L/m
cph	3,643	J/kg.K		
cpc	4,177	J/kg.K		
balanced r	0.029	kg/s		
(mcp)c/(mc	87%			
kt	400	W/m.K		
Ds	102	mm	4.016 in	
H	0.406	m	15.98 in	
m	0	exponent in Ajele's eq'n		

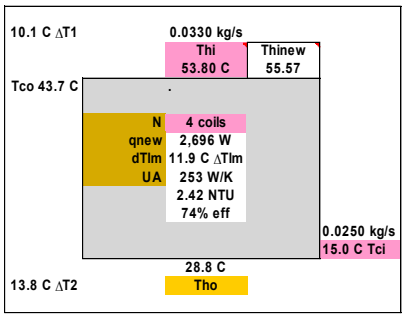

	40/60
cp	3732 + 2.32 T
k	0.379+0.00130 T-(0.00379 T)^2+(0.00431 T)^3
visc	11437-428T+6.1T^2-0.0297T^3

FALSE

Coil #		1	2	3	4	
Tube outer diameter, Do (in)		0.250	0.250	0.250	0.250	tube outer diameter, before bending
Tube outer diameter, Do (m	Do	6.35	6.35	6.35	6.35	Dot 6.35 mm
Wall thickness, tw (mm)	tw	0.761	0.761	0.761	0.761	0.030 in
Tube inner diameter, Di (mr	Di	4.83	4.83	4.83	4.83	tube inner diameter, before bending
Major axis, a, outer (mm)	a	7.51	6.74	6.72	6.55	Dele's measurements; [(a2+b2)/2]^0.5 below
Minor axis, b, outer (mm)	b	4.87	5.68	6.00	6.15	6.33 6.23 6.37 6.35
Major axis, ain, inner (mm)	ain	5.99	5.22	5.20	5.03	a-2*tw
Minor axis, bin, inner (mm)	bin	3.35	4.16	4.48	4.63	b-2*tw
Area of X-sect., mm2	Ac	15.75	17.04	18.28	18.28	π ain*bin/4
Ratio of turns	nrcp	1.00	1.05	0.92	0.85	as built (Oct.24,07)
Ratio of turns	nrc	1.00	1.00	1.00	1.00	for testing purposes
Ratio of turns	nrca	1.00	0.84	0.68	0.56	for constant Ti-To
coil factor, cnf: 0 = nrcp, 1 =	cnf	0				
No. of turns	nc	43	45	39	36	INT(nrc*NC1) NC1=35 - production model
Space between tubes (mm)	SL	1.93	2.28	3.69	4.73	
Space between tubes, SL (in)		0.076	0.090	0.145	0.186	1 given; 2,3,4: (H-nc*a)/nc
Coil pitch		1.26	1.34	1.55	1.72	
Hydraulic diameter (mm)	Dhi	4.13	4.60	4.80	4.82	(ain*bin)/((ain^2+bin^2)/2)^0.5
Coil mean dia (mm)	Dc	31.6	48.6	67.6	90.6	
Coil outer dia (mm)	Dco	36.5	54.3	73.6	96.8	Dc+b
Coil inner dia (mm)	Dci	26.7	42.9	61.6	84.5	Dc-b
Space between coils (mm)	Sc	3.2	3.7	5.4	2.6	
Dco^2 - Dci^2		616	1,104	1,622	2,229	
Area for water flow (mm2)	Acs	627	532	994	1,516	3,669 mm2
Deq 74.6		S 0.367		S=(Ds-Deq)/Deq		

Aot 0.592 m2

Coils in HX as per Oct.24, 2007
31
35 (=92 feet only)
40
39
Coils in Oakland HX
44
45
39
35
Coils in TDL HX, Nov5, 07
42
45
39
35

Calculation of hi, the inside heat transfer coefficient

Thmc (C)	Thmc	44.6	41.8	42.5	41.0	(Thi+To)/2 #VALUE!
Density (kg/m3)	rhohc	1,017	1,019	1,018	1,019	1044-0.5395T-(0.0384T)^2
Specific heat (J/kg.K)	cp	3,654	3,644	3,647	3,641	3732+2.32T / 3500+3.45T
Viscosity (N.s/m2)	muhc	0.00283	0.00312	0.00304	0.00320	11437-428T+6.1T^2-0.0297T^3
Thermal conductivity (W/m.(	khc	0.37	0.37	0.37	0.37	0.344+.00109T-(0.000346T)^2+(0.00375T)^3
Prandtl #	Prhc	27.7	30.5	29.8	31.4	muhc*cp/khc
Tube length (m)	Lc	4.27	6.87	8.28	10.25	nc πDc; Length, Lt 29.67 m
Tube length, Lc (ft)		14.0	22.5	27.2	33.6	97 ft
% flow received	pfc	28.0	24.5	25.4	22.1	100.0 %
% flow received (new values	pfnew	28.0	24.5	25.4	22.1	equal ΔP for each coil
Flow rate (kg/s)	mdhc	0.0092	0.0081	0.0084	0.0073	0.0330 kg/s
Velocity (m/s)	um	0.58	0.47	0.45	0.39	mdhc/(rhohc*Ac)
Reynolds#	ReD	856	700	725	599	rhohc*Dhi*um/muhc
Dean #, De	De	310	215	193	138	ReD*(Dhi/Dc)^0.5
Friction factor	f	0.164	0.173	0.160	0.173	64/ReD*[1+(1+Dhi/Dc/3)^2*De/88.33]^0.5
ΔP (kPa)		28.6	28.6	28.6	28.7	f*Lc/Dhi*rhohc*um^2/2
ΔP (psi)		4.2	4.1	4.2	4.2	ΔPave 4.15 psi
Constant	X3f	1.00	1.00	1.00	1.00	[1+1342/(De^2*Prhc)]^2
Constant	X4f	1.04	1.04	1.04	1.04	1+1.15/Prhc
Nusselt #, Nui	Nui	21.5	18.3	17.4	15.2	[(4.36+4.64/X3f)^3+1.82*(De/X4f)^1.5]^0.333
Heat transfer coef, hi (W/m	hi	1,944	1,480	1,353	1,172	Nui*khc/Dhi
Heat transfer area, Ai (m2)	Ai	0.065	0.104	0.126	0.155	πDi*Lc Ait (m2) 0.450
Ric, 1/(hiAi)	Ric	0.00795	0.00648	0.00588	0.00549	
hiAi (W/k)		126	154	170	182	hi(eq) = 1,405
Equivalent (1/hiAi)	Ri	0.00158				hiAi,total 632

Button

Click this button to re-calculate the values for "pfc".
pfc is the percentage of the flow taken by each coil

Wall resistance (Rwc)	Rwc	2.55E-05	1.59E-05	1.32E-05	1.06E-05
Equivalent Rw	Rw	3.67E-06			

Calculation of ho based on forced water flow and proportioning water flow over the coils

Twater,mean (°C)	Tcmc	34.5	33.3	33.9	33.3	(Tmsoc+Tmw)/2	#VALUE!
Density (kg/m3)	rhocc	994	994	994	994	1001-0.1026T-0.0033T^2	
Specific heat (J/kg.K)	cpcc	4,177	4,177	4,177	4,177	4215-2.849T+(0.2688T)^2-(0.0901T)^3+(0.0414T)^4	
Viscosity (N.s/m2)	mucc	0.000727	0.000747	0.000737	0.000747	0.0017-0.0000429T+(0.000704T)^2-(0.00126T)^3	
Th. conductivity (W/m.K)	kcc	0.62	0.62	0.62	0.62	0.569+0.00183T-0.00000724T^2	
Prandtl #	Prcc	4.9	5.0	4.9	5.0	mucc*cpcc/kcc	
Viscosity (m/s2)	nucc	0.73	0.75	0.74	0.75	mucc/rhocc * 1000000	
Th. diffusivity (m/s2)	acc	0.15	0.15	0.15	0.15	kcc/(rhocc*cpcc)*1000000	
Beta (1/K)	Bcc	332	322	327	322	(-10.1+11.2T-0.037T^2)	
Water flow (kg/s)	mwc	0.0061	0.0053	0.0059	0.0051	based on fraction of total q (qc/qh * n	#VALUE!
Water velocity (mm/s)	uwc	9.7	9.9	6.0	3.4	0.0224 mdc -calc	6.8 mm/s (ave.)
uw index	uwind	0	0 use uwc; 1 use uw				
Hydraulic diameter (mm)	Dho	5.78	6.14	6.33	6.34	(a*b)/((a^2+b^2)/2)^0.5	
Reynolds#, Re		69	75	46	26		
Nusselt #	NuDf	8.7	9.0	7.2	5.7	based on forced flow; single cylinder, Hilpert	
ho	hocf	923	903	703	550		
ratio		1.00	0.98	0.76	0.60		
1/(hoAo)		0.01272	0.00808	0.00861	0.00890	728 ho-effective for forced flow	

Calculation of ho for each coil, assuming natural convection only

?Tcc (°C)	dTcc	24.7	22.2	23.4	22.3	Tmsoc-Tci	#VALUE!
RaDcc	RaDcc	141,222	144,188	171,107	159,343	g*Bcc*dTcc*Do^3/(nucc*acc)	
Morgan coefficient	Cm	0.480	0.480	0.480	0.480		
Morgan exponent	nm	0.250	0.250	0.250	0.250		
NuDcc (RaDcc)	NuDcc	9.3	9.4	9.8	9.6	Morgan	
hoc (W/m2.K) (NuDcc)	hoc	1,004	947	960	941	NuDcc*kcc/Dho	
1/(hocAo)	Roc2	0.0117	0.0077	0.0063	0.0052	957 ho-effective	

?Tccx (C)	dTccx	10.3	7.8	9.1	7.9	Tmsoc-Tmw	#VALUE!
RaDccx	RaDccx	59,065	50,947	66,191	56,622	g*Bcc*dTccx*Do^3/(nucc*acc)	
Morgan coefficient	Cmx	0.480	0.480	0.480	0.480		
Morgan exponent	nmx	0.250	0.250	0.250	0.250		
NuDx (RaDccx)	NuDccx	7.48	7.21	7.70	7.40	Morgan	
hocx (W/m2.K) (NuDcc)	hocx	807	730	757	726		
1/(hocAo)	Rocx2	0.0145	0.0100	0.0080	0.0067	748 ho-effective	

Heat transfer area, Ao (m2)	Ao	0.085	0.137	0.165	0.204	Aot (m2)	0.592		
DoAo		0.54	0.87	1.05	1.30	6.35 Do-e (mm)			
0 - use one ho; 1 - use hoc		1	hoindex	677	(=Ajele's ho)				
ho or hocx (W/m2.K)		807	730	757	726	hocx - natural conv. for each coil			
correction factor for hoc		1.11	0.79	0.67	0.52	used to adjust ho to fit experimental	1.11	0.79	0.67
ho - corrected	hocc	896	577	507	378				
1/(hoAo), Roc	Roc	0.0131	0.0126	0.0119	0.0130	535 ho-effective			

penalty factor	NuDfff	0.70	0.66	0.53	0.53
combined conv.	NuDc	6.93	6.62	4.82	4.31
combined conv.	h-comb	748	670	475	423
combined conv.	Rocc	0.01570	0.01089	0.01275	0.01157

Calculate UA for each coil and qc for each coil

UAc (W/K)	UAc	42.2	57.5	53.6	58.6	1/(Ric+Rwc+Roc) (or use Rocc)		212 W/K
To (C) -assumed	To	35.4	29.8	31.2	28.2	53.8		
Toc (C) - calculated	Toc	35.4	29.8	31.2	28.2		Bu tto	Click this button to re-
To (C) (new values)	Tonew	35.4	29.8	31.2	28.2	x*To+(1-x)*Toc		
qc (W) - for the single coil	qc	619	707	692	678	2696	qnew	UAc*((Thi-Tco)-(To-Tci))/LN((Thi-Tc
q" (W/m2)		7,269	5,156	4,186	3,317	heat flux	Thonew	
							31.4	

Calculate the mean temp. of the outside surface of each coil (req'd for ho, nat conv.)

Tmsic (°C)	Tmsic	39.7	37.2	38.4	37.3	Thmc-qc*Ric surface temperature on the inside of the coil
Tmsi x Ai		2.57	3.88	4.83	5.80	37.94 Tmsi -ave

Model-3

Please open the macro program: HX4.macro

Modified on Feb. 16, 2008 by PLA input data

Data in bold is input information that is required.

q	2304	W		
Thm	51.2	C		
Tmw	39.9	C		
coil liquid (w or g	g			*50.4*
mdh	0.0310	kg/s	0.49 USGPM	1.86 L/m
mdc	0.0264	kg/s	0.42 USGPM	1.58 L/m
cph	3,851	J/kg.K	based on Thm	
cpc	4,177	J/kg.K	based on Tmw	
balanced mdc	0.0286	kg/s		
(mcp)c/(mcp)h	92%			
kt (Cu)	400	W/m.K		
m	0	exponent in Ajele's eq'n		
Ds, shell diamete	77.00	mm	3.031 in	
H, shell height	0.406	m	15.98 in	
		(based on height of coil #1)		

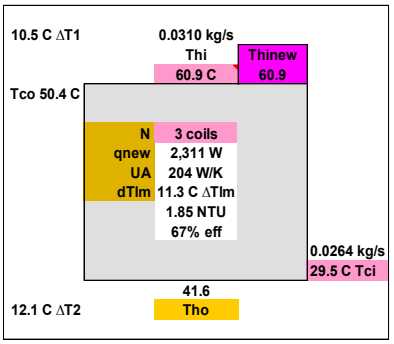

	Coil #	1	2	3	
Do (in)	tube outer dia., in	0.250	0.250	0.250	tube outer diameter, before bending
Do	tube outer dia., mm	6.35	6.35	6.35	
tw	wall thickness, mm	0.76	0.76	0.76	0.030 inch
Di	tube inner dia., mm	4.83	4.83	4.83	tube inner diameter, before bending
a	Major axis, outer, mm	7.51	6.74	6.72	Dele's measurements; [(a2+b2)/2]^0.5 below
b	Minor axis, outer, mm	4.87	5.68	6.00	6.33 6.23 6.37
ain	Major axis, inner, mm	5.99	5.22	5.20	a-2*tw
bin	Minor axis, inner, mm	3.35	4.16	4.48	b-2*tw
Ac	Area of X-sect., mm2	15.75	17.04	18.28	π ain*bin/4
nrcp	Ratio of turns	1.00	1.05	0.92	as built
nrc	Ratio of turns	1.00	1.00	1.00	for testing purposes
nrca	Ratio of turns	1.00	0.84	0.68	for constant Ti-To
coil factor, cnf: 0 = nrcp, 1 = nrc		0			
nc	number of turns	43	45	39	INT(nrc*NC1) NC1=35 - production model
Space between tubes, SL (mm)		1.93	2.28	3.69	
Space between tubes, SL (in)		0.076	0.090	0.145	1 given; 2,3: (H-nc*a)/nc
Coil pitch		1.26	1.34	1.55	
Dhi	hyd. diameter, mm	4.13	4.60	4.80	(ain*bin)/((ain^2+bin^2)/2)^0.5
Dc	coil mean dia., mm	31.6	48.6	67.6	
Dco	coil outer dia., mm	36.5	54.3	73.6	Dc+b
Dci	coil inner dia., mm	26.7	42.9	61.6	Dc-b
Space between coils (mm)		3.2	3.7	1.7	
Dco^2 - Dci^2		616	1,104	1,622	
Awf	area for flow, mm2	627	532	746	1,905 mm2
Deq	57.8	S	0.332		

Aot 0.387 m2

Calculation of hi, the inside heat transfer coefficient

Thmc	mean coil liquid temp.	52.5	50.2	50.8	(Thi+To)/2
rhohc	Density, (kg/m3)	1,012	1,013	1,013	1044-0.5395T-(0.0384T)^2
cp	Specific heat, (J/kg.K)	3,854	3,849	3,850	3732+2.32T
muhc	Viscosity, (N.s/m2)	0.00148	0.00156	0.00154	11437-428T+6.1T^2-0.0297T^3
khc	Ther. conductivity, (W/m.K)	0.419	0.418	0.418	.379+.0013T-(0.000379T)^2+(0.00431T)^3
Prhc	Prandtl number	13.62	14.40	14.21	muhc*cp/khc
Lc	tube length, m	4.27	6.87	8.28	nc πDc; Length, Lt 19.42 m 64 ft 76.23 mm Di 0.0
pfc	% flow received	35.1	31.8	33.1	equal ΔP for each coil
pfnew	% flow received (new)	35.1	31.8	33.1	equal ΔP for each coil
mdhc	flow rate, (kg/s)	0.0109	0.0099	0.0102	0.0310 kg/s
um	velocity, m/s	0.684	0.571	0.553	mdhc/(rhohc*Ac)
ReD	Reynolds #	1930	1700	1742	rhohc*Dhi*um/muhc
De	Dean #	698	523	464	ReD*(Dhi/Dc)^0.5
f	friction factor	0.103	0.102	0.094	64/ReD*[1+(1+Dhi/Dc/3)^2*De/88.33]^0.5
ΔP (Pa)		25.12	25.10	25.10	f*Lc/Dhi*rhohc*um^2/2
ΔP (psi)		3.64	3.64	3.64	ΔPave 3.64 psi
X3f	constant	1.000	1.001	1.001	[1+1342/(De^2*Prhc)]^2
X4f	constant	1.084	1.080	1.081	1+1.15/Prhc
Nui	Nusselt #	31.1	27.1	25.6	[(4.36+4.64/X3f)^3+1.82*(De/X4f)^1.5]^0.333
hi	W/m2.K	3,155	2,464	2,230	Nui*khc/Dhi
Ai	m2	0.0647	0.1042	0.1256	πDi*Lc Ait (m2) 0.295
Ric	1/(hiAi)	0.00490	0.00389	0.00357	
hiAi (W/k)		204	257	280	hi(eq) = 2,516
Ri	equivalent R	0.00135			hiAi,total 741

Button: Click on this button to re-calculate the values for "% flow received"

Rwc	wall resistance	2.55E-05	1.59E-05	1.32E-05
Rw	equivalent R	5.61E-06		

Coils in HX as per Oct.24, 2007
31
35 (=92 feet only)
40
39
Coils in Oakland HX
44
45
39
35
Coils in TDL HX, Nov5, 07
42
45
39
35

Calculation of ho based on forced water flow and proportioning water flow over the coils

Tcmc	°C	44.51	43.51	43.92	(Tmsoc+Tmw)/2	#VALUE!
rhocc	Density, (kg/m3)	990	990	990	1001-0.1026T-0.0033T^2	Tcmc
cpcc	Specific heat, (J/kg.K)	4,178	4,178	4,178	4215-2.849T+(0.2688T)^2-(0.0901T)^3+(0.0414T)^4	
mucc	Viscosity, (N.s/m2)	0.000596	0.000607	0.000602	0.0017-0.0000429T+(0.000704T)^2-(0.00126T)^3	
kcc	Th. conductivity, (W/m.K)	0.636	0.635	0.635	0.569+0.00183T-0.00000724T^2	
Prcc	Prandtl number	3.91	3.99	3.96	mucc*cpcc/kcc	
nucc	Viscosity, (m/s2)	0.602	0.613	0.608	mucc/rhocc * 1000000	
acc	Th. diffusivity, (m/s2)	0.154	0.153	0.154	kcc/(rhocc*cpcc)*1000000	
Bcc	Beta (1/K)	415	407	410	(-10.1+11.2T-0.037T^2)	
Water flow (kg/s)		0.0091	0.0082	0.0090	based on fraction of total q (qc/qh * mdc)	#VALUE!
Water velocity (m/s)		0.0147	0.0155	0.0122	0.0263 mdc -calc	
Dho	hyd. diameter, mm	5.78	6.14	6.33	(a*b)/((a^2+b^2)/2)^0.5	
Reynolds#		130.5	147.1	119.2		3 inch copper tube
NuDf	Nusselt #	10.72	11.33	10.27	based on forced flow; single cylinder	3.125 inches
hocf	W/m2.K	1,180	1,171	1,031		79.38 Do -mm
ratio		1.00	0.99	0.87		0.062 t-wall
1/(hoAo)		0.00995	0.00623	0.00587	1,113 ho-effective for forced flow	1.575 mm
						3.15 2 t-wall

Calculation of ho for each coil, assuming natural convection only

dTcc	°C	19.58	17.58	18.40	Tmsoc-Tci	#VALUE!
dTccx	°C	9.13	7.13	7.95	Tmsoc-Tmw (use this ΔT)	#VALUE!
RaDcc	based on dTcc	166,102	172,940	200,929	g*Bcc*dTcc*Do^3/(nucc*acc)	
RaDccx	based on dTccx	77,481	70,152	86,830	g*Bcc*dTccx*Do^3/(nucc*acc)	
NuDcc	based on Radcc	6.84	6.94	7.29	0.125*RaDcc^0.333 (Morgan, turbulent, RaD>10 million)	
NuD	based on RaDcc	9.69	9.79	10.16	0.48*RaDcc^0.25 (Morgan, laminar)	
NuDx	based on Radccx	8.01	7.81	8.24	0.48*RaDccx^0.25 (Morgan, laminar)	
hoc	W/m2.K	882	807	827	NuDx*kcc/Do (Morgan turbulent)	
Roc2	1/(hoAo)	0.01332	0.00904	0.00732	832 ho-effective	
Ao	area, m2	0.0852	0.1371	0.1652	Aot (m2) 0.387	
DoAo		0.5408	0.8704	1.0492	6.35 Do-e (mm)	
0 - use one ho; 1 - use hoc		1	1176		Ajele's value	
ho or hoc (W/m2.K)		882	807	827	hoc - natural conv. for each coil	
correction factor for hoc		1.11	0.79	0.67	used to adjust ho to fit experimental data	
hocc	ho corrected	979	638	554		
Roc	1/(hoAo)	0.01200	0.01144	0.01092	677 ho-effective for natural convection	

NuDfff	penalty factor	0.71	0.66	0.53		
NuDc	combined conv.	8.31	8.01	6.07		
h-comb	combined conv.	915	828	609		
Rocc	combined conv.	0.01284	0.00881	0.00993		

Calculate UA for each coil and qc for each coil

UAc	W/K	56.3	78.6	74.0	1/(Ric+Rwc+Roc) (or use Rocc)	
To	from HX4.macro	44.2	39.6	40.6		
Toc	calculated	44.2	39.6	40.6	Button	Click on this button to re-calculate the values for "To".
Tonew	new values	44.2	39.6	40.6	x*To+(1-x)*Toc	
qc	W - for the single coil	702	809	800	2311 W qnew	
q"	W/m2	8,248	5,902	4,842	heat flux	

Calculate the mean temp. of the outside surface of each coil (req'd for ho, nat conv.)

Tmsic	mean inner surf. temp.	49.10	47.09	47.91	Thmc-qc*Ric		
Tmsi x Ai		3.18	4.91	6.02	47.88	Tmsi -ave	
Tmsoc	mean outer surf. temp.	49.08	47.08	47.90	Tmsic-qc*R	48.02	Tmso-av
Tmsoc-Tmw		9.13	7.13	7.95	8.07		dT-av
(Tmsoc-Tmw)/dT-av		1.13	0.88	0.98			
Tmso x Ao		4.18	6.45	7.91	47.87	Tmso	*47.87*

Various methods for calculating ho (single value)

Thermophysical properties of water evaluated at Tmw

Tmw (C) *39.9*

kc	rhoc	cpc	alphac	muc	nuc	Prc	beta
0.631	992	4,177	1.52E-07	6.44E-04	6.49E-07	4.27	0.000378

Aot	As	Ap	Acf	Dhx	uw	ReDo
0.387	0.098	0.486	0.00191	0.00637	0.0140	136.7

	dT			
	18.4	Ajele	Ajele correlation is for 1-4 coils only!	

Ra(Dhx)	Ram	Ff	Nuo	ho	Ro	Ri
178,100	3,722	1.551	10.61	1176	0.00219	0.00135

RaDo	NuDo	Nuo	Nuo	1050
176,479	9.84	6.98	10.57	
ho=	977	693	1050	
	Morgan lam.	Morgan tur.	Churchill	

Ri+Rw+Ro	Thonew
0.00355	41.5

tube bank

NuDo
11.39

Zhukauskas

NuDo	ho	NuDo
10.95	1087	11.59

Hilpert (forced) Churchill (forced)

NuDo	ho
7.42	734

Nu=0.48Ra*^0.33

Ajele (general)

Model-4

Please open the macro program: HX4.macro

Modified o Feb. 17, 2008 by PLA

Data in bold is required input.

qh	3,000	W		
prop. gly. (	38	%		
Thm	42.4	C		43.7
Tmw	29.4	C	USGPM	
mdh	0.0330	kg/s	0.524	1.98 L/m
mdc	0.0250	kg/s	0.397	1.50 L/m
cph	4,000	J/kg.K		
cpc	4,177	J/kg.K		
balanced r	0.032	kg/s		
(mcp)c/(mc	79%			
kt	400	W/m.K		
Ds	102	mm	4.016 in	
H	0.406	m	15.98 in	
m	0	exponent in Ajele's eq'n		

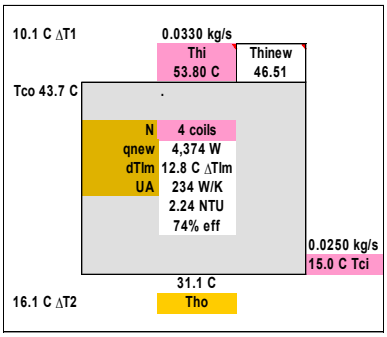

	40/60
cp	3732 + 2.32 T
k	0.379+0.00130 T-(0.00379 T)^2+(0.00431 T)^3
visc	11437-428T+6.1T^2-0.0297T^3

FALSE

Coil #		1	2	3	4	
Tube outer diameter, Do (in)		0.250	0.250	0.250	0.250	tube outer diameter, before bending
Tube outer diameter, Do (m	Do	6.35	6.35	6.35	6.35	Dot 6.35 mm
Wall thickness, tw (mm)	tw	0.761	0.761	0.761	0.761	0.030 in
Tube inner diameter, Di (mm	Di	4.83	4.83	4.83	4.83	tube inner diameter, before bending
Major axis, a, outer (mm)	a	7.51	6.74	6.72	6.55	Dele's measurements; [(a2+b2)/2]^0.5 below
Minor axis, b, outer (mm)	b	4.87	5.68	6.00	6.15	6.33 6.23 6.37 6.35
Major axis, ain, inner (mm)	ain	5.99	5.22	5.20	5.03	a-2*tw
Minor axis, bin, inner (mm)	bin	3.35	4.16	4.48	4.63	b-2*tw
Area of X-sect., mm2	Ac	15.75	17.04	18.28	18.28	π ain*bin/4
Ratio of turns	nrcp	1.00	1.05	0.92	0.85	as built (Oct.24,07)
Ratio of turns	nrc	1.00	1.00	1.00	1.00	for testing purposes
Ratio of turns	nrca	1.00	0.84	0.68	0.56	for constant Ti-To
coil factor, cnf: 0 = nrcp, 1 =	cnf	0				
No. of turns	nc	43	45	39	36	INT(nrc*NC1) NC1=35 - production model
Space between tubes (mm)	SL	1.93	2.28	3.69	4.73	
Space between tubes, SL (in)		0.076	0.090	0.145	0.186	1 given; 2,3,4: (H-nc*a)/nc
Coil pitch		1.26	1.34	1.55	1.72	
Hydraulic diameter (mm)	Dhi	4.13	4.60	4.80	4.82	(ain*bin)/((ain^2+bin^2)/2)^0.5
Coil mean dia (mm)	Dc	31.6	48.6	67.6	90.6	
Coil outer dia (mm)	Dco	36.5	54.3	73.6	96.8	Dc+b
Coil inner dia (mm)	Dci	26.7	42.9	61.6	84.5	Dc-b
Space between coils (mm)	Sc	3.2	3.7	5.4	2.6	
Dco^2 - Dci^2		616	1,104	1,622	2,229	
Area for water flow (mm2)	Acs	627	532	994	1,516	3,669 mm2
Deq 74.6		S 0.367		S=(Ds-Deq)/Deq		

Aot 0.592 m2

	Coils in HX as per Oct.24, 2007
	31
	35 (=92 feet only)
	40
	39
	Coils in Oakland HX
	44
	45
	39
	35
	Coils in TDL HX, Nov5, 07
	42
	45
	39
	35

Calculation of hi, the inside heat transfer coefficient

Thmc (C)	Thmc	44.6	41.8	42.5	41.0	(Thi+To)/2 #VALUE!
Density (kg/m3)	rhohc	1,017	1,019	1,018	1,019	1044-0.5395T-(0.0384T)^2
Specific heat (J/kg.K)	cp	4,000	4,000	4,000	4,000	3732+2.32T / 3500+3.45T
Viscosity (N.s/m2)	muhc	0.00000	0.00000	0.00000	0.00000	11437-428T+6.1T^2-0.0297T^3
Thermal conductivity (W/m.I	khc	0.45	0.45	0.45	0.45	0.344+.00109T-(0.000346T)^2+(0.00375T)^3
Prandtl #	Prhc	0.0	0.0	0.0	0.0	muhc*cp/khc
Tube length (m)	Lc	4.27	6.87	8.28	10.25	nc πD c; Length, L t 29.67 m
Tube length, Lc (ft)		14.0	22.5	27.2	33.6	97 ft
% flow received	pfc	26.3	24.6	25.6	23.5	100.0 %
% flow received (new values	pfnew	26.3	24.6	25.6	23.5	equal ΔP for each coil
Flow rate (kg/s)	mdhc	0.0087	0.0081	0.0084	0.0078	0.0330 kg/s
Velocity (m/s)	um	0.54	0.47	0.45	0.42	mdhc/(rhohc*Ac)
Reynolds#	ReD	2,279,740,982	2,188,893,060	2,217,405,499	2,043,279,666	rhohc*Dhi*um/muhc
Dean #, De	De	824437992	673330000	590744260	471073026	ReD*(Dhi/Dc)^0.5
Friction factor	f	0.000	0.000	0.000	0.000	64/ReD*[1+(1+Dhi/Dc/3)^2*De/88.33]^0.5
ΔP (kPa)		0.0	0.0	0.0	0.0	f*Lc/Dhi*rhohc*um^2/2
ΔP (psi)		0.0	0.0	0.0	0.0	ΔPave 0.00 psi
Constant	X3f	1.00	1.00	1.00	1.00	[1+1342/(De^2*Prhc)]^2
Constant	X4f	129376.00	129376.00	129376.00	129376.00	1+1.15/Prhc
Nusselt #, Nui	Nui	97.0	87.7	82.1	73.3	[(4.36+4.64/X3f)^3+1.82*(De/X4f)^1.5]^0.333
Heat transfer coef, hi (W/m	hi	10,559	8,577	7,701	6,854	Nui*khc/Dhi
Heat transfer area, Ai (m2)	Ai	0.065	0.104	0.126	0.155	πDi*Lc Ait (m2) 0.450
Ric, 1/(hiAi)	Ric	0.00146	0.00112	0.00103	0.00094	
hiAi (W/k)		684	894	968	1065	hi(eq) = 8,023
Equivalent (1/hiAi)	Ri	0.00028				hiAi,total 3,610

Wall resistance (Rwc)	Rwc	2.55E-05	1.59E-05	1.32E-05	1.06E-05
Equivalent Rw	Rw	3.67E-06			

But ton

Click this button to re-calculate the values for "pfc".

pfc is the percentage of the flow taken by each coil

Calculation of ho based on forced water flow and proportioning water flow over the coils

Twater,mean (°C)	Tcmc	36.2	34.9	35.4	34.7	(Tmsoc+Tmw)/2	#VALUE!
Density (kg/m3)	rhocc	993	993	993	993	1001-0.1026T-0.0033T^2	
Specific heat (J/kg.K)	cpcc	4,177	4,177	4,177	4,177	4215-2.849T+(0.2688T)^2-(0.0901T)^3+(0.0414T)^4	
Viscosity (N.s/m2)	mucc	0.000701	0.000722	0.000714	0.000725	0.0017-0.0000429T+(0.000704T)^2-(0.00126T)^3	
Th. conductivity (W/m.K)	kcc	0.63	0.62	0.62	0.62	0.569+0.00183T-0.00000724T^2	
Prandtl #	Prcc	4.7	4.8	4.8	4.9	mucc*cpcc/kcc	
Viscosity (m/s2)	nucc	0.71	0.73	0.72	0.73	mucc/rhocc * 1000000	
Th. diffusivity (m/s2)	acc	0.15	0.15	0.15	0.15	kcc/(rhocc*cpcc)*1000000	
Beta (1/K)	Bcc	347	335	340	334	(-10.1+11.2T-0.037T^2)	
Water flow (kg/s)	mwc	0.0097	0.0099	0.0090	0.0077	based on fraction of total q (qc/qh * m	#VALUE!
Water velocity (mm/s)	uwc	15.6	18.6	9.1	5.1	0.0363 mdc -calc	6.8 mm/s (ave.)
uw index	uwind	0	0 use uwc; 1 use uw				
Hydraulic diameter (mm)	Dho	5.78	6.14	6.33	6.34	(a*b)/((a^2+b^2)/2)^0.5	
Reynolds#, Re		110	140	70	40		
Nusselt #	NuDf	10.8	12.1	8.8	6.6	based on forced flow; single cylinder, Hilpert	
ho	hocf	1,151	1,210	853	644		
ratio		1.00	1.05	0.74	0.56		
1/(hoAo)		0.01020	0.00603	0.00710	0.00759	906	ho-effective for forced flow

Calculation of ho for each coil, assuming natural convection only

ΔTcc (°C)	dTcc	28.1	25.4	26.4	25.0	Tmsoc-Tci	#VALUE!
RaDcc	RaDcc	173,524	176,817	205,992	190,640	g*Bcc*dTcc*Do^3/(nucc*acc)	
Morgan coefficient	Cm	0.480	0.480	0.480	0.480		
Morgan exponent	nm	0.250	0.250	0.250	0.250		
NuDcc (RaDcc)	NuDcc	9.8	9.8	10.2	10.0	Morgan	
hoc (W/m2.K) (NuDcc)	hoc	1,061	1,000	1,009	987	NuDcc*kcc/Dho	
1/(hocAo)	Roc2	0.0111	0.0073	0.0060	0.0050	1,007	ho-effective

ΔTccx (C)	dTccx	13.8	11.0	12.0	10.7	Tmsoc-Tmw	#VALUE!
RaDccx	RaDccx	84,916	76,658	93,869	81,262	g*Bcc*dTccx*Do^3/(nucc*acc)	
Morgan coefficient	Cmx	0.480	0.480	0.480	0.480		
Morgan exponent	nmx	0.250	0.250	0.250	0.250		
NuDx (RaDccx)	NuDccx	8.19	7.99	8.40	8.10	Morgan	
hocx (W/m2.K) (NuDcc)	hocx	887	811	829	797		
1/(hocAo)	Rocx2	0.0132	0.0090	0.0073	0.0061	822	ho-effective

Heat transfer area, Ao (m2	Ao	0.085	0.137	0.165	0.204	Aot (m2)	0.592			
DoAo		0.54	0.87	1.05	1.30	6.35	Do-e (mm)			
0 - use one ho; 1 - use hoc		1	hoindex	726	(=Ajele's ho)					
ho or hocx (W/m2.K)		887	811	829	797	hocx - natural conv. for each coil				
correction factor for hoc		1.11	0.79	0.67	0.52	used to adjust ho to fit experimental d	1.11	0.79	0.67	0.52
ho - corrected	hocc	985	641	556	415					
1/(hoAo), Roc	Roc	0.0119	0.0114	0.0109	0.0118	588	ho-effective			

penalty factor	NuDfff	0.70	0.66	0.53	0.53
combined conv.	NuDc	8.28	8.45	5.55	4.82
combined conv.	h-comb	897	859	547	474
combined conv.	Rocc	0.01309	0.00850	0.01106	0.01032

Calculate UA for each coil and qc for each coil

UAc (W/K)	UAc	68.6	103.8	82.6	88.7	1/(Ric+Rwc+Roc) (or use Rocc)		344 W/K
To (C) -assumed	To	35.4	29.8	31.2	28.2	53.8		
Toc (C) - calculated	Toc	24.9	15.1	22.3	20.7	Bu		Click this button to re-calculate the values for "To".
To (C) (new values)	Tonew	31.2	23.9	28.5	26.7	x*To+(1-x)*Toc		
qc (W) - for the single coil	qc	1005	1276	1066	1027	4374	qnew	*UAc*((Thi-Tco)-(To-Tci))/LN((Thi-Tco)/(To-Tci))*
q" (W/m2)		11,804	9,311	6,449	5,024	heat flux	Thonew	
							20.7	

Calculate the mean temp. of the outside surface of each coil (req'd for ho, nat conv.)

Tmsic (°C)	Tmsic	43.2	40.4	41.4	40.0	Thmc-qc*Ric	surface temperature on the inside of the coil
Tmsi x Ai		2.79	4.21	5.20	6.22	40.95	Tmsi -ave
Tmsoc (°C)	Tmsoc	43.1	40.4	41.4	40.0	Tmsic-qc*Rw	surface temperature on the ouside of th #### Tmso-av
Tmsoc-Tmw		13.8	11.0	12.0	10.7	11.86	dT-av
(Tmsoc-Tmw)/dT-av		1.16	0.93	1.01	0.90		
Tmso x Ao		3.67	5.53	6.84	8.18	*40.93*	*Tmso* *40.93*

Various methods for calculating ho (single value) Thermophysical properties of water evaluated at Tmw

Tmw (C) *29.4*

kc	rhoc	cpc	alphac	muc	nuc	Prc	beta
0.616	995	4,177	1.48E-07	8.15E-04	8.19E-07	5.52	0.000287

Aot (m2)	As	Ap	Acf	Dhx	uw	ReDo
0.592	0.130	0.722	0.00367	8.25 mm	6.8 mm/s	53

Tmso-Tci=dT 25.9 Ajele

Ajele correlation is for 1-4 coils only!

Ra(Dhx)	Ram	Ff	Nuo	ho	Ro	Ri
337,685	4,620	1.149	8.68	726	0.00233	0.00028

RaDo	NuDo	NuDo
153,838	9.51	10.47
ho=	923	1017
	Morgan	Churchill

649

Ri+Rw+Ro 0.0026

NuDo	ho	NuDo	ho
7.7	746	7.7	747
Hilpert (forced)		Churchill (forced)	

tube bank

NuDo	ho
7.2	
Zhukauskas	

NuDo	ho
8.0	596

Nu=0.48Ra*^0.33 Ajele (general)

APPENDIX D

SYSTEM MONITORING PROGRAM

```
CLEAR: CLS: CLOSE
BREAK ON
DEFSNG A-H,J-Z: DEFINT I
DEF FN CPWCAL(T)=4215-2.849*T+.07637*T^2-
.0008403*T^3+.000003701#*T^4
DEF FN CPGCAL(T)=3733+2.33*T+(3500+3.45*T-3733-2.33*T)*(PGC-40)/10
DIM xlist$(66),lab$(66),T2(10)
GOSUB "LISTS": GOSUB "DEFAULTS"
OPEN"C",-1,9600,0,0,1
HANDSHAKE -1,-1
PRINT#-1,"ECHO 0"
PRINT#-1,"SETCAL
1,9.998,98.92,480.3,989.89,1001.6,9985,682506,1000000"
PRINT#-1,"SETAZ 0,1"
PRINT#-1,"SETREF 1,1"
INPUT#-1, A$,B$,C$,D$,E$
PRINT A$,B$,C$,D$,E$
send$="TCP 7,3,0"
GOSUB "GETNUM"
PRINT temp;
send$="THMST 1,2"
GOSUB "GETNUM"
PRINT temp
GOTO "KEYIN"

"GETNUM"
PRINT#-1,send$
"INAGAIN"
INPUT#-1, A$
NUM=VAL(A$)
IF NUM>500000 THEN BEEP:BEEP
IF NUM>500000 THEN GOTO "INAGAIN"
AR$=RIGHT$(A$,LEN(A$)-1)
temp=VAL(AR$)
RETURN

"KEYIN"
PRINT:PRINT "Press a key and then RETURN":PRINT
PRINT "M,m  E,e  S,s  P,p or X,x (END)": BEEP
INPUT B$
        IF B$ = "M" OR B$="m" GOTO "MONITOR"
        IF B$ = "E" OR B$="e" GOTO "EXALL"
        IF B$ = "S" OR B$="s" GOTO "SINGLE"
```

```
        IF B$ = "P" OR B$="p" GOTO "PFILE"
        IF B$ = "X" OR B$="x" GOTO "END"
GOTO "KEYIN"

"PFILE"
DEF OPEN "TEXT"
filename$="mDATA"
OPEN "O",2,filename$
PRINT#2, "testing"
CLOSE#2
GOTO "KEYIN"

"MONITOR"
PRINT "Write data to file (1 for yes,0 for no; then RETURN)"
INPUT B$
       IF B$="" GOTO "MONITOR"
       IF B$="1" THEN PF=1
filename$="TDATA"
IF PF=0 THEN GOTO "MON5"
DEF OPEN "TEXT"
IF PF=1 THEN OPEN "O",#2,filename$
PRINT #2, "Time";CHR$(9);"Tgi";CHR$(9);"Tgo1";CHR$(9);"Tgo2";
PRINT #2, CHR$(9);"Tgo3";CHR$(9);"Tgo4";
PRINT #2, CHR$(9);"TgoFM";CHR$(9);"Thti";CHR$(9);"Thto";
PRINT #2, CHR$(9);"Two";CHR$(9);"Twi";CHR$(9);"DT1";CHR$(9);"DT2";
PRINT #2,
CHR$(9);"DTLM";CHR$(9);"Cpht";CHR$(9);"Cphx";CHR$(9);"Cpwc";
PRINT #2, CHR$(9);"GPM";CHR$(9);"mdot";CHR$(9);"md1";CHR$(9);"md2";
PRINT #2, CHR$(9);"md3";CHR$(9);"md4";
PRINT #2,
CHR$(9);"m1pc";CHR$(9);"m2pc";CHR$(9);"m3pc";CHR$(9);"m4pc";
PRINT #2, CHR$(9);"mdcw";CHR$(9);"qele";CHR$(9);"qht";CHR$(9);"qhx";
PRINT #2, CHR$(9);"qhx4c";CHR$(9);"qhx1";CHR$(9);"qhx2";
PRINT #2, CHR$(9);"qhx3";CHR$(9);"qhx4";
PRINT #2, CHR$(9);"UA1";CHR$(9);"UA2";CHR$(9);"Tlab"

"MON5"
IMI=-1
CLS
"MON2"
IMI=IMI+1
FOR I=7 TO 17
send$=xlist$(I):GOSUB "GETNUM"
PRINT USING "####.#";temp;:PRINT "   ";
IF I=7 THEN Tgi=temp
IF I=8 THEN Tgo1=temp
IF I=9 THEN Tgo2=temp
IF I=10 THEN Tgo3=temp
IF I=16 THEN Tgo4=temp
IF I=11 THEN Tgo=temp
IF I=12 THEN Thti=temp
IF I=13 THEN Thto=temp
```

```
IF I=14 THEN Two=temp
IF I=15 THEN Twi=temp
IF I=17 THEN Tlab=temp
NEXT I
Tave=(Tgi+Tgo)/2
PRINT
IF IMI>0 THEN GOTO "MON4"
"MON6"
       PRINT "Type in heater voltage"
                  INPUT Vht
       qelec=Vht*Vht/Rht
       delq=6.3*(Tave-Tlab)
       qhxact=qelec-delq
       GPM1=.00000000000666*qhxact^3-
.00000008#*qhxact^2+.000312*qhxact+.175
       RFM=-1.96*GPM1^2+2.28*GPM1+.215
                   PRINT "RFM = ", RFM
       GPMFM=GPM1/RFM
       PRINT "qhxact is  ";:PRINT USING "######";qelec;
       PRINT "   GPM (actual) should be ";:PRINT USING "##.###";GPM1
       PRINT "   GPM (flow meter) should be ";:PRINT USING
"##.###";GPMFM
       PRINT "Type in actual flow meter reading in USGPM"
       INPUT GPMFM1
       GPM=RFM*GPMFM1
       PRINT "GPM = ",GPM
       PRINT "Type in flow rate coil 1": INPUT fr1
IF ICOIL=1 THEN GOTO "FREND"
       PRINT "Type in flow rate coil 2": INPUT fr2
       PRINT "Type in flow rate coil 3": INPUT fr3
IF ICOIL=3 THEN GOTO "FREND"
       PRINT "Type in flow rate coil 4": INPUT fr4
"FREND"

IF IMI=0 THEN GOTO "MON2"
PRINT
"MON4"
mdot=GPM*3.789/60
totfr=fr1+fr2+fr3+fr4
mdot1=mdot*fr1/totfr: mdot2=mdot*fr2/totfr
mdot3=mdot*fr3/totfr: mdot4=mdot*fr4/totfr
m1PC=fr1/totfr*100: m2PC=fr2/totfr*100
m3PC=fr3/totfr*100: m4PC=fr4/totfr*100
Tmht=(Thti+Thto)/2: CPHT=FN CPGCAL(Tmht)
Tmhx=(Tgi+Tgo)/2: CPHX=FN CPGCAL(Tmhx)
Tmwc=(Two+Twi)/2: CPWC=FN CPWCAL(Tmwc)
PRINT "Tgi  (7)=";:PRINT  USING "####.#";Tgi
PRINT "Tgo1 (8)=";:PRINT USING "####.#";Tgo1;
PRINT " Tgo2 (9)=";:PRINT USING "####.#";Tgo2;
PRINT " Tgo3(10)=";:PRINT USING "####.#";Tgo3;
PRINT " Tgo4(16)=";:PRINT USING "####.#";Tgo4;
PRINT "Tgo (11)=";:PRINT USING "####.#";Tgo
```

```
PRINT "Thti(12)=";:PRINT USING "####.#";Thti;
PRINT " Thto(13)=";:PRINT USING "####.#";Thto
PRINT "Two (14)=";:PRINT USING "####.#";Two;
PRINT " Twi (15)=";:PRINT USING "####.#";Twi
PRINT "Tlab(17)=";:PRINT USING "####.#";Tlab
DT1=Tgi-Two: DT2=Tgo-Twi
IF DT1<0 THEN DT1=.1
IF DT1=0 THEN DT1=.1
IF DT2<0 THEN DT2=.1
IF DT2=0 THEN DT2=.1
IF DT2=DT1 THEN DT1=DT2+.01
DTLM=(DT1-DT2)/LOG(DT1/DT2)
PRINT "DT1=";:PRINT USING "####.#";DT1;
PRINT "   DT2=";:PRINT USING "####.#";DT2;
PRINT "   DTLM=";:PRINT USING "####.#";DTLM
PRINT "cpht=";:PRINT USING "######";CPHT;
PRINT "   cphx=";:PRINT USING "######";CPHX;
PRINT "   cpwc=";:PRINT USING "######";CPWC
PRINT "GPM=";:PRINT USING "####.###";GPM;
mdotcw=mdot*CPHX/CPWC*(Tgi-Tgo)/(Two-Twi)
PRINT "   mdot (kg/s)=";:PRINT USING "####.####";mdot;
PRINT "   mdotcw (kg/s)=";:PRINT USING "####.####";mdotcw
PRINT "mdot1, mdot2, mdot3, mdot4 (kg/s)=";:PRINT USING
"###.####";mdot1;
PRINT USING "###.####";mdot2;:PRINT USING "###.####";mdot3;
PRINT USING "###.####";mdot4
PRINT "m1PC, m2PC, m3PC, m4PC (%)=";:PRINT USING "######";m1PC;
PRINT USING "######";m2PC;:PRINT USING "######";m3PC;
PRINT USING "######";m4PC
qelec=Vht*Vht/Rht
qht=mdot*CPHT*(Thto-Thti): qhx=mdot*CPHX*(Tgi-Tgo)
qhx1=mdot1*CPHX*(Tgi-Tgo1): qhx2=mdot2*CPHX*(Tgi-Tgo2)
qhx3=mdot3*CPHX*(Tgi-Tgo3): qhx4=mdot4*CPHX*(Tgi-Tgo4)
qhx4c=qhx1+qhx2+qhx3+qhx4
PRINT "qelec=";:PRINT USING "#####";qelec;
PRINT "   qht=";:PRINT USING "#####";qht;
PRINT "   qhx=";:PRINT USING "#####";qhx;
PRINT "   qhx4c=";:PRINT USING "#####";qhx4c
PRINT "qhx1, qhx2, qhx3, qhx4=";:PRINT USING "#####";qhx1;
PRINT USING "#####";qhx2;:PRINT USING "#####";qhx3;
PRINT USING "#####";qhx4
UAhx1=qhx/DTLM: UAhx2=qhx4c/DTLM: UAqel=qelec/DTLM
PRINT "UAqel, UAhx1, UAhx2 (W/K)=";:PRINT USING "######";UAqel;
PRINT USING "######";UAhx1;:PRINT USING "######";UAhx2
PRINT
IF PF=0 THEN GOTO "MON3"
PRINT #2, TIME$;
PRINT #2, CHR$(9);:PRINT #2,  USING "####.#";Tgi;
PRINT #2, CHR$(9);:PRINT #2, USING "####.#";Tgo1;
PRINT #2, CHR$(9);:PRINT #2, USING "####.#";Tgo2;
PRINT #2, CHR$(9);:PRINT #2,USING "####.#";Tgo3;
PRINT #2, CHR$(9);:PRINT #2,USING "####.#";Tgo4;
```

```
PRINT #2, CHR$(9);:PRINT #2, USING "####.#";Tgo;
PRINT #2, CHR$(9);:PRINT #2, USING "####.#";Thti;
PRINT #2, CHR$(9);:PRINT #2, USING "####.#";Thto;
PRINT #2, CHR$(9);:PRINT #2, USING "####.#";Two;
PRINT #2, CHR$(9);:PRINT #2, USING "####.#";Twi;
PRINT #2, CHR$(9);:PRINT #2, USING "####.#";DT1;
PRINT #2, CHR$(9);:PRINT #2, USING "####.#";DT2;
PRINT #2, CHR$(9);:PRINT #2, USING "####.#";DTLM;
PRINT #2, CHR$(9);:PRINT #2, USING "######";CPHT;
PRINT #2, CHR$(9);:PRINT #2, USING "######";CPHX;
PRINT #2, CHR$(9);:PRINT #2, USING "######";CPWC;
PRINT #2, CHR$(9);:PRINT #2, USING "####.###";GPM;
PRINT #2, CHR$(9);:PRINT #2, USING "####.####";mdot;
PRINT #2, CHR$(9);:PRINT #2, USING "####.####";mdot1;
PRINT #2, CHR$(9);:PRINT #2, USING "####.####";mdot2;
PRINT #2, CHR$(9);:PRINT #2, USING "####.####";mdot3;
PRINT #2, CHR$(9);:PRINT #2, USING "####.####";mdot4;
PRINT #2, CHR$(9);:PRINT #2, USING "######";m1PC;
PRINT #2, CHR$(9);:PRINT #2, USING "######";m2PC;
PRINT #2, CHR$(9);:PRINT #2, USING "######";m3PC;
PRINT #2, CHR$(9);:PRINT #2, USING "######";m4PC;
PRINT #2, CHR$(9);:PRINT #2, USING "####.####";mdotcw;
PRINT #2, CHR$(9);:PRINT #2, USING "#####";qelec;
PRINT #2, CHR$(9);:PRINT #2, USING "#####";qht;
PRINT #2, CHR$(9);:PRINT #2, USING "#####";qhx;
PRINT #2, CHR$(9);:PRINT #2, USING "#####";qhx4c;
PRINT #2, CHR$(9);:PRINT #2, USING "#####";qhx1;
PRINT #2, CHR$(9);:PRINT #2, USING "#####";qhx2;
PRINT #2, CHR$(9);:PRINT #2, USING "#####";qhx3;
PRINT #2, CHR$(9);:PRINT #2, USING "#####";qhx4;
PRINT #2, CHR$(9);:PRINT #2, USING "######";UAhx1;
PRINT #2, CHR$(9);:PRINT #2, USING "######";UAhx2;
PRINT #2, CHR$(9);:PRINT #2, USING "####.#";Tlab

"MON3"
IF B$="D" OR B$="d" THEN GOTO "MON2"
PRINT "c to continue; f to enter flow; . to stop; d to file data
(then RETURN)"
"LOOP2"
INPUT B$
       IF B$="" GOTO "LOOP2"
       IF B$="D" OR B$="d" THEN GOTO "MON2"
       IF B$="." AND PF=1 THEN CLOSE #2
       IF B$="." THEN GOTO "KEYIN"
       IF B$="C" OR B$= "c" THEN GOTO "MON2"
       IF B$="F" OR B$= "f" THEN  GOTO "MON6"
GOTO "MON2"

"EXALL"
CLS
"EXA6"
FOR i=7 TO 10: FOR td=1 TO 2500: NEXT td
```

```
send$=xlist$(i):GOSUB "GETNUM"
PRINT USING "##";i;:PRINT " ";lab$(i),:PRINT USING "####.#";temp
NEXT i
i=16
send$=xlist$(i):GOSUB "GETNUM"
PRINT USING "##";i;:PRINT " ";lab$(i),:PRINT USING "####.#";temp
FOR i=11 TO 15: FOR td=1 TO 2500: NEXT td
send$=xlist$(i):GOSUB "GETNUM"
PRINT USING "##";i;:PRINT " ";lab$(i),:PRINT USING "####.#";temp
NEXT i
i=17
send$=xlist$(i):GOSUB "GETNUM"
PRINT USING "##";i;:PRINT " ";lab$(i),:PRINT USING "####.#";temp
PRINT
GOTO "EXA6"

"SINGLE"
CLS
PRINT "thermistor reference temp. 1"
PRINT "HX, glycol: inlet:         7"
PRINT "HX, glycol: outlet 1:      8"
PRINT "HX, glycol: outlet 2:      9"
PRINT "HX, glycol: outlet 3:     10"
PRINT "Glycol: flow meter outlet:11"
PRINT "Heater inlet;             12"
PRINT "Heater outlet;            13"
PRINT "HX water outlet;          14"
PRINT "HX water inlet;           15"
PRINT "HX, glycol: outlet 4:     16"
PRINT "Tlab:                     17"

"SINGLE4"
PRINT
BEEP:PRINT "Type in desired channel number (0 to stop); then
RETURN/ENTER"
PRINT "Type in N (or n) at anytime to change to a NEW channel"
INPUT nch
IF nch = 0 THEN GOTO "KEYIN"
PRINT:PRINT "Channel:  ";nch;":   ";lab$(nch)

"MORE"
PRINT TIME$;"  ";
FOR i=1 TO 10
FOR td=1 TO 2500: NEXT td
send$=xlist$(nch):  GOSUB "GETNUM"
PRINT USING "####.#";temp;

NEXT i

"SINGLE2"
      INPUT B$
      IF B$="." THEN GOTO "KEYIN"
```

```
      IF B$="N" OR B$="n" THEN GOTO "SINGLE4"
PRINT
GOTO "MORE"

"LISTS"

xlist$(0)="OHMS2W 0": lab$(0)="zero resistance"
xlist$(1)="THMST 1,2": lab$(1)="thermistor temp"

xlist$(7)="TCP 7,3,0":xlist$(8)="TCP 8,3,0"
xlist$(9)="TCP 9,3,0":xlist$(10)="TCP 10,3,0":xlist$(11)="TCP
11,3,0"
xlist$(12)="TCP 12,3,0":xlist$(13)="TCP 13,3,0":xlist$(14)="TCP
14,3,0"
xlist$(15)="TCP 15,3,0":xlist$(16)="TCP 16,3,0":xlist$(17)="TCP
17,3,0"

lab$(7)="HX glycol inlet":  lab$(8)="HX glycol exit #1"
lab$(9)="HX glycol exit #2":  lab$(10)="HX glycol exit #3"
lab$(11)="glycol at FM exit"
REM  FM = flow meter
lab$(12)="glycol heater inlet"
lab$(13)="glycol heater outlet":  lab$(14)="HX water outlet"
lab$(15)="HX water inlet":  lab$(16)="HX glycol exit #4"
lab$(17)="Tlab"

RETURN

REM  Default settings
"DEFAULTS"
Tcw=21: Rht=12.2: PGC=40: ICOIL=1
RETURN

"DATEMOD"
IF LEFT$(DATE$,2)="01" THEN MN$="Jan ": nday=0
IF LEFT$(DATE$,2)="02" THEN MN$="Feb ": nday=31
IF LEFT$(DATE$,2)="03" THEN MN$="Mar ": nday=59
IF LEFT$(DATE$,2)="04" THEN MN$="Apr ": nday=90
IF LEFT$(DATE$,2)="05" THEN MN$="May ": nday=120
IF LEFT$(DATE$,2)="06" THEN MN$="Jun ": nday=151
IF LEFT$(DATE$,2)="07" THEN MN$="Jul ": nday=181
IF LEFT$(DATE$,2)="08" THEN MN$="Aug ": nday=212
IF LEFT$(DATE$,2)="09" THEN MN$="Sep ": nday=243
IF LEFT$(DATE$,2)="10" THEN MN$="Oct ": nday=273
IF LEFT$(DATE$,2)="11" THEN MN$="Nov ": nday=304
IF LEFT$(DATE$,2)="12" THEN MN$="Dec ": nday=334

nday=nday+VAL(MID$(DATE$,4,2))
nweek=FIX(nday/7)
derr=1+nday-nweek*7
REM    at the start of a new year the number below must be advanced.
derr=derr+2
```

```
IF derr>7 THEN derr=derr-7
IF derr=2 THEN day$="Monday, "
IF derr=3 THEN day$="Tuesday, "
IF derr=4 THEN day$="Wednesday, "
IF derr=5 THEN day$="Thursday, "
IF derr=6 THEN day$="Friday, "
IF derr=7 THEN day$="Saturday, "
IF derr=1 THEN day$="Sunday, "
DATEM$=day$+MN$+MID$(DATE$,4,2)+", "+RIGHT$(DATE$,4)
DATEMS$=MN$+MID$(DATE$,4,2)+","+RIGHT$(DATE$,2)+" "+LEFT$(day$,3)
RETURN

BREAK OFF
"END"
PRINT#-1,"ECHO 1"
END
```